

# Trainability of Quantum Models Beyond Known Classical Simulability

Sabri Meyer,<sup>1</sup> Francesco Scala,<sup>1</sup> Francesco Tacchino,<sup>2</sup> and Aurelien Lucchi<sup>1</sup>

<sup>1</sup>*Department of Mathematics and Computer Science, University of Basel, 4051 Basel, Switzerland\**

<sup>2</sup>*IBM Quantum, IBM Research Europe – Zurich, 8803 Rüschlikon, Switzerland*

(Dated: July 10, 2025)

Variational Quantum Algorithms (VQAs) are promising candidates for near-term quantum computing, yet they face scalability challenges due to barren plateaus, where gradients vanish exponentially in the system size. Recent conjectures suggest that avoiding barren plateaus might inherently lead to classical simulability, thus limiting the opportunities for quantum advantage. In this work, we advance the theoretical understanding of the relationship between the trainability and computational complexity of VQAs, thus directly addressing the conjecture. We introduce the *Linear Clifford Encoder (LCE)*, a novel technique that ensures constant-scaling gradient statistics on optimization landscape regions that are close to Clifford circuits. Additionally, we leverage classical Taylor surrogates to reveal computational complexity phase transitions from polynomial to super-polynomial as the initialization region size increases. Combining these results, we reveal a deeper link between trainability and computational complexity, and analytically prove that barren plateaus can be avoided in regions for which no classical surrogate is known to exist. Furthermore, numerical experiments on LCE transformed landscapes confirm in practice the existence of a super-polynomially complex “transition zone” where gradients decay polynomially. These findings indicate a plausible path to practically relevant, barren plateau-free variational models with potential for quantum advantage.

## I. INTRODUCTION

Variational Quantum Algorithms (VQAs) [1] are promising tools for near-term quantum computers, with applications such as Variational Quantum Eigensolvers (VQE) [2] for estimating molecular ground state energies in quantum chemistry and condensed matter physics [3–7], and Quantum Machine Learning (QML) [8–10], where Parameterized Quantum Circuits (PQCs) [11] process data similarly to neural networks. However, characterizing and demonstrating indisputable advantages of VQAs over their classical counterparts remains an open and challenging question. Recently, a strong focus has been placed on the relationship between trainability and classical simulability of PQCs. Notably, it has been conjectured that a provable absence of so-called barren plateaus [12, 13], a gradient concentration phenomenon severely hindering trainability at large scale, implies – at least in many cases of practical interest – the existence of efficient classical simulation techniques for the corresponding class of circuits [14]. Intuitively, for instance, high expressivity of PQCs is known to be one of the major causes of barren plateaus [15, 16], while it is also known to potentially limit classical simulability [17, 18].

In this work, we advance the theoretical understanding of the relationship between trainability and computational complexity of PQCs. Starting with a Taylor approximation of the PQC optimization landscape, we

establish a mathematical framework to rigorously analyze both computational complexity and trainability of VQAs. More specifically, we expand around Clifford circuits, proposing a generalization of the quadratic Taylor approximation [19], leveraging the Gottesman-Knill theorem [20, 21] to efficiently compute Taylor coefficients. As a result, we establish a novel classical surrogate [22] of PQCs that demonstrates competitive performance compared to related approaches [17, 18, 23, 24].

The efficiency in computing derivatives evaluated at Clifford circuits has significant implications for the understanding of trainability in PQCs as well. Specifically, this insight enables us to effectively address the issue of trainability by introducing a classical algorithm that manages linear Taylor coefficients, the *Linear Clifford Encoder (LCE)*. This technique ensures constant-scaling gradient norm statistics within small regions of the landscape (or patches [18]) near Clifford circuits, even for large-scale models, at the cost of adding certain Clifford gates to the quantum circuit. Related work by Park et al. [25] achieves constant scaling gradients as well, but relies on stronger assumptions.

In addition, the Taylor surrogate enables us to capture the runtime complexity across various surrogate patch sizes, revealing a *phase transition in computational complexity*. This critical threshold separates the regimes where VQAs exhibit polynomially complex landscapes from those with super-polynomial hardness. Below this threshold, VQAs are simultaneously classically simulable and free of barren plateaus, with constant scaling gradients thanks to LCE. However, as the patch size increases beyond this threshold, the runtime of known classical simulation techniques saturates to an exponential scaling

---

\* [sabri.meyer@unibas.ch](mailto:sabri.meyer@unibas.ch)

behavior, accompanied by an expected exponential decay of the gradient. For arbitrary VQE problems whose observable includes at most  $\mathcal{O}(1)$  Pauli terms, we demonstrate that the transition is smooth, analytically proving that the gradient statistics decay polynomially over a transition patch where our Taylor surrogate demands super-polynomial computational resources. At the time of writing, no classical simulation technique is known to exist that can efficiently surrogate this transition patch. Our findings thus directly address a central conjecture raised by Cerezo et al. [14]. Numerical experiments support our theoretical results.

The rest of this document is structured as follows. In Sec. II we introduce the necessary concepts to lay the foundation for our main theoretical results, presented in Sec. III. There, we mathematically address the challenge of balancing trainability and computational complexity. In Sec. IV, we apply our theoretical findings and analytically prove that barren plateaus are avoidable on landscape patches for which no classical surrogate is currently known to exist. Sec. V discusses numerical experiments, providing evidence of potential *quantum advantage* [26] without barren plateaus. Finally, we summarize our findings in Sec. VI. A compact overview comparing our theoretical results with related works is found in Appendix A.

## II. PRELIMINARIES

In this section, we establish the four key ideas that we will leverage to yield our main results: the stabilizer formalism, the expressive power of PQC, barren plateau mitigation, and a novel class of classical Taylor surrogates.

### A. Stabilizer Formalism

The stabilizer formalism efficiently describes a large class of quantum states, named *stabilizer states*, by tracking the Pauli operators that leave them invariant [27]. This underlies the Gottesman-Knill theorem [20, 21] which guarantees efficient classical simulation for circuits made solely of Clifford operators. Here, we briefly recall the definitions of the Pauli and Clifford groups; see also Refs. [27, 28].

Let  $N \geq 1$  be the number of qubits. The  $N$ -qubit Pauli group is defined as

$$\mathcal{P}_N := \{\pm P, \pm iP : P \in \{I, X, Y, Z\}^{\otimes N}\}. \quad (1)$$

The  $N$ -qubit Clifford group is the subgroup of the unitary group  $U(2^N)$  that normalizes  $\mathcal{P}_N$  modulo global phases:

$$\text{Clifford}(N) := \{Q \in U(2^N) : Q \mathcal{P}_N Q^\dagger = \mathcal{P}_N\} / U(1). \quad (2)$$

It is generated by the ensemble  $\{H, S, CX\}$ . The space of stabilizer states is then

$$\text{Stab}(N) := \{Q|0\rangle : Q \in \text{Clifford}(N)\}, \quad (3)$$

where  $|0\rangle \equiv |0\rangle^{\otimes N}$ . For further details, including a review of related simulation techniques, see Appendices B and D.

### B. Variational Quantum Algorithms

An ideal  $N$ -qubit quantum system resides in a Hilbert space  $\mathcal{H}_N$  spanned by  $\{|b\rangle : b \in \{0, 1\}^N\}$ . We focus on a PQC [11] defined by

$$U(\theta) = \prod_{k=D}^1 R_{V_k}(\theta_k) W_k, \quad (4)$$

with  $D \geq 1$  parameterized rotation gates and Clifford operators  $W_k$ . Here,  $R_{V_k}(\theta_k) := \exp(-i\frac{\theta_k}{2}V_k)$  with  $V_k \in \{X, Y, Z\}$  acting on single qubits, using the notation  $V_j := I_{2^{j-1}} \otimes V \otimes I_{2^{N-j}}$ . We then define  $|\psi(\theta)\rangle := U(\theta)|0\rangle$ . Note that for  $\theta = 0$ ,  $U(0)$  is Clifford and  $|\psi(0)\rangle \in \text{Stab}(N)$ . Without loss of generality, we may only consider expanding around  $\theta = 0$ .

We consider a non-identity observable

$$H = \sum_{i \in \mathcal{I}} c_i P_i, \quad (5)$$

with Pauli strings  $P_i \in \mathcal{P}_N \setminus \{I\}$  and coefficients  $c_i \in \mathbb{R}$  satisfying  $c_i \in \mathcal{O}(1)$  as  $N \rightarrow \infty$ . The expectation value (cost function) is

$$C(\theta) := \langle \psi(\theta) | H | \psi(\theta) \rangle = \sum_{i \in \mathcal{I}} c_i \langle \psi(\theta) | P_i | \psi(\theta) \rangle, \quad (6)$$

which is smooth,  $2\pi$ -periodic in each parameter, and bounded by  $\|H\|$ . A typical VQA [1] utilizes a quantum processor to estimate the cost  $C(\theta)$ , which a classical optimizer (e.g. gradient descent or ADAM [29]) uses to update the parameters  $\theta$ , e.g. in Variational Quantum Eigensolver (VQE) [2] tasks that seek

$$\theta_* = \arg \min_{\theta \in [-\pi, \pi]^D} C(\theta). \quad (7)$$

If the ansatz  $U(\cdot)$  is sufficiently expressive, then  $C(\theta_*)$  provides a good estimate of the lowest eigenvalue of  $H$ . The expressivity of a PQC refers to its ability to explore  $\mathcal{H}_N$  in an unbiased manner [15]. Notably, expressivity is also closely linked to the barren plateau phenomenon [12, 16].

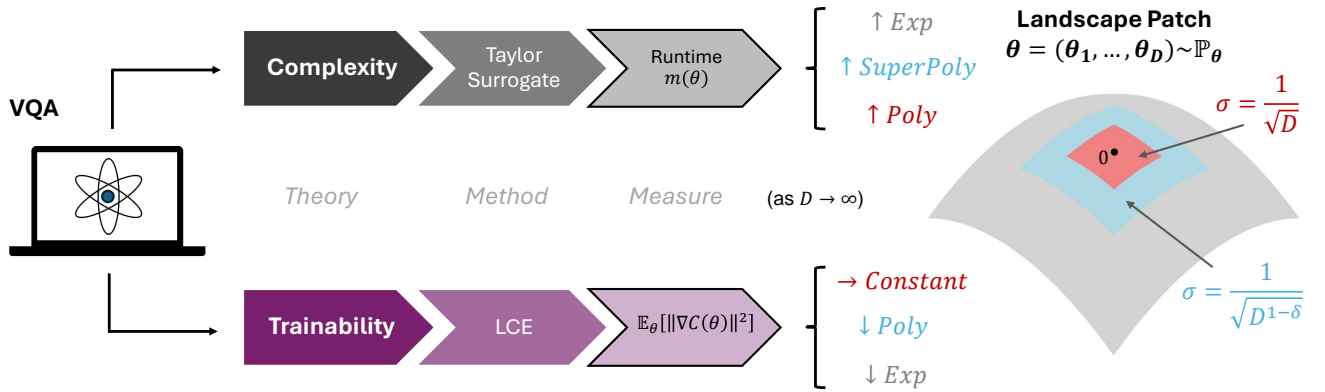


FIG. 1. Illustration of our decomposition of the theoretical link between complexity and trainability in VQAs. These two theories relate to each other with the landscape patch size  $\sigma > 0$  around  $\theta = 0$ . The Linear Clifford Encoder (LCE) and the classical Taylor surrogate reveal how gradient scalability and computational complexity interact, exposing a super-polynomially complex transition patch (blue), where for sufficiently small  $\delta > 0$ , gradients provably decay polynomially with the model size. The scaling results hold true for observables with at most  $\mathcal{O}(1)$  Pauli terms.

### C. Barren Plateaus

We typically initialize  $\theta \sim \mathbb{P}_\theta$ , and the choice of the probability distribution  $\mathbb{P}_\theta$  is crucial to avoid the barren plateau problem [12, 13, 30–32]. Barren plateaus occur whenever the expected squared gradient norm vanishes as

$$\mathbb{E}_\theta[\|\nabla_\theta C(\theta)\|^2] = \mathcal{O}(2^{-\eta N}) \quad (8)$$

for some  $\eta > 0$ , while the expected gradient satisfies  $\mathbb{E}_\theta[\nabla_\theta C(\theta)] = 0$ , making optimization intractable. Due to higher-order parameter-shift rules, the gradient is sufficient to characterize barren plateaus [33].

Here and in the following, we make use of the standard Landau notations to describe asymptotic behavior of functions. Specifically, asymptotically as  $D \rightarrow \infty$ ,  $\mathcal{O}$  denotes an upper bound,  $\Omega$  a lower bound, and  $\Theta$  a tight bound. These notations are formally introduced in Appendix J.

Various mitigation strategies [25, 34–42] provide a polynomial lower bound of the form

$$\mathbb{E}_\theta[\|\nabla_\theta C(\theta)\|^2] = \Omega(\text{Poly}(N)^{-1}). \quad (9)$$

Our contribution introduces the *Linear Clifford Encoder (LCE)* technique, which ensures constant scaling gradients on classically simulable landscape patches. In this work, we assume  $D = \Theta(\text{Poly}(N))$ , meaning that the number of parameters  $D$  scales polynomially with the number of qubits  $N$ . The polynomial is determined by the specifics of the circuit architecture, such as its layer depth.

### D. Classical Taylor Surrogate Patches

For complexity benchmarking, we consider a *classical surrogate* of a quantum learning model [22] that classically reproduces its input-output relations, with high accuracy, efficiency and low probability of failure. Following ideas from Pauli path methods [18, 24], small-angle techniques [31, 32], and quadratic Clifford expansion [19], we approximate  $C(\theta)$  using a truncated Taylor expansion of arbitrary order  $m - 1$  around  $\theta = 0$ :

$$C(\theta) \approx \sum_{\|\alpha\|_1 < m} (D_\theta^\alpha C)(0) \frac{\theta^\alpha}{\alpha!} =: C_m(\theta), \quad (10)$$

where for each multi-index  $\alpha = (\alpha_1, \dots, \alpha_D)$  we use the notations  $D_\theta^\alpha := \partial_{\theta_1}^{\alpha_1} \dots \partial_{\theta_D}^{\alpha_D}$ ,  $\theta^\alpha := \theta_1^{\alpha_1} \dots \theta_D^{\alpha_D}$ ,  $\alpha! := \alpha_1! \dots \alpha_D!$ , and  $\|\alpha\|_1 := |\alpha_1| + \dots + |\alpha_D|$  denoting the  $\ell_1$ -norm of  $\alpha$ .

As we will show below, the Taylor coefficients  $(D_\theta^\alpha C)(0)$  can be classically simulated by combining higher-order parameter-shift rules [33, 43, 44] and the Gottesman-Knill theorem [20, 21], with a complexity of at most  $\mathcal{O}(|\mathcal{I}| D^{\|\alpha\|_1})$ . Thus,  $C_m(\theta)$  serves as an efficient polynomial surrogate of  $C(\theta)$  for near-Clifford patches, where parameters are initialized as

$$\mathbb{P}_\theta \in \{\mathcal{N}(0, \sigma^2 I_D), \text{Unif}([- \sigma, \sigma]^D)\}, \quad (11)$$

with  $\sigma > 0$  determining the patch size.

While small patches limit PQC expressivity (since a Clifford ensemble covers only a discrete subset of  $\mathcal{H}_N$ ), increasing non-Clifford resources eventually render classical simulation intractable [17, 23]. Our framework aims to maximize the landscape patch size while maintaining both trainability and classical intractability. An illustration of our approach is summarized in Fig. 1.

### III. THEORETICAL RESULTS

This section presents the main theoretical contributions of our work. The central idea is to employ the Gottesman-Knill theorem [20, 21] to classically simulate the Taylor coefficients of our Taylor surrogate. These can be used to systematically adapt the Clifford structure of the PQC, ensuring constant gradient norms within the surrogate patch. This technique, termed *Linear Clifford Encoder (LCE)*, can be implemented efficiently using classical resources for large-scale PQCs.

After establishing the LCE transformation, we present complexity-theoretical insights showing that our Taylor surrogate simulation technique can also be leveraged to measure the circuit computational complexity as a function of the initialization strategy. We further identify a critical patch size where runtime complexity transitions from polynomial to super-polynomial, indicating a phase transition in computational complexity. Combined with the LCE theory, these results are used to prove the existence of super-polynomially complex landscape patches where gradient norms still decay only polynomially (cf. Sec. IV).

#### A. Backpropagation of High-Order Clifford structures in the Heisenberg Picture

We begin by outlining the core technical contribution and intuition behind our method. Since our proposed Taylor surrogate expands around Clifford circuits (recalling from Eq. (4) that  $U(0)$  is Clifford), we introduce the notion of *Clifford structures*—specific sets of Clifford operators that arise from the evaluation of the Taylor coefficients  $(D_\theta^\alpha C)(0)$ . These structures generate, via Heisenberg backpropagation [45], a set of efficiently computable Pauli strings and can be used to classically benchmark [20, 21] optimization landscape patches prior to the deployment of the corresponding quantum algorithm on quantum processors.

As shown in Appendix E, the Taylor coefficients take the explicit parameter-shift [33, 43, 44] form:

$$(D_\theta^\alpha C)(0) = \frac{1}{2^{\|\alpha\|_1}} \sum_{j \leq \alpha} (-1)^{\|j\|_1} \binom{\alpha}{j} C(\xi_{j,\alpha}), \quad (12)$$

where  $\xi_{j,\alpha} := \frac{\pi}{2}(\alpha - 2j)$  for fixed multi-indices  $\alpha \in \mathbb{N}_0^D$ , and  $0 \leq j \leq \alpha$ .

For each shift  $j \leq \alpha$ , we establish in Appendix J that evaluating the PQC in Eq. (4) at  $\xi_{j,\alpha}$  results in a Clifford operator  $U(\xi_{j,\alpha})$ , enabling Gottesman-Knill-based simulation [20, 21]. This leads to an algorithm evaluating Eq. (12) in polynomial time  $\mathcal{O}(|\mathcal{I}| D^{\|\alpha\|_1})$ , motivating the following:

**Definition 1** (High-Order Clifford Structures). *For a variational ansatz  $U(\theta)$  composed of Clifford gates and single-qubit Pauli rotations with  $D \geq 1$  parameters, the Clifford structure up to order  $m - 1$  is the set*

$$\{U(\xi_{j,\alpha}) : j \leq \alpha, \|\alpha\|_1 < m\}, \quad (13)$$

where  $\xi_{j,\alpha} := \frac{\pi}{2}(\alpha - 2j)$  and each  $U(\xi_{j,\alpha})$  is a Clifford unitary transformation.

Since we expand around  $\theta = 0$ ,  $U(0)$  always belongs to the Clifford structure. For instance, the linear Clifford structure derived from the standard parameter-shift rule [43, 44] consists of  $\{U(0), U(\pm\pi/2)\}$ , which is used to build the LCE in the next section.

Due to the transitive action of the Clifford group on  $\mathcal{P}_N$ , we obtain for each  $j \leq \alpha$ :

$$\begin{aligned} C(\xi_{j,\alpha}) &= \sum_{i \in \mathcal{I}} c_i \langle 0 | U(\xi_{j,\alpha})^\dagger P_i U(\xi_{j,\alpha}) | 0 \rangle \\ &= \sum_{i \in \mathcal{I}} c_i \langle 0 | P_i^{j,\alpha} | 0 \rangle, \end{aligned} \quad (14)$$

where  $P_i^{j,\alpha} := U(\xi_{j,\alpha})^\dagger P_i U(\xi_{j,\alpha}) \in \mathcal{P}_N \setminus \{I\}$  defines a list of Heisenberg-evolved Pauli strings. These evolved strings are efficiently computable via the Aaronson-Gottesman check matrix algorithm [21], producing Pauli strings [27] indexed by  $i \in \mathcal{I}$  (cf. Eq. (5)).

Fig. 2a depicts three views of the  $\alpha$ -order Clifford structure. The leftmost picture shows an equidistant grid of points  $\xi_{j,\alpha} = \frac{\pi}{2}(\alpha - 2j)$  in parameter space. The central one shows Clifford circuits  $U(\xi_{j,\alpha})$  evaluated at each grid point. Finally, the rightmost one shows the Heisenberg-evolved list of Pauli strings  $P_i^{j,\alpha}$ , classically encoding the  $\alpha$ -order Clifford structure.

To analyze the influence of  $U(\cdot)$  on the optimization landscape, we combine Eqs. (12) and (14):

$$\begin{aligned} (D_\theta^\alpha C)(0) &= \frac{1}{2^{\|\alpha\|_1}} \sum_{j \leq \alpha} (-1)^{\|j\|_1} \binom{\alpha}{j} C(\xi_{j,\alpha}) \\ &= \frac{1}{2^{\|\alpha\|_1}} \sum_{j \leq \alpha} (-1)^{\|j\|_1} \binom{\alpha}{j} \sum_{i \in \mathcal{I}} c_i \langle 0 | P_i^{j,\alpha} | 0 \rangle. \end{aligned} \quad (15)$$

Thus, each Taylor coefficient depends on Pauli coefficients  $\{c_i\}$ , and Heisenberg-evolved Pauli strings  $P_i^{j,\alpha}$  generated by the Clifford structure. Together with prefactors  $(-1)^{\|j\|_1} \binom{\alpha}{j}$ , manipulating the set of Pauli strings

$$\{P_i^{j,\alpha} : j \leq \alpha, \|\alpha\|_1 < m, i \in \mathcal{I}\}, \quad (16)$$

e.g. by adding or removing Clifford gates in  $U(\cdot)$ , allows one to influence summation cancellations and contributions in Eq. (15), for example to ensure a non-zero gradient component  $(\partial_{\theta_k} C)(0) \neq 0$ . Since Eq. (12) can

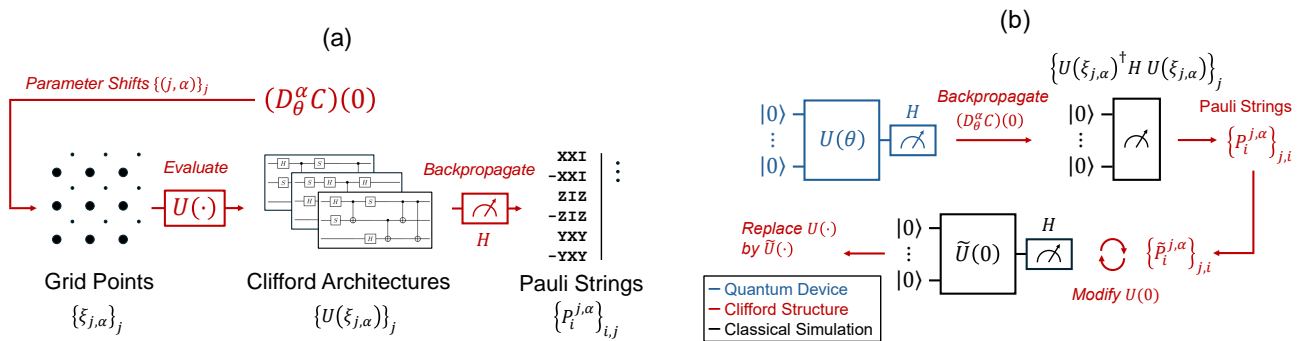


FIG. 2. (a) Three possible interpretations of the  $\alpha$ -order Clifford structure. (b) Classical framework for engineering Clifford structures.

be evaluated using Gottesman-Knill [20, 21], this establishes an efficient classical framework for engineering the Clifford architecture of  $U(\cdot)$  in order to achieve better gradients at  $\theta = 0$ .

Fig. 2b illustrates this framework: each Taylor coefficient  $(D_\theta^\alpha C)(0)$  induces an  $\alpha$ -order Clifford structure that backpropagates through the observable [45], producing a list of Pauli strings  $\{P_i^{j,\alpha}\}_{i,j}$  which encode the  $\alpha$ -order contribution to the surrogate patch.

## B. The Linear Clifford Encoder (LCE)

Having introduced the mathematical framework, this prompts a central question: can we systematically engineer the Clifford architecture of  $U(\cdot)$  to enhance landscape properties (e.g. trainability) without sacrificing expressivity? In the following, we demonstrate that this is, in principle, achievable. We now propose a novel technique that leverages the use of first-order Clifford structures (cf. Definition 1) to ensure trainability on near-Clifford patches. Proofs are deferred to Appendix F.

The previously discussed Taylor surrogation framework allows the explicit construction of a pair of Clifford operators  $(Q, \tilde{Q})$  defining the transformation  $\tilde{U}(\cdot) := \tilde{Q}U(\cdot)Q$  and yielding a *LCE transformed cost*  $\tilde{C}(\cdot)$ , where LCE stands for *Linear Clifford Encoder*. As a matter of fact, these operators are used to explicitly control one linear Taylor coefficient  $(\partial_{\theta_k} C)(0)$  (i.e.  $\alpha = e_k$  for some unit vector  $e_k$ ). Hence, given an arbitrary  $k \in [D]$ , our first main result shows how to use the first-order Clifford structure to transform any cost  $C(\cdot) \mapsto \tilde{C}(\cdot)$  such that the gradient component satisfies  $(\partial_{\theta_k} \tilde{C})(0) = \Omega(1)$ , independently from  $D$  or  $N$ .

The following theorem employs LCE to control the summation in Eq. (15) and isolate a fixed coefficient  $c_{i_0}$  of the observable  $H$ . Observe that the operators  $(Q, \tilde{Q})$  depend on the choice of  $k$  and  $i_0$ .

**Theorem 1.** Consider an arbitrary observable  $H$  indexed by  $\mathcal{I}$  in Eq. (5). Then, for every  $k \in [D]$  and  $i_0 \in \mathcal{I}$ , there exists a pair of Clifford operators  $(Q, \tilde{Q})$  such that the gradient component  $(\partial_{\theta_k} \tilde{C})(0)$  is equal to

$$\beta_{i_0}(H) := \pm c_{i_0} + \frac{1}{2} \sum_{i \in \mathcal{I} \setminus \{i_0\}} c_i \{ \langle 0 | \tilde{P}_i^{0, e_k} | 0 \rangle - \langle 0 | \tilde{P}_i^{e_k, e_k} | 0 \rangle \},$$

defining  $\tilde{P}_i^{j,\alpha} := Q^\dagger U(\xi_{j,\alpha})^\dagger \tilde{Q}^\dagger P_i \tilde{Q} U(\xi_{j,\alpha}) Q$  and  $\xi_{j,\alpha} := \frac{\pi}{2}(\alpha - 2j)$  for  $0 \leq j \leq \alpha$ .

The operators  $(Q, \tilde{Q})$  may be used to ensure constant-scaling gradients at the origin as shown below. Note that the choice of the coefficient  $c_{i_0}$  is independent of  $k$ , thus allowing a total of  $k|\mathcal{I}|$  candidates for the LCE construction. The proof of the theorem shows how to construct  $(Q, \tilde{Q})$  explicitly using only few Clifford gates (also see Fig. 8 in Appendix C). The gradient is evaluated by differentiating expectations of transformed Pauli strings, efficiently computable using the stabilizer formalism as shown in Appendix B. Furthermore, multiple gradient components may simultaneously benefit from the LCE, as discussed in Appendix F.

Notably, it is possible to explicitly construct the LCE such that  $\beta_{i_0}(H) = 1$  if  $H = P$  is a single Pauli string (cf. Theorem 7 in Appendix F). For general observables  $H$ , understanding the scaling behavior of  $\beta_{i_0}(H)$  is more subtle due to potential cancellations among the Pauli terms. The lemma below shows that the probability of complete cancellation, that is  $\beta_{i_0}(H) = 0$ , decreases exponentially with the number of qubits  $N$ :

**Lemma 1.** Let  $H = \sum_{i \in \mathcal{I}} c_i P_i$  be a random observable with  $P_i \stackrel{i.i.d.}{\sim} \text{Unif}(\mathcal{P}_N \setminus \{I\})$ . Then, for each  $i_0 \in \mathcal{I}$ , we have the conditional probability that

$$\mathbb{P}(\beta_{i_0}(H)^2 = c_{i_0}^2 \mid P_{i_0}) \geq 1 - \mathcal{O}(|\mathcal{I}| 2^{-N}),$$

as  $N \rightarrow \infty$ .

Intuitively, LCE is applied to isolate the Pauli coefficient  $c_{i_0}$ , while the remaining terms in  $\beta_{i_0}(H)$  decay exponentially in  $N$ . We condition the probability on  $P_{i_0}$  since this Pauli string is fixed for the LCE construction as shown in the proof of Theorem 1. If  $c_{i_0} = \Omega(1)$ , then this almost surely guarantees a constant gradient lower bound, as long as  $|\mathcal{I}| = \mathcal{O}(\text{Poly}(N))$ . Numerical experiments in Sec. V (cf. Fig. 5) and Appendix K demonstrate that the probability of complete cancellation is indeed negligible, and the expected behavior closely matches the case  $H = P$  where  $\beta_{i_0}(H) = 1$  if we additionally assume i.i.d. coefficients  $c_i \sim \text{Unif}([-1, 1])$ .

### C. Escaping Barren Plateaus with the Linear Clifford Encoder (LCE)

Combined with the Taylor surrogate in Eq. (10), Theorem 1 provides a constant lower bound in Eq. (9) for arbitrary Pauli decompositions  $H$  with at least one constant scaling coefficient as per Eq. (5):

**Theorem 2.** *Let  $H$  be an arbitrary, uniformly randomly sampled observable as in Eq. (5) with Pauli terms indexed by  $\mathcal{I}$ . Let  $\delta > 0$  and initialize  $\theta \sim \mathbb{P}_\theta \in \{\mathcal{N}(0, \sigma^2 I_D), \text{Unif}([- \sigma, \sigma]^D)\}$  with i.i.d. components and  $\sigma = \mathcal{O}(\|H\|^{-1} D^{-\frac{1+\delta}{2}})$ . Then, for each  $k \in [D]$  and  $i_0 \in \mathcal{I}$  with  $c_{i_0} = \Omega(1)$ , there exists a pair of Clifford operators  $(Q, \tilde{Q})$  such that, with probability at least  $1 - \mathcal{O}(|\mathcal{I}| 2^{-N})$  (conditioned on  $P_{i_0}$ ), as  $D \rightarrow \infty$ ,*

$$\mathbb{E}_{\theta \sim \mathbb{P}_\theta} [(\partial_{\theta_k} \tilde{C}(\theta))^2] \geq \Omega(1) + \mathcal{O}(D^{-\delta}),$$

where  $\tilde{C}(\cdot)$  denotes the LCE transformed cost.

Theorem 2 shows how to apply LCE (cf. Theorem 1) in order to achieve a constant lower bound on the expected gradient square norm. This is achieved by initializing the parameters on a sufficiently small patch, with a size  $\sigma$  that depends on the number of parameters  $D$  and the operator norm  $\|H\|$  of the observable. In the case where  $\|H\| = \mathcal{O}(1)$ , the effective patch size  $\sigma$  for escaping barren plateaus thus scales as  $\mathcal{O}(D^{-1/2})$ , which is consistent with the findings of Puig et al. [46]. Otherwise, if  $\|H\|$  depends on  $D$  (or  $N$ ), then  $\sigma$  also scales with  $\|H\|^{-1}$  as shown in Theorem 2. Additionally, since we require that  $c_{i_0} = \Omega(1)$  for some Pauli term  $i_0 \in \mathcal{I}$ , the condition  $\|H\| = \mathcal{O}(1)$  limits the possible candidates for  $H$ . Recalling from Eq. (5) that  $c_i = \mathcal{O}(1)$  for all  $i \in \mathcal{I}$ , by the triangle inequality,

$$\|H\| \leq \sum_{i \in \mathcal{I}} |c_i| \underbrace{\|P_i\|}_{=1} \leq |\mathcal{I}| \max_{i \in \mathcal{I}} |c_i| = \mathcal{O}(|\mathcal{I}|). \quad (17)$$

Hence, if we additionally assume  $\|H\| = \mathcal{O}(1)$ , then it is necessary that  $|\mathcal{I}| = \mathcal{O}(1)$ . As a result, LCE establishes constant lower gradient bounds within  $\mathcal{O}(D^{-\frac{1}{2}})$  patches only when considering observables satisfying  $|\mathcal{I}| = \mathcal{O}(1)$ .

A summary that compares various barren-plateau mitigation methods on small landscape regions with LCE is provided in Table I in Appendix A.

It is also worth recalling that the total number of possible LCE candidates equals to  $k|\mathcal{I}|$  if  $c_i = \Omega(1)$  for all  $i \in \mathcal{I}$ ; one for each direction  $k \in [D]$ , and Pauli term  $i \in \mathcal{I}$ , respectively. This additional degree of freedom increases the likelihood of finding an optimal minimum  $\theta_*$  by employing various LCE constructions at initialization.

Since the location of the solution  $\theta_*$  is a priori unknown, a reasonable initialization strategy is to randomly sample  $k \in [D]$  and  $i \in \mathcal{I}$ , ensuring a random descent momentum in the  $k$ -th direction. Importantly, however, while a random walk lacks directional guidance, LCE uses structured gradient information to drive efficient optimization from the start. In fact, note that for any given  $k$ , LCE reshapes the loss landscape itself so that the gradient at initialization captures a stronger, more informative signal, effectively steepening the landscape along that direction. This effect of LCE on the loss landscape is visually demonstrated in Appendix F.

Crucially, we must ensure that the LCE transformation  $C(\cdot) \mapsto \tilde{C}(\cdot)$  does not compromise expressivity of the PQC and does not significantly change the value of the minimum  $\tilde{C}(\theta_*)$  (while the minimizer in Eq. (7) may change). Heuristically, this is plausible: the operator  $Q$  merely changes the initial stabilizer state  $|0\rangle \mapsto |\psi_0\rangle = Q|0\rangle$ , corresponding to a landscape translation, while  $\tilde{Q}^\dagger H \tilde{Q}$  constitutes a basis change. More formally, we prove in Appendix H that both expressivity and global optimality are preserved under LCE transformations via a geometric notion of  $\varepsilon$ -state-expressivity. This implies that the LCE transformed PQC ansatz is able to explore the same regions as the original Hilbert space  $\{|\psi(\theta)\rangle : \theta \in [-\pi, \pi]^D\}$ , even though the optimal point  $\theta_*$  might be different.

While LCE preserves the global minima, the risk of getting trapped in local minima remains. In such cases, Quantum Optimal Control (QOC) [47] and the theory of overparameterization [48] may help transform local minima into global ones [49]. We leave the study of this topic to future work.

Having introduced the LCE technique, which allows us to circumvent barren plateaus on  $\mathcal{O}(D^{-1/2})$ -sized surrogate patches, we now ask whether larger patch sizes are achievable. The next section explores how computational complexity scales with increasing parameter norms  $\|\theta\|_1$ , providing a measure of non-Cliffordness, relating patch sizes to classical simulability, and revealing a phase transition in computational complexity.

## D. Phase Transitions in Computational Complexity

Let us now consider again the task of approximating a target PQC with the Taylor surrogate  $C_m(\theta)$  from Eq. (10), with truncation threshold  $m = m(\theta)$ . The truncation threshold directly determines its computational complexity, as  $m$  directly determines the number of terms in the summation in Eq. (10) (cf. Lemma 10 in Appendix I). We analyze the minimal threshold required to satisfy a surrogate error tolerance via two approaches:

1. *Worst-case error analysis:*  $m = m(\theta)$  is deterministic for a fixed configuration  $\theta \in [-\pi, \pi]^D$ ;
2. *Mean-squared error analysis:*  $m = m(\mathbb{P}_\theta)$  is probabilistic, depending on an initialization strategy  $\mathbb{P}_\theta$ .

This separation, previously explored by Lerch et al. [18], reveals distinct trade-offs in simulability and trainability. We show in Appendix I that the worst-case analysis characterizes computational complexity for arbitrary patch sizes, while mean-squared error is limited to  $\mathcal{O}(D^{-1/2})$ -sized patches. Notably, this threshold marks the boundary between polynomial and super-polynomial regimes (cf. Appendix J) and identifies the largest patch where barren plateaus can be provably mitigated [46] (cf. Theorem 2).

### 1. Worst-Case Error Analysis

In Appendix I we show the worst-case error obeys

$$|C(\theta) - C_m(\theta)| \leq \frac{\|H\|}{m!} \|\theta\|_1^m. \quad (18)$$

Thus, for any fixed  $\theta \in [-\pi, \pi]^D$ , one can determine the minimal  $m = m(\theta)$  needed to satisfy the error bound in Eq. (18) as a function of  $\|\theta\|_1$ , which in this context serves as a way to measure the level of non-Cliffordness of the configuration. This leads to the following  $\ell_1$ -characterization of a super-polynomial computational phase transition (cf. Appendix J):

**Theorem 3.** *If  $\|\theta\|_1 = \mathcal{O}(1)$ , the runtime of evaluating  $C_m(\theta)$  is polynomial, namely  $\mathcal{O}(|\mathcal{I}|D^m)$ . If  $\|\theta\|_1 \rightarrow \infty$  as  $D \rightarrow \infty$ , the runtime becomes super-polynomial:*

$$\mathcal{O}\left(\text{Poly}(D) \exp\left[e\|\theta\|_1 \left(1 + \log\left(2 + \frac{2D}{e\|\theta\|_1}\right)\right)\right]\right),$$

*saturating to exponential scaling  $\mathcal{O}(|\mathcal{I}|D2^{2D})$  if and only if  $\|\theta\|_1 = \Theta(D)$ .*

Appendix D 4 (cf. Fig. 10) demonstrates how to compare the polynomial complexity across various PQC models, and how to identify computational overheads.

For  $\theta \sim \mathbb{P}_\theta \in \{\mathcal{N}(0, \sigma^2 I_D), \text{Unif}([-\sigma, \sigma]^D)\}$  with i.i.d. components and  $\sigma = D^{-r}$  for  $r \in [0, 1)$ , the law of large numbers yields

$$\mathbb{E}_\theta[m(\theta)] = \Theta(D^{1-r}) \quad (19)$$

as  $D \rightarrow \infty$ .

Thus, the Taylor surrogate captures computational complexity across all patch sizes  $\mathcal{O}(D^{-r})$  parametrized by  $r \geq 0$ . Combining the lower bound  $m(\theta) = \Omega(\|\theta\|_1)$  as  $D \rightarrow \infty$  (cf. Lemma 9 in Appendix I) with Theorem 3 thus reveals a *phase transition in computational complexity* at  $r = 1$ , separating polynomial from super-polynomial regimes. As  $r \rightarrow 0$ , the runtime saturates to exponential scaling.

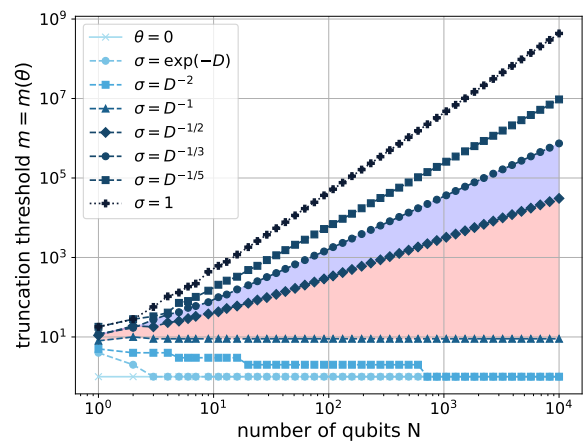


FIG. 3. Worst-case analysis truncation threshold  $m = m(\theta)$  of a model with  $D = 2N(N + 1)$  parameters, as predicted by the expected truncation threshold in Eq. (19). Here, we set  $\|H\| = 1$  and  $\varepsilon = 10^{-6}$ . The red region is easy to simulate classically (cf. Theorem 4), while the blue region is not (cf. Theorem 3).

### 2. Mean-Squared Error Analysis

For  $\theta \sim \mathbb{P}_\theta \in \{\mathcal{N}(0, \sigma^2 I_D), \text{Unif}([-\sigma, \sigma]^D)\}$  with i.i.d. components, the mean-squared error satisfies

$$\mathbb{E}_\theta[(C(\theta) - C_m(\theta))^2] \leq c \|H\|^2 D^m \sigma^{2m}, \quad (20)$$

for some  $c > 0$  (cf. Appendix I). This implies  $\sigma$  cannot exceed  $\Omega(D^{-1/2})$  without incurring significant error. Thus, mean-squared analysis fails beyond  $\mathcal{O}(D^{-1/2})$ -patches, while worst-case analysis remains valid across the full parameter space.

Fig. 3 illustrates the scaling of  $m(\theta)$  when simulating a model with  $D = 2N(N + 1)$  parameters, such as the linear-depth mHEA (minimalistic Hardware Efficient Ansatz [50, 51]) defined in Appendix C, with patch sizes  $\mathcal{O}(\sigma)$  under various distributions  $\mathbb{P}_\theta$ . The red-shaded region corresponds to the regime where barren plateaus are provably avoided (cf. Theorem 2). The blue-shaded region marks the regime requiring super-polynomial computational resources. As further shown in Theorem 4, the mean-squared error analysis collapses the red-shaded region to constant scaling  $m(\mathbb{P}_\theta) = \mathcal{O}(1)$ , implying classical simulability of  $\mathcal{O}(D^{-1/2})$ -patches—consistent with the findings of Lerch et al. [18].

To ensure a small mean-squared error, we analyze two initialization strategies:

- (i) *Asymptotic Local Initialization:*  
For  $\sigma = \mathcal{O}(\|H\|^{-1/m} D^{-(1+\delta)/2})$  with  $\delta > 0$ , the error decays as  $\mathcal{O}(D^{-\delta m})$ .
- (ii) *Non-Asymptotic Local Initialization:*  
For  $\sigma = q \|H\|^{-1/m} D^{-1/2}$  with  $0 < q < 1$ , the error decays as  $\mathcal{O}(q^{2m})$ .

The first mitigates the problem of barren plateaus; the second facilitates runtime comparison with state-of-the-art methods. Both yield polynomial-time surrogates:

**Theorem 4.** *Let  $\theta \sim \mathbb{P}_\theta \in \{\mathcal{N}(0, \sigma^2 I_D), \text{Unif}([- \sigma, \sigma]^D)\}$  with i.i.d. components, according to Eq. (20) with constant  $c > 0$ . Then, with probability at least  $1 - \rho$ , the computational cost of simulating  $C(\theta)$  via  $C_m(\theta)$  up to an error  $\varepsilon > 0$ , is of polynomial order,*

$$\mathcal{O}\left(|\mathcal{I}| D^{\frac{1}{\delta \log D} \log\left(\frac{c}{\rho \varepsilon^2}\right)}\right)$$

for asymptotic local initialization, i.e.

$\sigma = \mathcal{O}(\|H\|^{-\frac{1}{m}} D^{-\frac{1+\delta}{2}})$  for some  $\delta > 0$ , and

$$\mathcal{O}\left(|\mathcal{I}| D^{\frac{1}{2 \log\left(\frac{1}{q}\right)} \log\left(\frac{c}{\rho \varepsilon^2}\right)}\right)$$

for non-asymptotic local initialization, i.e.

$\sigma = q \|H\|^{-\frac{1}{m}} D^{-\frac{1}{2}}$  for some  $0 < q < 1$ , respectively.

For  $\|H\| = \mathcal{O}(1)$ , Theorem 4 aligns with the main results of Lerch et al. [18], who study a classical surrogate based on the Pauli path formalism [24]. As shown in Appendix J (cf. Corollary 3), our Taylor surrogate outperforms such a method on sufficiently small surrogate patches (i.e.  $0.35 < q < 1$ ) under non-asymptotic local initialization. A visual comparison of the two surrogate complexities is shown in Fig. 4. While Lerch et al. characterize complexity only at  $r \in \{0, \frac{1}{2}, 1\}$  for  $\theta \sim \text{Unif}([- \sigma, \sigma]^D)$  with  $\sigma = \mathcal{O}(D^{-r})$ , our analysis extends to the entire spectrum  $r \geq 0$  via Eq. (19).

Table II in Appendix A compares our complexity results with the Pauli path surrogate [18] of small landscape patches.

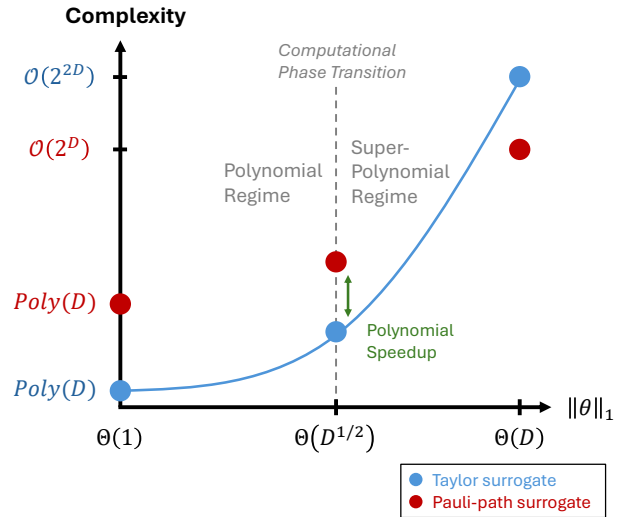


FIG. 4. Comparing the computational complexity of the Taylor surrogate and the Pauli path surrogate of Lerch et al. [18] as a function of the measure  $\|\theta\|_1$  of non-Cliffordness. Furthermore, Ref. [18] does not contain a complexity result as a continuous function of  $\|\theta\|_1$ .

#### IV. ABSENCE OF BARREN PLATEAUS BEYOND SMALL PATCHES

Finally, we now turn to an analytical investigation of super-polynomially complex patches, namely those regions where opportunities for quantum advantage exist. Here, by applying the LCE technique alongside principles from Lebesgue measure theory, we demonstrate that barren plateaus can in principle be avoided beyond the critical  $\sigma = \mathcal{O}(D^{-1/2})$  patch, namely for a class of models for which no classical surrogate is currently known [18]. This result holds with high probability, for any uniformly sampled observable  $H$  of the form given in Eq. (5), indexed by  $\mathcal{I}$ , that satisfies  $|\mathcal{I}| = \mathcal{O}(1)$ . The proof of the following theorem is deferred to Appendix G.

**Theorem 5.** *Let  $H$  be an arbitrary, uniformly randomly sampled observable as in Eq. (5) with Pauli terms indexed by  $\mathcal{I}$ . Let  $r > 0$  and initialize the parameters  $\theta \stackrel{i.i.d.}{\sim} \mathbb{P}_{-\frac{r}{D}} := \text{Unif}([- \sigma, \sigma]^D)$  with  $\sigma = \|H\|^{-1} D^{-\frac{1-r/D}{2}}$ . Then, for each  $k \in [D]$  and  $i \in \mathcal{I}$  with  $c_i = \Omega(1)$ , there exists a pair of Clifford operators  $(Q, \tilde{Q})$  such that, with probability at least  $1 - \mathcal{O}(|\mathcal{I}| 2^{-N})$  (conditioned on  $P_i$ ), as  $D \rightarrow \infty$ ,*

$$\mathbb{E}_{\theta \sim \mathbb{P}_{-\frac{r}{D}}} [(\partial_{\theta_k} \tilde{C}(\theta))^2] \geq D^{-r} (\Omega(1) + \mathcal{O}(D^{-\frac{r}{D}})),$$

where  $\tilde{C}(\cdot)$  is the LCE transformed cost.

Therefore, under the assumption that no classical surrogate exists beyond the patch  $\mathcal{O}(D^{-1/2})$ , Theorem 5 suggests that super-polynomial quantum advantage [26] might co-exist with barren-plateau-free optimization landscapes. Although we extend only slightly

beyond the critical patch, our earlier deterministic complexity findings (cf. Theorem 3) indicate that classically simulating the larger patch  $\sigma = \mathcal{O}(D^{-(1-\delta)/2})$  requires at least super-polynomial resources for all  $\delta$ . On the other hand, Theorem 5 establishes trainability on the same patch as long as  $\|H\| = \mathcal{O}(1)$  and  $c_i = \Omega(1)$  for some  $i \in \mathcal{I}$  are simultaneously satisfied. As discussed in Sec. III C, these two conditions hold true for all observables  $H$  of the form in Eq. (5) satisfying  $|\mathcal{I}| = \mathcal{O}(1)$ .

## V. NUMERICAL EXPERIMENTS

We now present numerical experiments supporting our theoretical results. First, we benchmark the trainability of LCE transformed PQCs using the Taylor surrogate to confirm that proper Clifford design yields constant-scaling gradients (cf. Theorems 2 and 5). We then apply these insights to VQE optimization, leveraging improved gradients on near-Clifford patches.

### A. Initial Gradient Scalability

We evaluate the scaling of the gradient norm  $\|(\nabla_\theta C)(0)\|$  for increasing qubit numbers  $N$  focusing on the mHEA [50] model—a minimalistic Hardware-Efficient Ansatz based on Qiskit’s EfficientSU2 [51], comprising  $Y/Z$ -rotations and circular entanglement. Appendix C shows additional PQC models with their respective LCE modifications. Note that Theorem 2 applies in general even to deep PQCs.

Fig. 5 compares initial gradient norms at  $\theta = 0$  with and without LCE, employing mHEA with linear circuit depth  $L = N$ . Gradients are computed analytically via Eq. (15). Each run uses a randomly sampled observable  $H$ , and a random LCE construction. Panel (a) of Fig. 5 focus on uniformly random single Pauli strings  $H = P$ . Without LCE, constructive contributions in Eq. (15) vanish with increasing  $N$ , leading to zero expected gradient for sufficiently large  $N$ . With LCE, gradient norms remain constant in  $N$ . Panels (b) and (c) of Fig. 5 extend results to random observables with  $|\mathcal{I}| = \lfloor \sqrt{N} \rfloor$  Pauli terms. For observables with uniformly sampled Pauli strings  $P_i$  and  $c_i = 1$  for all  $i \in \mathcal{I}$  (called random unweighted  $H$ ), the scaling compares to the single-Pauli case. For observables with uniformly sampled Pauli strings  $P_i$  and i.i.d.  $c_i \sim \text{Unif}([-1, 1])$  for all  $i \in \mathcal{I}$  (called random weighted  $H$ ), gradient norms tend to behave more randomly due to random Pauli coefficients. This is evidence that the LCE transformation remains effective for arbitrary observables.

As previously mentioned, evaluation at  $\theta = 0$  is classically efficient by Gottesman-Knill [20, 21], allowing simulation even for large  $N$ . Specifically, evaluating the

gradient norm  $\|(\nabla_\theta C)(0)\|$  takes  $\mathcal{O}(|\mathcal{I}|D^2)$  operations: the vanilla parameter-shift rule [43, 44] requires  $\mathcal{O}(|\mathcal{I}|D)$  operations to evaluate  $(\partial_{\theta_k} C)(0)$  (cf. Lemma 3 in Appendix E), of which there are exactly  $D$  distinct gradient components  $k \in [D]$ .

Appendix K contains gradient norm scaling experiments with up to  $N = 32$  qubits for mHEA with  $L = 1$  layer.

Fig. 6 repeats the experiment of the left panel in Fig. 5 on near-Clifford patches, varying patch sizes via Gaussian initialization  $\sigma = D^{-r}$ . Each run uses a randomly sampled parameter, a random single-Pauli string observable  $H = P$ , and a random LCE construction. The red-shaded region corresponds to classically efficient regimes (cf. Fig. 3); blue-shaded to super-polynomial regimes, where gradients still decay only polynomially. Interestingly, the LCE construction not only maintains trainability but also alters how the gradient scales as  $N \rightarrow \infty$ . This new scaling behavior closely resembles that shown in Fig. 3, suggesting a deeper link between trainability and complexity. LCE transformed norms scale predictably, while non-LCE trends are more erratic. Within the constant-scaling regime (red-shaded), LCE ensures trainability. For large  $\sigma$ , gradients decay exponentially. This confirms the existence of a transition patch (contained in the blue-shaded region) where gradients asymptotically smoothly transitions from constant to polynomially decay (cf. Eq. (9)) in alignment with Theorem 5. We refer to Appendix K for comparisons across additional hardware-efficient PQC models.

### B. Variational Quantum Eigensolvers

We now perform an ablation study on VQE optimization dynamics with LCE. Since theory applies to initialization only, we empirically test whether improved gradients translate to practical optimization benefits—especially under barren plateau-prone observables like global ones [52] such as:

$$H_{\text{global}} := Z^{\otimes N}. \quad (21)$$

Fig. 7 shows VQE optimization of  $H_{\text{global}}$  employing the mHEA ansatz ( $L = 5$ ,  $N = 15$ ) via vanilla gradient descent (update rules defined as  $\theta_{t+1} = \theta_t - \eta \nabla_\theta C(\theta_t)$  with constant learning rate  $\eta > 0$ ) over 5 runs with Gaussian initializations  $\theta \sim \mathcal{N}(0, \sigma^2 I_D)$  across varying patch sizes. The top row displays the cost minimization, highlighting faster convergence with LCE across all patch dimensions. The central row shows gradient norms, reflecting improved trainability both at initialization (cf. Theorem 2) and throughout the minimization. The bottom row tracks the parameter norm  $\|\theta_t\|_2$ , indicative of classical hardness (cf. Theorem 3) showing that indeed this increases when enlarging the patch

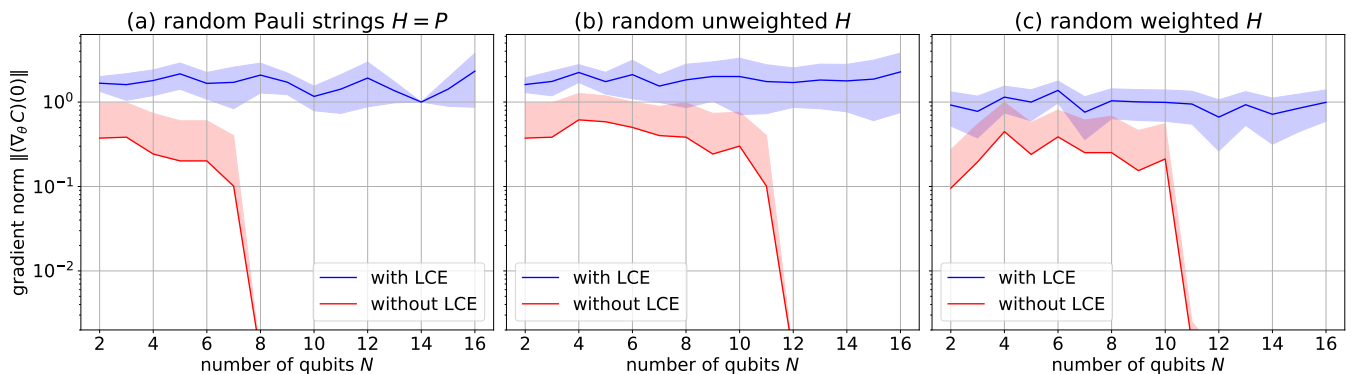


FIG. 5. Scaling behavior of the initial gradient norm at  $\theta = 0$  for the mHEA-model with  $L = N$  layers. The panels vary across types of random observables. The experiment highlights the effect of the LCE transformation. We average over 10 independent runs.

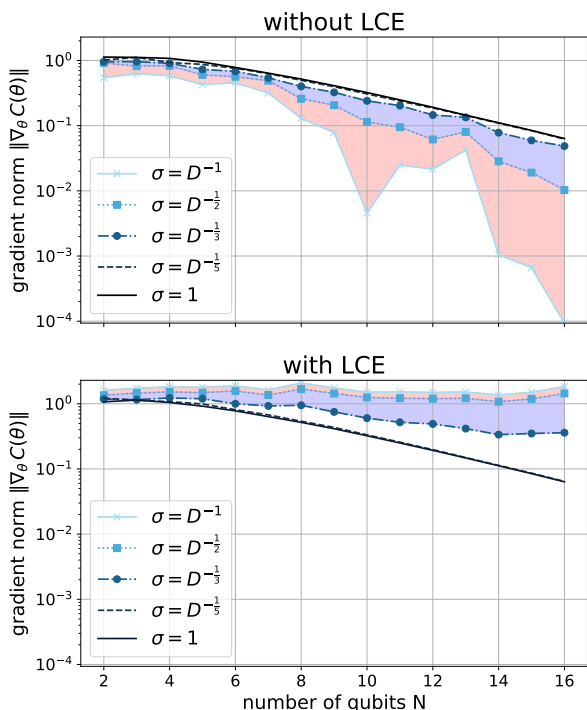


FIG. 6. Scaling behavior of the gradient norm on various landscape patches for the mHEA-model with  $L = N$  layers. We average over 50 independent runs of random  $\theta \sim \mathbb{P}_\theta$  and uniformly sampled Pauli strings  $H = P$ .

size. While our theory guarantees trainability slightly beyond  $\sigma = D^{-1/2}$  (cf. Theorem 5), numerical results continue to demonstrate successful convergence on the larger patch size  $\sigma = \mathcal{O}(D^{-1/3})$ . As the patch size  $\sigma$  increases, the gap between standard VQE and VQE with LCE gradually decreases, eventually approaching the situation where convergence rates appear to become more

similar (cf.  $\sigma = \mathcal{O}(D^{-1/5})$ ). This means that the benefits of LCE are most significant when employed on patches of moderate size. Additional experiments are compiled in Appendix K, where we show that changing learning rates leaves the effect of LCE invariant, that LCE is compatible with finite sampling noise [53], and conducting VQE experiments with the Heisenberg model [54].

## VI. CONCLUSION

In this work, we advanced the theoretical understanding of trainability and computational complexity in Variational Quantum Algorithms (VQAs) [1]. More specifically, we connected these two aspects via Taylor surrogate methods, demonstrating their effectiveness through numerical experiments.

To address trainability, we introduced the *Linear Clifford Encoder (LCE)*, a novel technique that leverages the stabilizer formalism [20, 21, 27] to modify the first-order Clifford structure of Parameterized Quantum Circuits (PQCs) [11]. This ensures constant gradient scaling within a near-Clifford landscape patch—without sacrificing expressivity or global landscape quality. Implemented efficiently as a classical algorithm, the LCE facilitates testing large-scale PQCs and alleviates barren plateaus. Numerical results confirm accelerated training dynamics in Variational Quantum Eigensolver (VQE) [2] tasks due to improved gradient statistics at initialization.

On the complexity front, we observed a computational phase transition as PQCs deviate from the Clifford regime. This threshold, characterized by the  $\ell_1$ -norm of parameters, aligns precisely with the regime where LCE ensures favorable gradient scaling, consistently with prior results [18, 46]. Importantly, our Theorem 5 goes significantly beyond the previous literature, and proves that barren-plateau-free landscape patches extend into

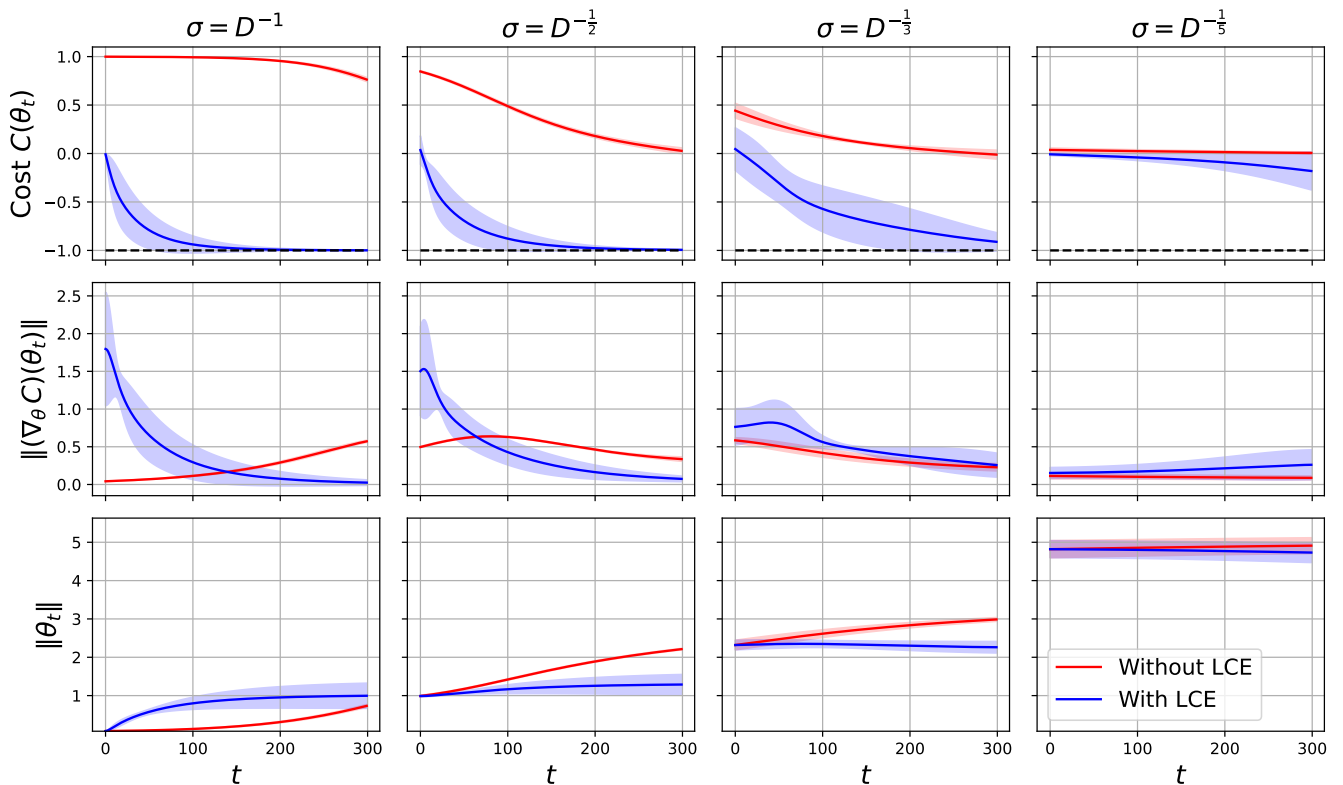


FIG. 7. VQE Optimization using vanilla gradient descent with a learning rate of 0.01, averaging over 5 runs of random Gaussian initialization across varying patch sizes. We find the ground energy of the global observable  $Z^{\otimes N}$  with  $N = 15$ , employing the mHEA ansatz with  $L = 5$  layers.

regions for which no efficient classical surrogate is currently known, thus suggesting novel opportunities for super-polynomial quantum advantage in VQAs.

Despite these promising results, several open questions remain. The LCE technique is currently incompatible with quantum machine learning (QML) tasks that rely on quantum feature maps [55], which typically disrupt to such settings—possibly by encoding data into observables [56]—may extend some of our analytical guarantees to data-driven settings. Moreover, while LCE addresses first-order structure, the role of higher-order Clifford encoders remains unexplored. Theoretical understanding of the training dynamics with LCEs, namely to the model behavior beyond initialization [48, 57–61], is also lacking. For instance, while the optimizer choice affects dynamics, it does not alter the landscape itself. Exploring this interplay with LCEs is a promising direction for future

work.

## VII. ACKNOWLEDGMENTS

We are grateful to Matthis Lehmkuhler for his valuable input on the classical simulation of PQCs via Taylor surrogates and for discussions on the phenomenon of barren plateaus. We also thank Christa Zoufal, David Sutter, Stefan Woerner, and Zoë Holmes for their constructive feedback, Jiří Černý for his insightful comments, and Enea Monzio Compagnoni and Jim Zhao for discussions on optimization. Sabri Meyer, Francesco Scala and Aurelien Lucchi acknowledge the support from SNF grant No. 214919. Francesco Tacchino acknowledges support from the Swiss National Science Foundation (grant number 225229 RESQUE).

[1] Marco Cerezo, Andrew Arrasmith, Ryan Babbush, Simon C. Benjamin, Suguru Endo, Keisuke Fujii, Jarrod R. McClean, Kosuke Mitarai, Xiao Yuan, Lukasz Cincio, and Patrick J. Coles. Variational quantum algorithms.

*Nature Reviews Physics*, 3(9):625–644, 2021.  
 [2] Alberto Peruzzo, Jarrod McClean, Peter Shadbolt, Man-Hong Yung, Xiao-Qi Zhou, Peter J. Love, Alán Aspuru-Guzik, and Jeremy L. O’Brien. A variational eigenvalue

- solver on a photonic quantum processor. *Nat. Commun.*, 5(1), 2014.
- [3] Viacheslav V. Kuzmin and Pietro Silvi. Variational quantum state preparation via quantum data buses. *Quantum*, 4:290, 2020.
- [4] Gabriel Matos, Sonika Johri, and Zlatko Papić. Quantifying the efficiency of state preparation via quantum variational eigensolvers. *PRX Quantum*, 2:010309, 2021.
- [5] Gaurav Gyawali and M. Lawler. Adaptive variational preparation of the fermi-hubbard eigenstates. *Physical Review A*, 2021.
- [6] Roland C. Farrell, Marc Illa, Anthony N. Ciavarella, and Martin J. Savage. Scalable circuits for preparing ground states on digital quantum computers: The schwinger model vacuum on 100 qubits. *PRX Quantum*, 5:020315, 2024.
- [7] Jakob S. Kottmann and Francesco Scala. Quantum algorithmic approach to multiconfigurational valence bond theory: Insights from interpretable circuit design. *Journal of Chemical Theory and Computation*, 20(9):3514–3523, 2024.
- [8] Peter Wittek. *Quantum Machine Learning*. Academic Press, Boston, 2014.
- [9] Jacob Biamonte, Peter Wittek, Nicola Pancotti, Patrick Rebentrost, Nathan Wiebe, and Seth Lloyd. Quantum machine learning. *Nature*, 549(7671):195–202, 2017.
- [10] Marco Cerezo, Guillaume Verdon, Hsin-Yuan Huang, Lukasz Cincio, and Patrick J. Coles. Challenges and opportunities in quantum machine learning. *Nature Computational Science*, 2(9):567–576, 2022.
- [11] Marcello Benedetti, Erika Lloyd, Stefan Sack, and Mattia Fiorentini. Parameterized quantum circuits as machine learning models. *@article{Abedi2023quantumlazytraining, doi = 10.22331/q-2023-04-27-989, url = https://doi.org/10.22331/q-2023-04-27-989, title = Quantum Lazy Training, author = Abedi, Erfan and Beigi, Salman and Taghavi, Leila, journal = Quantum, issn = 2521-327X, publisher = Verein zur Förderung des Open Access Publizierens in den Quantenwissenschaften, volume = 7, pages = 989, month = apr, year = 2023, 5(1):019601, 2020.*
- [12] Jarrod R. McClean, Sergio Boixo, Vadim N. Smelyanskiy, Ryan Babbush, and Hartmut Neven. Barren plateaus in quantum neural network training landscapes. *Nature communications*, 9(1):4812, 2018.
- [13] Martín Larocca, Supanut Thanasilp, Samson Wang, Kunal Sharma, Jacob Biamonte, Patrick J. Coles, Lukasz Cincio, Jarrod R. McClean, Zoë Holmes, and M. Cerezo. Barren plateaus in variational quantum computing. *Nature Reviews Physics*, 2025.
- [14] M. Cerezo, Martín Larocca, Diego García-Martín, N. L. Diaz, Paolo Braccia, Enrico Fontana, Manuel S. Rudolph, Pablo Bermejo, Aroosa Ijaz, Supanut Thanasilp, et al. Does provable absence of barren plateaus imply classical simulability? or, why we need to rethink variational quantum computing. *arXiv preprint arXiv:2312.09121*, 2023.
- [15] Sukin Sim, Peter D. Johnson, and Alán Aspuru-Guzik. Expressibility and entangling capability of parameterized quantum circuits for hybrid quantum-classical algorithms. *Advanced Quantum Technologies*, 2(12):1900070, 2019.
- [16] Zoë Holmes, Kunal Sharma, M. Cerezo, and Patrick J. Coles. Connecting ansatz expressibility to gradient magnitudes and barren plateaus. *PRX Quantum*, 3:010313, 2022.
- [17] Sergey Bravyi, Dan Browne, Pdraic Calpin, Earl Campbell, David Gosset, and Mark Howard. Simulation of quantum circuits by low-rank stabilizer decompositions. *Quantum*, 3:181, 2019.
- [18] Sacha Lerch, Ricard Puig, Manuel S. Rudolph, Armando Angrisani, Tyson Jones, M. Cerezo, Supanut Thanasilp, and Zoë Holmes. Efficient quantum-enhanced classical simulation for patches of quantum landscapes. *arXiv preprint arXiv:2411.19896*, 2024.
- [19] Kosuke Mitarai, Yasunari Suzuki, Wataru Mizukami, Yuya O Nakagawa, and Keisuke Fujii. Quadratic clifford expansion for efficient benchmarking and initialization of variational quantum algorithms. *Physical Review Research*, 4(3):033012, 2022.
- [20] Daniel Gottesman. The heisenberg representation of quantum computers. *arXiv preprint quant-ph/9807006*, 1998.
- [21] Scott Aaronson and Daniel Gottesman. Improved simulation of stabilizer circuits. *Physical Review A—Atomic, Molecular, and Optical Physics*, 70(5):052328, 2004.
- [22] Franz J. Schreiber, Jens Eisert, and Johannes Jakob Meyer. Classical surrogates for quantum learning models. *Physical Review Letters*, 131(10):100803, 2023.
- [23] Sergey Bravyi and David Gosset. Improved classical simulation of quantum circuits dominated by clifford gates. *Physical Review Letters*, 116(25):250501, 2016.
- [24] Tomislav Begušić, Kasra Hejazi, and Garnet Kin Chan. Simulating quantum circuit expectation values by clifford perturbation theory. *arXiv preprint arXiv:2306.04797*, 2023.
- [25] Chae-Yeun Park, Minhyeok Kang, and Joonsuk Huh. Hardware-efficient ansatz without barren plateaus in any depth. *arXiv preprint arXiv:2403.04844*, 2024.
- [26] Alexander M. Dalzell, Sam McArdle, Mario Berta, Przemyslaw Bienias, Chi-Fang Chen, András Gilyén, Connor T. Hann, Michael J. Kastoryano, Emil T. Khabiboulline, Aleksander Kubica, et al. Quantum algorithms: A survey of applications and end-to-end complexities. *arXiv preprint arXiv:2310.03011*, 2023.
- [27] Michael A. Nielsen and Isaac L. Chuang. *Quantum computation and quantum information*. Cambridge University Press, 2010.
- [28] Kieran Mastel. The clifford theory of the  $n$ -qubit clifford group. *arXiv preprint arXiv:2307.05810*, 2023.
- [29] Diederik P Kingma and Jimmy Ba. Adam: A method for stochastic optimization. *arXiv preprint arXiv:1412.6980*, 2014.
- [30] Edward Grant, Leonard Wossnig, Mateusz Ostaszewski, and Marcello Benedetti. An initialization strategy for addressing barren plateaus in parametrized quantum circuits. *Quantum*, 3:214, 2019.
- [31] Kaining Zhang, Liu Liu, Min-Hsiu Hsieh, and Dacheng Tao. Escaping from the barren plateau via gaussian initializations in deep variational quantum circuits. *Advances in Neural Information Processing Systems*, 35:18612–18627, 2022.
- [32] Yabo Wang, Bo Qi, Chris Ferrie, and Daoyi Dong. Trainability enhancement of parameterized quantum circuits via reduced-domain parameter initialization. *Physical Review Applied*, 22(5):054005, 2024.
- [33] Marco Cerezo and Patrick J. Coles. Higher order derivatives of quantum neural networks with barren plateaus.

- Quantum Science and Technology*, 6(3):035006, 2021.
- [34] Kaining Zhang, Min-Hsiu Hsieh, Liu Liu, and Dacheng Tao. Toward trainability of deep quantum neural networks. *arXiv preprint arXiv:2112.15002*, 2021.
- [35] Alistair Letcher, Stefan Woerner, and Christa Zoufal. Tight and Efficient Gradient Bounds for Parameterized Quantum Circuits. *Quantum*, 8:1484, 2024.
- [36] Chae-Yeun Park and Nathan Killoran. Hamiltonian variational ansatz without barren plateaus. *Quantum*, 8:1239, 2024.
- [37] Xiao Shi and Yun Shang. Avoiding barren plateaus via gaussian mixture model. *arXiv preprint arXiv:2402.13501*, 2024.
- [38] Andrea Skolik, Jarrod R. McClean, Masoud Mohseni, Patrick Van Der Smagt, and Martin Leib. Layerwise learning for quantum neural networks. *Quantum Machine Intelligence*, 3:1–11, 2021.
- [39] Taylor L. Patti, Khadijeh Najafi, Xun Gao, and Susanne F. Yelin. Entanglement devised barren plateau mitigation. *Physical Review Research*, 3(3):033090, 2021.
- [40] Tyler Volkoff and Patrick J. Coles. Large gradients via correlation in random parameterized quantum circuits. *Quantum Science and Technology*, 6(2):025008, 2021.
- [41] Arthur Pesah, Marco Cerezo, Samson Wang, Tyler Volkoff, Andrew T. Sornborger, and Patrick J. Coles. Absence of barren plateaus in quantum convolutional neural networks. *Physical Review X*, 11(4):041011, 2021.
- [42] Hela Mhiri, Ricard Puig, Sacha Lerch, Manuel S Rudolph, Thiparat Chotibut, Supanut Thanasilp, and Zoë Holmes. A unifying account of warm start guarantees for patches of quantum landscapes. *arXiv preprint arXiv:2502.07889*, 2025.
- [43] Kosuke Mitarai, Makoto Negoro, Masahiro Kitagawa, and Keisuke Fujii. Quantum circuit learning. *Physical Review A*, 98(3):032309, 2018.
- [44] Maria Schuld, Ville Bergholm, Christian Gogolin, Josh Izaac, and Nathan Killoran. Evaluating analytic gradients on quantum hardware. *Physical Review A*, 99(3):032331, 2019.
- [45] Bryce Fuller, Minh C. Tran, Danylo Lykov, Caleb Johnson, Max Rossmannek, Ken Xuan Wei, Andre He, Youngseok Kim, DinhDuy Vu, Kunal Sharma, et al. Improved quantum computation using operator backpropagation. *arXiv preprint arXiv:2502.01897*, 2025.
- [46] Ricard Puig, Marc Drudis, Supanut Thanasilp, and Zoë Holmes. Variational quantum simulation: A case study for understanding warm starts. *PRX Quantum*, 6:010317, 2025.
- [47] Alicia B. Magann, Christian Arenz, Matthew D. Grace, Tak-San Ho, Robert L. Kosut, Jarrod R. McClean, Herschel A. Rabitz, and Mohan Sarovar. From pulses to circuits and back again: A quantum optimal control perspective on variational quantum algorithms. *PRX Quantum*, 2:010101, 2021.
- [48] Martin Larocca, Nathan Ju, Diego García-Martín, Patrick J Coles, and Marco Cerezo. Theory of overparametrization in quantum neural networks. *Nature Computational Science*, 3(6):542–551, 2023.
- [49] Herschel A. Rabitz, Michael M. Hsieh, and Carey M. Rosenthal. Quantum optimally controlled transition landscapes. *Science*, 303(5666):1998–2001, 2004.
- [50] Lorenzo Leone, Salvatore F.E. Oliviero, Lukasz Cincio, and M. Cerezo. On the practical usefulness of the Hardware Efficient Ansatz. *Quantum*, 8:1395, 2024.
- [51] <https://docs.quantum.ibm.com/api/qiskit/qiskit.circuit.library.EfficientSU2>, 2023.
- [52] Marco Cerezo, Akira Sone, Tyler Volkoff, Lukasz Cincio, and Patrick J. Coles. Cost function dependent barren plateaus in shallow parametrized quantum circuits. *Nature communications*, 12(1):1791, 2021.
- [53] David A. Kreplin and Marco Roth. Reduction of finite sampling noise in quantum neural networks. *Quantum*, 8:1385, 2024.
- [54] F. Bonechi, E. Celeghini, Riccardo Giachetti, E. Sorace, and M. Tarlini. Heisenberg xxz model and quantum galilei group. *Journal of Physics A: Mathematical and General*, 25(15):L939, 1992.
- [55] Amira Abbas, David Sutter, Christa Zoufal, Aurélien Lucchi, Alessio Figalli, and Stefan Woerner. The power of quantum neural networks. *Nature Computational Science*, 1(6):403–409, 2021.
- [56] Federico Tibljas, Anna Schroeder, Yue Zhang, Mariami Gachechiladze, and Iryna Gurevych. An efficient quantum classifier based on hamiltonian representations. *arXiv preprint arXiv:2504.10542*, 2025.
- [57] Junyu Liu, Francesco Tacchino, Jennifer R. Glick, Liang Jiang, and Antonio Mezzacapo. Representation learning via quantum neural tangent kernels. *PRX Quantum*, 3:030323, 2022.
- [58] Junyu Liu, Khadijeh Najafi, Kunal Sharma, Francesco Tacchino, Liang Jiang, and Antonio Mezzacapo. Analytic theory for the dynamics of wide quantum neural networks. *Phys. Rev. Lett.*, 130:150601, 2023.
- [59] Erfan Abedi, Salman Beigi, and Leila Taghavi. Quantum Lazy Training. *Quantum*, 7:989, 2023.
- [60] Xuchen You, Shouvanik Chakrabarti, Boyang Chen, and Xiaodi Wu. Analyzing convergence in quantum neural networks: Deviations from neural tangent kernels. In *International Conference on Machine Learning*, pages 40199–40224. PMLR, 2023.
- [61] Francesco Scala, Christa Zoufal, Dario Gerace, and Francesco Tacchino. Towards practical quantum neural network diagnostics with neural tangent kernels. *arXiv preprint arXiv:2503.01966*, 2025.
- [62] Robert M. Corless, Gaston H Gonnet, David EG Hare, David J Jeffrey, and Donald E Knuth. On the lambert w function. *Advances in Computational mathematics*, 5:329–359, 1996.
- [63] Herbert Robbins. A remark on stirling’s formula. *The American mathematical monthly*, 62(1):26–29, 1955.
- [64] William Feller. *An introduction to probability theory and its applications, Volume 2*, volume 2. John Wiley & Sons, 1991.

## CONTENTS

I. Introduction	1
II. Preliminaries	2
A. Stabilizer Formalism	2
B. Variational Quantum Algorithms	2
C. Barren Plateaus	3
D. Classical Taylor Surrogate Patches	3
III. Theoretical Results	4
A. Backpropagation of High-Order Clifford structures in the Heisenberg Picture	4
B. The Linear Clifford Encoder (LCE)	5
C. Escaping Barren Plateaus with the Linear Clifford Encoder (LCE)	6
D. Phase Transitions in Computational Complexity	7
1. Worst-Case Error Analysis	7
2. Mean-Squared Error Analysis	7
IV. Absence of barren plateaus beyond small patches	8
V. Numerical Experiments	9
A. Initial Gradient Scalability	9
B. Variational Quantum Eigensolvers	9
VI. Conclusion	10
VII. Acknowledgments	11
References	11
A. Comparing Barren-Plateau Mitigation Techniques and Classical Surrogates	15
a. Comparing Barren-Plateau Mitigation Techniques	16
b. Comparing Classical Surrogates	16
B. Stabilizer Formalism and the Gottesman-Knill Theorem	17
1. Quantum States in an Exponential Hilbert Space	17
2. Stabilizer Group	18
3. $N$ -qubit Pauli Group	18
4. The Clifford Group and Stabilizer States	19
5. The Gottesman-Knill Theorem	19
6. Computing Expectations with the Stabilizer Formalism	21
C. PQC Ansatz Architectures	23

D. Comparing State-of-the-Art Simulation Techniques	24
1. Naive Evaluation of the Exponential Quadratic Form	24
2. Low-Rank Stabilizer Decomposition	24
3. Pauli Path Formalism	25
4. Truncated Taylor series	27
E. High-Order Parameter-Shift Rules and Cost Regularity	28
F. Construction of the Linear Clifford Encoder (LCE)	31
1. Explicit Construction of the Linear Clifford Encoder (LCE)	31
2. Generalization to Arbitrary Observables	35
G. Escaping Barren Plateaus	36
1. Taylor Perturbation around Clifford Points	36
2. Constant Gradient Lower Bound in Small Patches	37
3. Polynomial Gradient Lower Bound beyond Small Patches	40
H. State Expressivity of Parameterized Quantum Circuits	41
I. Minimal Truncation Threshold of the Taylor Surrogate	43
1. Worst-Case Error Analysis	43
2. Mean-Squared Error Analysis	46
J. Computational Complexity	49
1. Deterministic Worst-Case Simulation Complexity	49
2. Probabilistic Mean-Squared Simulation Complexity	51
3. Complexity Comparison with the Pauli Path Surrogate	52
4. Efficient Recursive Classical Implementation	54
K. Additional Numerical Experiments	56
1. Gradient Scaling Experiments	56
2. VQE Optimization with different Learning Rates and Finite Sampling Noise	57
3. VQE Optimization of the Heisenberg Model	60

## Appendix A: Comparing Barren-Plateau Mitigation Techniques and Classical Surrogates

In order to provide an overview of our results in trainability and classical computational complexity, and how they fit into the literature, we compare related barren-plateau mitigation techniques trainability and the performance of classical surrogates with related works, respectively.

	gradient bounds within $\mathcal{O}(D^{-\frac{1}{2}})$ patches	gradient bounds beyond $\mathcal{O}(D^{-\frac{1}{2}})$ patches	model assumptions
<b>Linear Clifford Encoder (LCE)</b>	$\Omega(1)$ on $\mathcal{O}\left(D^{-\frac{1+\delta}{2}}\right)$ with $\delta > 0$	$\Omega(\text{Poly}(N)^{-1})$	LCE transformed expectation $C(\theta) = \text{Tr}(U(\theta)^\dagger  0\rangle\langle 0  U(\theta) H)$ with arbitrary PQC $U(\theta)$ , and any observable $H$ with at most $\mathcal{O}(1)$ Pauli terms.
<b>Park et al. [25]</b>	$\Omega(1)$ on $\mathcal{O}(D^{-1})$	none	expectation cost function $\text{Tr}(U(\theta)^\dagger  \psi_0\rangle\langle \psi_0  U(\theta) H)$ with $ \psi_0\rangle$ s.t. $\ (\nabla_\theta C)(0)\  = \Omega(1)$ , imposing single-Pauli or local observable $H$ .
<b>Warm Start [46]</b>	$\Omega(\text{Poly}(N)^{-1})$ on $\mathcal{O}(D^{-\frac{1}{2}})$	none	warm-started cost function $1 -  \langle \psi_0   U(\theta)^\dagger e^{-i\delta t H} U(\theta^*)   \psi_0 \rangle ^2$ with arbitrary PQC $U(\theta)$ , and arbitrary observable $H$ .
<b>Small Angles [32]</b>	$\Omega(\text{Poly}(N)^{-1})$ on $\mathcal{O}(\sqrt{N} D^{-\frac{1}{2}})$	none	expectation value of the form $\text{Tr}(U(\theta)^\dagger  0\rangle\langle 0  U(\theta) H)$ with $\Theta(D/N)$ layers, and local observable $H$ .

TABLE I. Comparison of barren-plateau mitigation on small patches. Models within the  $\mathcal{O}(D^{-1/2})$  patch are classically simulable (cf. Theorem 4), while only our method proves trainability beyond this patch (cf. Theorem 5), where no classical surrogate is currently known to exist.

#### a. Comparing Barren-Plateau Mitigation Techniques

Refer to Table I in order to compare barren-plateau mitigation techniques. In this work, we established the *Linear Clifford Encoder (LCE)* which ensures constant scaling gradient lower bounds on  $\mathcal{O}(D^{-\frac{1}{2}})$  patches (cf. Theorem 2), and is currently the only known mitigation technique able to achieve polynomially decaying gradient lower bounds beyond that patch (Theorem 5). Notably, Park et al. [25] also established constant lower gradient bounds, where their assumption is satisfied with the special case where the initial state  $|\psi_0\rangle = \tilde{Q}U(\xi^{j,ek})Q|0\rangle$  matches the LCE transformation. However, they achieve these asymptotics solely within the  $\mathcal{O}(D^{-1})$  patch, and they also impose locality of the observable, or  $H = P$  being a single Pauli string. Puig et al. [46] use a warm start approach in order to achieve polynomially decaying gradients on the larger  $\mathcal{O}(D^{-\frac{1}{2}})$  but do not extend their analysis beyond that patch size. Additionally, we compare with uniform small angle initialization of parameters, where Wang et al. [32] establish polynomially decaying gradients on patches  $\mathcal{O}(L^{-\frac{1}{2}})$  depending on the number of layers  $L = \Theta(D/N)$ . Increasing the number of layers while keeping  $N$  fixed thus increases the number of parameters  $D$ , which makes their results comparable to our  $\mathcal{O}(D^{-\frac{1}{2}})$  patch framework. Likewise, they require locality of the observable  $H$ . A Gaussian small angles initialization strategy is studied by Zhang et al. [31], where they employ gradients evaluated at  $\theta = 0$  to lower bound the expected gradient norm, thus bearing resemblance to our Taylor approximation technique (cf. Theorem 8). Similarly, they achieve polynomially decaying asymptotics on  $\mathcal{O}(L^{-\frac{1}{2}})$  patches, and require locality of the observable.

#### b. Comparing Classical Surrogates

Table II compares our Taylor surrogate performance to that relying on the Pauli path technique in the work of Sasha et al. [18]. Both techniques are able to simulate the patch  $\mathcal{O}(D^{-1})$  in polynomial time up to a certain approximation error  $\varepsilon > 0$ . In our case, the degree of the polynomial is given by the explicitly determined truncation threshold

	worst-case simulation of $\mathcal{O}(D^{-1})$ patches	MSE simulation of $\mathcal{O}(D^{-1/2})$ patches	model assumptions
<b>Taylor Surrogate</b>	$\mathcal{O}( \mathcal{I} D^{m(\theta,\varepsilon)})$	$\mathcal{O}\left( \mathcal{I} D^{\frac{1}{2\log(\frac{1}{q})}\log(\frac{c}{\rho\varepsilon^2})}\right)$	expectation $\text{Tr}(U(\theta)^\dagger 0\rangle\langle 0 U(\theta)H)$ with arbitrary PQC $U(\theta)$ , generated by Clifford and single-qubit Pauli rotation gates.
<b>Pauli Path Surrogate [18]</b>	$\mathcal{O}( \mathcal{I} D^{\log(\frac{1}{\varepsilon})})$	$\mathcal{O}( \mathcal{I} D^{\log(\frac{1}{\varepsilon^{2\rho}})})$	expectation $\text{Tr}(\mathcal{E}_\theta(\rho)H)$ with density matrix $\rho$ , and parameterized channel $\mathcal{E}_\theta$ , imposing classically feasible derivatives $D_\theta^\alpha C(\theta)$ with certain bounds.

TABLE II. Comparing classical surrogates of small landscape patches.

$m(\theta, \varepsilon)$  of the Taylor surrogate (cf. Lemma 9). When allowing a small probability of failure  $\rho > 0$ , both surrogates are able to extend classical simulability to the larger patch  $\mathcal{O}(D^{-\frac{1}{2}})$  (cf. Theorem 4). This is achieved with the mean-squared error:

$$\mathbb{E}_\theta[(C(\theta) - C_m(\theta))^2] \leq c \|H\|^2 D^m \sigma^{2m}, \quad (\text{A1})$$

for some  $c > 0$  (cf. Appendix I). When initializing the parameters with  $\sigma = q \|H\|^{-\frac{1}{m}} D^{-\frac{1}{2}}$  for some sufficiently small  $0.35 \geq q < 1$ , we are able to prove that the Taylor surrogate outperforms the Pauli path approach (cf. Corollary 3), where the efficiency of Gottesman-Knill [20, 21] starts to emerge.

## Appendix B: Stabilizer Formalism and the Gottesman-Knill Theorem

We presume a familiarity of the reader with basic concepts in group theory. The content of this section may be seen as a summary and a slightly alternative point of view of the introductory works on stabilizer formalism in Ref. [27]. We begin by refreshing the necessary terminology, and conclude with a proof sketch of the version of the Gottesman-Knill theorem [20, 21] that we employ in this work. For a more in-depth review of the Pauli and Clifford theory, we encourage the reader to look into Refs. [28].

### 1. Quantum States in an Exponential Hilbert Space

Consider a  $N$ -qubit quantum system on which we intend to perform error-free computation. That system may be described by a Hilbert space

$$\mathcal{H}_N := \left\{ |\psi\rangle = \sum_{b \in \{0,1\}^N} a_b |b\rangle : a_b \in \mathbb{C} \right\}, \quad (\text{B1})$$

spanned by the computational basis  $\{|b\rangle : b \in \{0,1\}^N\}$ , where valid quantum states satisfy the normalization condition,

$$\sum_{b \in \{0,1\}^N} |a_b|^2 = 1 \quad (\text{B2})$$

for all  $b \in \{0,1\}^N$ .

The Hilbert space  $\mathcal{H}_N$  is exponentially large and generally difficult to fully describe classically. Of course there are states that are given by polynomially many amplitudes  $a_b$  which remain classically feasible. However, a groundbreaking insight lead to the discovery of *stabilizer states* which are quantum states spanned by exponentially many amplitudes that may be classically described using polynomial resources. These states may be derived with basic concepts from group theory.

## 2. Stabilizer Group

Stabilizer formalism is motivated from a concept in group theory called *stabilizer*. In the context of the quantum computing, we say that a unitary operator  $U \in \text{U}(2^N)$  *stabilizes* a quantum state  $|\psi\rangle \in \mathcal{H}_N$  if  $U|\psi\rangle = |\psi\rangle$ , i.e.  $|\psi\rangle$  is an eigenstate of  $U$  with eigenvalue  $+1$ . From a group-theoretic perspective, the *stabilizer* of a quantum state  $|\psi\rangle \in \mathcal{H}_N$  is defined as

$$\text{Stab}(|\psi\rangle) := \{U \in \text{U}(2^N) : U|\psi\rangle = |\psi\rangle\} \quad (\text{B3})$$

consisting of all unitary operators that stabilize the state  $|\psi\rangle$ . It can be shown that  $\text{Stab}(|\psi\rangle) \subset \mathcal{H}_N$  defines an abelian subgroup for every  $|\psi\rangle \in \mathcal{H}_N$ . Similarly, we say that  $|\psi\rangle$  is a *stabilizer* of a unitary operator  $U \in \text{U}(2^N)$  if  $U|\psi\rangle = |\psi\rangle$ .

## 3. $N$ -qubit Pauli Group

The Pauli matrices are defined as

$$I = \begin{pmatrix} 1 & 0 \\ 0 & 1 \end{pmatrix}, \quad X = \begin{pmatrix} 0 & 1 \\ 1 & 0 \end{pmatrix}, \quad Y = \begin{pmatrix} 0 & -i \\ i & 0 \end{pmatrix}, \quad \text{and} \quad Z = \begin{pmatrix} 1 & 0 \\ 0 & -1 \end{pmatrix}, \quad (\text{B4})$$

where  $i$  denotes the imaginary unit. The multiplicative group dynamics of  $\mathcal{P}_1 := \langle X, Y, Z \rangle$  (modulo phases  $\pm 1, \pm i$ ) is fully determined by the *Cayley table*,

	$X$	$Y$	$Z$
$X$	$I$	$iZ$	$-iY$
$Y$	$-iZ$	$I$	$iX$
$Z$	$iY$	$-iX$	$I$

In particular, we have the commutator rules

$$[P, Q] = 0 \quad \text{or} \quad \{P, Q\} = 0 \quad (\text{B5})$$

for all  $P, Q \in \mathcal{P}_1$ .

The following table represents the set of stabilizer states for each element in the single-qubit Pauli group  $\mathcal{P}_1$  (with  $-I$  being the sole pathological case):

Operator	$I$	$X$	$Y$	$Z$	$-I$	$-X$	$-Y$	$-Z$
Stabilizers	$\mathcal{H}_N$	$ +\rangle$	$ i\rangle$	$ 0\rangle$	$\emptyset$	$ -\rangle$	$  -i\rangle$	$ 1\rangle$

where the quantum states

$$\begin{aligned} |0\rangle &:= \begin{pmatrix} 1 \\ 0 \end{pmatrix}, \quad |1\rangle := \begin{pmatrix} 0 \\ 1 \end{pmatrix} \quad (Z\text{-axis}) \\ |\pm\rangle &:= \frac{1}{\sqrt{2}}(|0\rangle \pm |1\rangle) \quad (X\text{-axis}) \\ |\pm i\rangle &:= \frac{1}{\sqrt{2}}(|0\rangle \pm i|1\rangle) \quad (Y\text{-axis}) \end{aligned} \quad (\text{B6})$$

are known as the main axes of the *Bloch sphere*.

A generalization of the group  $\mathcal{P}_1$  leads to the definition of the  $N$ -qubit Pauli group:

$$\mathcal{P}_N := \left\{ \phi \cdot \bigotimes_{j=1}^N P_j : P_j \in \{I, X, Y, Z\}, \phi \in \{\pm 1, \pm i\} \right\}, \quad (\text{B7})$$

and it can be shown that this defines a finite group with  $|\mathcal{P}_N| = 4^{N+1}$  elements. The elements of  $\mathcal{P}_N$  are known as *Pauli strings* or *Pauli words*.

In the Clifford theory, setting the stage of the Gottesman-Knill theorem discussed further below, we are particularly interested in the stabilizer group consisting of Pauli strings only. For that purpose, we introduce the  $N$ -qubit *Pauli stabilizer group* of a given quantum state  $|\psi\rangle \in \mathcal{H}_N$  which is defined as

$$\text{Stab}_{\mathcal{P}_N}(|\psi\rangle) := \text{Stab}(|\psi\rangle) \cap \mathcal{P}_N. \quad (\text{B8})$$

The intersection of two groups forms a group, and  $\text{Stab}_{\mathcal{P}_N}(|\psi\rangle)$  is abelian since  $\text{Stab}(|\psi\rangle)$  is abelian.

#### 4. The Clifford Group and Stabilizer States

The  $N$ -qubit Clifford is defined to be the subgroup of  $2^N \times 2^N$  unitary operators that map tensor products of Pauli matrices to tensor products of Pauli matrices through conjugation modulo global phases,  $U(1) = \{e^{i\theta} : \theta \in [-\pi, \pi]\}$ :

$$\text{Clifford}(N) := \{Q \in U(2^N) : Q \mathcal{P}_N Q^\dagger = \mathcal{P}_N\} / U(1). \quad (\text{B9})$$

In other words, these operators normalize the  $N$ -qubit Pauli group  $\mathcal{P}_N$  modulo global phases. The Clifford group is well-known to be finite, and generated by  $H$ ,  $S$ , and CX-gates, i.e.  $\text{Clifford}(N) = \langle H, S, \text{CX} \rangle_N$  (modulo global phases).

The *stabilizer states* are simply given by the set of all states achieved by applying a Clifford operator to the zero state, i.e.

$$\text{Stab}(N) := \{Q|0\rangle : Q \in \text{Clifford}(N)\} \quad (\text{B10})$$

It can be shown that for each  $|\psi\rangle \in \text{Stab}(N)$  there exists a set of basis states  $S \equiv \{b\}_{b \in S} \subseteq \{0, 1\}^N$  and  $k_b \in \mathbb{N}_0$  such that

$$|\psi\rangle = \frac{1}{\sqrt{|S|}} \sum_{b \in S} i^{k_b} |b\rangle \quad (\text{B11})$$

defines an equal superposition of basis states with relative phases in  $\{e^{i\phi} : \phi \in \frac{\pi}{2}\mathbb{Z}\}$ . Stabilizer states may always be efficiently described classically with the help of the Gottesman-Knill theorem, as elaborated next.

#### 5. The Gottesman-Knill Theorem

We focus on the following version of the Gottesman-Knill theorem [20, 21]. We provide a proof sketch in the sense that we skip minor technical details in order to focus on the main idea behind the argumentation. The goal is to develop an intuitive formal understanding on how the group theory in the stabilizer formalism grants access to exponential savings in the classical description of stabilizer states. For more details, see Ref. [27].

The version of Gottesman-Knill (cf. Theorem 6) that we are going to prove states that every stabilizer state  $|\psi\rangle \in \text{Stab}(N)$  is *uniquely* determined by its underlying Pauli stabilizer group  $\text{Stab}_{\mathcal{P}_N}(|\psi\rangle) = \langle g_1, \dots, g_N \rangle$ , generated by  $N$  independent generators  $g_1, \dots, g_N \in \mathcal{P}_N$ . The generators  $g_1, \dots, g_N$  are efficiently described classically with the help of *check matrices* [21, 27], which establishes that stabilizer states are indeed easy to simulate classically. The proof of Theorem 6 below breaks down into three main steps:

- I. *Zero State Description:* First, we establish by induction that the zero state  $|0\rangle \in \text{Stab}(N)$  may always be described in terms of group generators  $Z_1, \dots, Z_N$  of the corresponding Pauli stabilizer group  $\text{Stab}_{\mathcal{P}_N}(|0\rangle)$ . That is,  $\text{Stab}_{\mathcal{P}_N}(|0\rangle) = \langle Z_1, \dots, Z_N \rangle$ .
- II. *Zero State Evolution:* Next, we employ the previous step to prove that any stabilizer state  $|\psi\rangle \in \text{Stab}(N)$  may be fully described by evolving the zero state through the underlying Clifford operator. Indeed, by definition there exists  $C \in \text{Clifford}(N)$  such that  $|\psi\rangle = C|0\rangle$ . With the help of the previous step, we then establish that the generators of  $\text{Stab}_{\mathcal{P}_N}(|\psi\rangle) = \langle g_1, \dots, g_N \rangle$  are simply obtained by evolving the generators of  $\text{Stab}_{\mathcal{P}_N}(|0\rangle)$  through  $C$  in the Heisenberg picture, i.e.  $g_j = CZ_jC^\dagger$  for all  $j \in [N]$ . This establishes that each stabilizer state is fully described by  $N$  generators.
- III. *Stabilizer State Uniqueness:* Finally, it remains to prove that the generators of  $\text{Stab}_{\mathcal{P}_N}(|\psi\rangle)$  are uniquely determined. This is achieved by introducing a certain projector operator  $P_{\text{Stab}_{\mathcal{P}_N}(|\psi\rangle)} : \mathcal{H}_N \rightarrow V_{\text{Stab}_{\mathcal{P}_N}(|\psi\rangle)}$ , that projects the full Hilbert space  $\mathcal{H}_N$  onto a certain linear subspace  $V_{\text{Stab}_{\mathcal{P}_N}(|\psi\rangle)}$  characterized by the Pauli stabilizer group  $\text{Stab}_{\mathcal{P}_N}(|\psi\rangle)$ . Afterwards, by using the fact that non-identity Pauli operators are traceless, we establish that the dimension of the subspace  $V_{\text{Stab}_{\mathcal{P}_N}(|\psi\rangle)}$  is equal to one. Thus, by normalization of quantum state, this shows that the group generators  $g_1, \dots, g_N$  of  $\text{Stab}_{\mathcal{P}_N}(|\psi\rangle)$  are sufficient to uniquely determine the stabilizer state  $|\psi\rangle$ .

**Theorem 6** (Gottesman-Knill). *Every stabilizer state  $|\psi\rangle \in \text{Stab}(N)$  is uniquely determined by its Pauli stabilizer group,  $\text{Stab}_{\mathcal{P}_N}(|\psi\rangle)$ . Moreover, the group  $\text{Stab}_{\mathcal{P}_N}(|\psi\rangle)$  is spanned by  $N$  pair-wise independent generators.*

*Proof Sketch.* Let  $|\psi\rangle \in \text{Stab}(N)$  be arbitrary. Then, by definition,  $|\psi\rangle = C|0\rangle$  for some  $C \in \text{Clifford}(N)$ . By induction, one establishes that the group

$$\text{Stab}_{\mathcal{P}_N}(|0\rangle) = \langle Z_1, \dots, Z_N \rangle, \quad (\text{B12})$$

is uniquely generated by the pair-wise independent Pauli strings  $Z_1, \dots, Z_N$ , where we use the conventional notations  $V_j := I_{2^{j-1}} \otimes V \otimes I_{2^{N-j}}$ . We use this as a basis to show that

$$\text{Stab}_{\mathcal{P}_N}(|\psi\rangle) = \langle CZ_1C^\dagger, \dots, CZ_NC^\dagger \rangle \quad (\text{B13})$$

is uniquely generated by the pair-wise independent Pauli strings  $CZ_1C^\dagger, \dots, CZ_NC^\dagger$ , where  $C \in \text{Clifford}(N)$ . To prove Eq. (B13), first note that

$$P \in \text{Stab}_{\mathcal{P}_N}(C|0\rangle) \iff PC|0\rangle = C|0\rangle \iff (C^\dagger PC)|0\rangle = |0\rangle \iff \underbrace{C^\dagger PC}_{\in \mathcal{P}_N} \in \text{Stab}_{\mathcal{P}_N}(|0\rangle), \quad (\text{B14})$$

again using  $C \in \text{Clifford}(N)$ . Next, we apply Eq. (B12) to establish that there exist exponents  $e_1, \dots, e_N \in \{0, 1\}$  such that

$$\begin{aligned} C^\dagger PC \in \text{Stab}_{\mathcal{P}_N}(|0\rangle) = \langle Z_1, \dots, Z_N \rangle &\iff C^\dagger PC = Z_1^{e_1} \dots Z_N^{e_N} \\ &\iff P = C \left( \prod_{j=1}^N Z_j^{e_j} \right) C^\dagger = \prod_{j=1}^N (CZ_jC^\dagger)^{e_j} \\ &\iff P \in \langle CZ_1C^\dagger, \dots, CZ_NC^\dagger \rangle, \end{aligned} \quad (\text{B15})$$

using  $C^\dagger C = CC^\dagger = I$ . Combined with Eq. (B14) this proves the equality in Eq. (B13). Next, we show that  $CZ_1C^\dagger, \dots, CZ_NC^\dagger$  are independent generators. For that purpose, we assume for absurd that the contrary is true. Then there exists an index  $i \in [N]$  such that

$$\text{Stab}_{\mathcal{P}_N}(C|0\rangle) = \langle CZ_jC^\dagger \rangle_{j \in [N]} = \langle CZ_jC^\dagger \rangle_{j \in [N] \setminus \{i\}}. \quad (\text{B16})$$

But by the previous equivalence in Eq. (B15), this would imply  $Z_i \in \langle Z_j \rangle_{j \in [N]} = \langle Z_j \rangle_{j \in [N] \setminus \{i\}}$ , which is absurd.

It remains to show that the group  $\text{Stab}_{\mathcal{P}_N}(|\psi\rangle)$  (and thus the set of its generators) uniquely determines the stabilizer state  $|\psi\rangle$ . Consider the space

$$V_{\text{Stab}_{\mathcal{P}_N}(|\psi\rangle)} := \{ |v\rangle \in \mathcal{H}_N : P|v\rangle = |v\rangle \text{ for all } P \in \text{Stab}_{\mathcal{P}_N}(|\psi\rangle) \}. \quad (\text{B17})$$

It can be shown that  $V_{\text{Stab}_{\mathcal{P}_N}(|\psi\rangle)} \subset \mathcal{H}_N$  defines a linear subspace, and it consists of all states that are fixed by elements of the Pauli stabilizer group  $\text{Stab}_{\mathcal{P}_N}(|\psi\rangle)$  (in particular by its generators). We are going to establish that its dimension equals  $\dim V_{\text{Stab}_{\mathcal{P}_N}(|\psi\rangle)} = 1$ . Indeed, this completes the proof because by normalization of quantum states, together with the one-dimensionality, Eq. (B17) implies the existence of a unique quantum state  $|\psi\rangle \in \mathcal{H}_N$ .

By Eq. (B13) there exist Pauli generators  $g_1, \dots, g_N \in \mathcal{P}_N$  such that  $\text{Stab}_{\mathcal{P}_N}(|\psi\rangle) = \langle g_1, \dots, g_N \rangle$ . Consider the operator

$$P_{\text{Stab}_{\mathcal{P}_N}(|\psi\rangle)} := \frac{1}{2^N} \prod_{j=1}^N (I + g_j). \quad (\text{B18})$$

Then, we note that  $P_{\text{Stab}_{\mathcal{P}_N}(|\psi\rangle)} : \mathcal{H}_N \rightarrow V_{\text{Stab}_{\mathcal{P}_N}(|\psi\rangle)}$  defines a projector. Indeed, for each  $j \in [N]$  we have

$$\left( \frac{I + g_j}{2} \right)^2 = \frac{1}{4} (I + 2g_j + g_j^2) = \frac{I + g_j}{2} \quad \text{and} \quad \left( \frac{I + g_j}{2} \right) |\psi\rangle = \frac{|\psi\rangle + g_j|\psi\rangle}{2} = |\psi\rangle, \quad (\text{B19})$$

using  $g_j^2 = I$  and  $g_j|\psi\rangle = |\psi\rangle$  since  $g_j \in \langle g_j \rangle_{j \in [N]} = \text{Stab}_{\mathcal{P}_N}(|\psi\rangle)$  is a Pauli string that stabilizes  $|\psi\rangle$ . In other words, for each  $j \in [N]$ ,  $\frac{1}{2}(I + g_j)$  is the projector onto the +1-eigenspace of  $g_j$ . Taking the product, this shows that  $P_{\text{Stab}_{\mathcal{P}_N}(|\psi\rangle)}$  defines the claimed projector, and it can be shown that it is surjective.

The crucial observation now is that this projector decomposes as

$$P_{\text{Stab}_{\mathcal{P}_N}(|\psi\rangle)} = \frac{1}{2^N} \prod_{j=1}^N (I + g_j) = \frac{1}{2^N} \sum_{e_1, \dots, e_N \in \{0,1\}} g_1^{e_1} \cdots g_N^{e_N} = \frac{1}{2^N} \sum_{g \in \text{Stab}_{\mathcal{P}_N}(|\psi\rangle)} g, \quad (\text{B20})$$

where the second equality is obtained by expanding the product, and the fact that all  $g_j$  commute pair-wise (else they must anti-commute which is impossible because of  $g_j g_i |\psi\rangle = -g_i g_j |\psi\rangle = -|\psi\rangle$ ). The last equality simply follows from  $\text{Stab}_{\mathcal{P}_N}(|\psi\rangle) = \langle g_1, \dots, g_N \rangle$ . This observation immediately implies that taking its trace yields

$$\text{Tr } P_{\text{Stab}_{\mathcal{P}_N}(|\psi\rangle)} = \frac{1}{2^N} \sum_{g \in \text{Stab}_{\mathcal{P}_N}(|\psi\rangle)} \text{Tr } g = \frac{1}{2^N} \underbrace{\text{Tr } I}_{=2^N} = 1, \quad (\text{B21})$$

using that  $\text{Tr } g = 0$  if and only if  $g \neq I$ . On the other hand, since the trace of an operator equals the sum of its eigenvalues, we find

$$1 = \text{Tr } P_{\text{Stab}_{\mathcal{P}_N}(|\psi\rangle)} = \sum_{k=1}^{2^N} \underbrace{\lambda(\text{Stab}_{\mathcal{P}_N}(|\psi\rangle))}_{\in \{0,1\}} = \dim \text{Image}(P_{\text{Stab}_{\mathcal{P}_N}(|\psi\rangle)}) = \dim V_{\text{Stab}_{\mathcal{P}_N}(|\psi\rangle)}. \quad (\text{B22})$$

Here, we used that the eigenvalues of a projector are either 0 or 1. The sum over all eigenvalues of the (linear) projector operator  $P_{\text{Stab}_{\mathcal{P}_N}(|\psi\rangle)} : \mathcal{H}_N \rightarrow V_{\text{Stab}_{\mathcal{P}_N}(|\psi\rangle)}$  thus counts the dimensions that are not in its kernel, and thus counts the dimension of its image, which precisely equals the dimension of the subspace  $V_{\text{Stab}_{\mathcal{P}_N}(|\psi\rangle)}$ , proving Eq. (B17). This completes the proof sketch.  $\square$

This version of Gottesman-Knill proves that there exist states  $|\psi\rangle$  (stabilizer states) with  $2^N$  non-zero amplitudes, that are classically fully characterized by only  $N$  generators of the underlying Pauli stabilizer group  $\text{Stab}_{\mathcal{P}_N}(|\psi\rangle)$ . Aaronson and Gottesman developed an efficient method, known as the *check matrix algorithm* [21], establishing that a stabilizer state  $C|0\rangle$  requires space resources of order  $\mathcal{O}(D_C^2)$ , where  $D_C$  is the number of elementary gates in the circuit  $C \in \text{Clifford}(N)$ . Furthermore, they showed that the time resources required to obtain  $C|0\rangle$  from  $|0\rangle$  is of order  $\mathcal{O}(D_C)$ . In our setting, where we consider a PQC  $U(\theta)$  generated by  $D_C \geq 1$  elementary Clifford gates and  $D \geq 1$  parameterized single-qubit (generally non-Clifford) rotation gates, we may generally assume that  $D_C = cD$  for some constant factor  $c > 0$ , so that simulating  $U(0)|0\rangle$  requires  $\mathcal{O}(D^2)$  space resources, since  $U(0) \in \text{Clifford}(N)$ .

Next, we show that simulating the expectation  $\langle 0|U(0)^\dagger H U(0)|0\rangle$  yields a runtime of order  $\mathcal{O}(D|\mathcal{I}|)$ , where  $|\mathcal{I}|$  is the number of Pauli terms in the observable  $H$ .

## 6. Computing Expectations with the Stabilizer Formalism

We may use the Gottesman-Knill theorem (Theorem 6) in order to prove that Hamiltonian expectations of the form  $\langle 0|C^\dagger H C|0\rangle$  may be computed in polynomial time for each Clifford operator  $C \in \text{Clifford}(N)$ . The result particularly holds true for PQCs evaluated at Clifford configurations, i.e.  $C = U(0)$ .

**Corollary 1.** *Let  $|\psi\rangle \in \text{Stab}(N)$  be a stabilizer state, and  $P \in \mathcal{P}_N$  a Pauli string. Let  $g_1, \dots, g_N \in \mathcal{P}_N$  be the generators of Pauli stabilizer group  $\text{Stab}_{\mathcal{P}_N}(|\psi\rangle)$ . Then,*

$$\langle \psi|P|\psi\rangle = \begin{cases} \text{sign } P, & \text{if } [P, g_j] = 0 \text{ for all } j \in [N], \\ 0, & \text{if there exists } j \in [N] \text{ such that } \{P, g_j\} = 0, \end{cases}$$

where  $\text{sign } P \in \{\pm 1\}$  denotes the sign of the Pauli string.

*Proof.* Since  $P \in \mathcal{P}_N$  is a Pauli string, it has eigenvalues in  $\{\pm 1\}$ . Therefore, we have

$$\langle \psi|P|\psi\rangle = p(+1) \cdot 1 + p(-1) \cdot (-1) = p(+1) - p(-1), \quad (\text{B23})$$

where  $p(\pm 1)$  is the probability of measuring the outcome  $\pm 1$  when the system is prepared in the state  $|\psi\rangle$ . By linearity and the cyclic property of the trace operator, we first establish that

$$p(+1) - p(-1) = \langle \psi | P | \psi \rangle = \text{Tr}(P|\psi\rangle\langle\psi|) = \text{Tr}\left(\frac{I+P}{2}|\psi\rangle\langle\psi|\right) - \text{Tr}\left(\frac{I-P}{2}|\psi\rangle\langle\psi|\right), \quad (\text{B24})$$

and by Born's rule, it immediately follows that

$$p(\pm 1) = \text{Tr}\left(\frac{I \pm P}{2}|\psi\rangle\langle\psi|\right). \quad (\text{B25})$$

Therefore, the projectors  $\frac{1}{2}(I \pm P)$  determine the probability distributions  $p(\pm 1)$  (of the outcomes  $\pm 1$ ) needed for the computation of the expectation value  $\langle \psi | P | \psi \rangle$ . It turns out that certain commutation rules of the Pauli operators involved suffice to explicitly determine these probabilities. More precisely, if the following holds true:

$$\begin{cases} [P, g_j] = 0 \text{ for all } j \in [N] \implies p(\text{sign } P) = 1 \text{ and } p(-\text{sign } P) = 0 & (\text{deterministic outcome}) \\ \text{there exists } j \in [N] \text{ such that } \{P, g_j\} = 0 \implies p(+1) = p(-1) = \frac{1}{2} & (\text{coin flip outcome}) \end{cases} \quad (\text{B26})$$

then, combining Eq. (B26) with Eq. (B24) would yield

$$\langle \psi | P | \psi \rangle = p(+1) - p(-1) \stackrel{(\text{B26})}{=} \begin{cases} \text{sign } P, & \text{if } [P, g_j] = 0 \text{ for all } j \in [N], \\ 0, & \text{if there exists } j \in [N] \text{ such that } \{P, g_j\} = 0. \end{cases} \quad (\text{B27})$$

Therefore, it remains to prove Eq. (B26). First, let us handle the case where  $[P, g_j] = 0$  for all  $j \in [N]$ . Recall the definition of the linear subspace  $V_{\text{Stab}_{\mathcal{P}_N}(|\psi\rangle)}$  in Eq. (B17) introduced in the proof of Theorem 6. By assumption, we have for all  $j \in [N]$  that

$$g_j P |\psi\rangle = P g_j |\psi\rangle = P |\psi\rangle \implies P |\psi\rangle \in V_{\text{Stab}_{\mathcal{P}_N}(|\psi\rangle)}. \quad (\text{B28})$$

We are going to use this observation in order to establish that  $p(\text{sign } P) = 1$ . Indeed, since  $\dim V_{\text{Stab}_{\mathcal{P}_N}(|\psi\rangle)} = 1$  (as shown in Theorem 6), we know that there exists a phase  $\phi \in \mathbb{C}$  such that  $P|\psi\rangle = \phi|\psi\rangle$ . Since  $P \in \mathcal{P}_N$ , we must have that  $\phi \in \{\pm 1\}$  (eigenvalues of  $P$ ). As a result, we find that  $P|\psi\rangle = \text{sign}(P)|\psi\rangle$ . Consequently,

$$p(\text{sign } P) \stackrel{(\text{B25})}{=} \text{Tr}\left(\frac{I + \text{sign}(P)P}{2}|\psi\rangle\langle\psi|\right) = \text{Tr}\left(\frac{I + \text{sign}(P)^2 I}{2}|\psi\rangle\langle\psi|\right) = \text{Tr}(|\psi\rangle\langle\psi|) = 1. \quad (\text{B29})$$

In particular,  $p(-\text{sign } P) = 1 - p(\text{sign } P) = 1 - 1 = 0$ , which proves the deterministic outcome in Eq. (B26).

On the other hand, if there exists  $j \in [N]$  such that  $\{P, g_j\} = 0$ , then

$$g_j P |\psi\rangle = -P g_j |\psi\rangle = -P |\psi\rangle, \quad (\text{B30})$$

which in turn, once again making use of the cyclic property of the trace operator, implies that

$$\begin{aligned} p(-1) &\stackrel{(\text{B25})}{=} \text{Tr}\left(\frac{I - P}{2}|\psi\rangle\langle\psi|\right) = \text{Tr}\left(\frac{I + g_j P}{2}|\psi\rangle\langle\psi|\right) = \frac{1}{2}\langle \psi | \psi \rangle + \frac{1}{2}\underbrace{\langle \psi | g_j P | \psi \rangle}_{\langle \psi | \psi \rangle} \\ &= \frac{1}{2}\langle \psi | (I + P) | \psi \rangle = \text{Tr}\left(\frac{I + P}{2}|\psi\rangle\langle\psi|\right) = p(+1). \end{aligned} \quad (\text{B31})$$

In particular,  $p(+1) = p(-1) = \frac{1}{2}$ , as claimed.  $\square$

As previously established by Theorem 6 we already know that all states involved only require polynomial classical space resources. Together with Corollary 1 this implies that any cost function,  $C(0) = \langle 0 | U(0)^\dagger H U(0) | 0 \rangle$ , evaluated at Clifford configurations (without loss of generality  $\theta = 0$ ) may be classically evaluated in polynomial time. Indeed, the time complexity of classically evaluating  $\langle \psi | P | \psi \rangle$  for a single Pauli string  $P \in \mathcal{P}_N$  scales as  $\mathcal{O}(N)$  since at most  $N$  of the generators  $g_1, \dots, g_N$  need to be compared with  $P$  in order to determine the commutator rules in Eq. (B26). Doing this for each of the Pauli terms in the observable yields a runtime scaling as  $\mathcal{O}(N |\mathcal{I}|)$ , where  $|\mathcal{I}|$  is the number of Pauli terms in the observable  $H$ .

In this work we make the assumption that the ansatz  $U(\theta)$  satisfies that  $D = \Theta(N)$  (i.e. the number of parameters is a multiple of the number of qubits) so that the time complexity of evaluating  $C(0) = \langle 0 | U(0)^\dagger H U(0) | 0 \rangle$  scales as  $\mathcal{O}(D |\mathcal{I}|)$  as established in our complexity theory results.

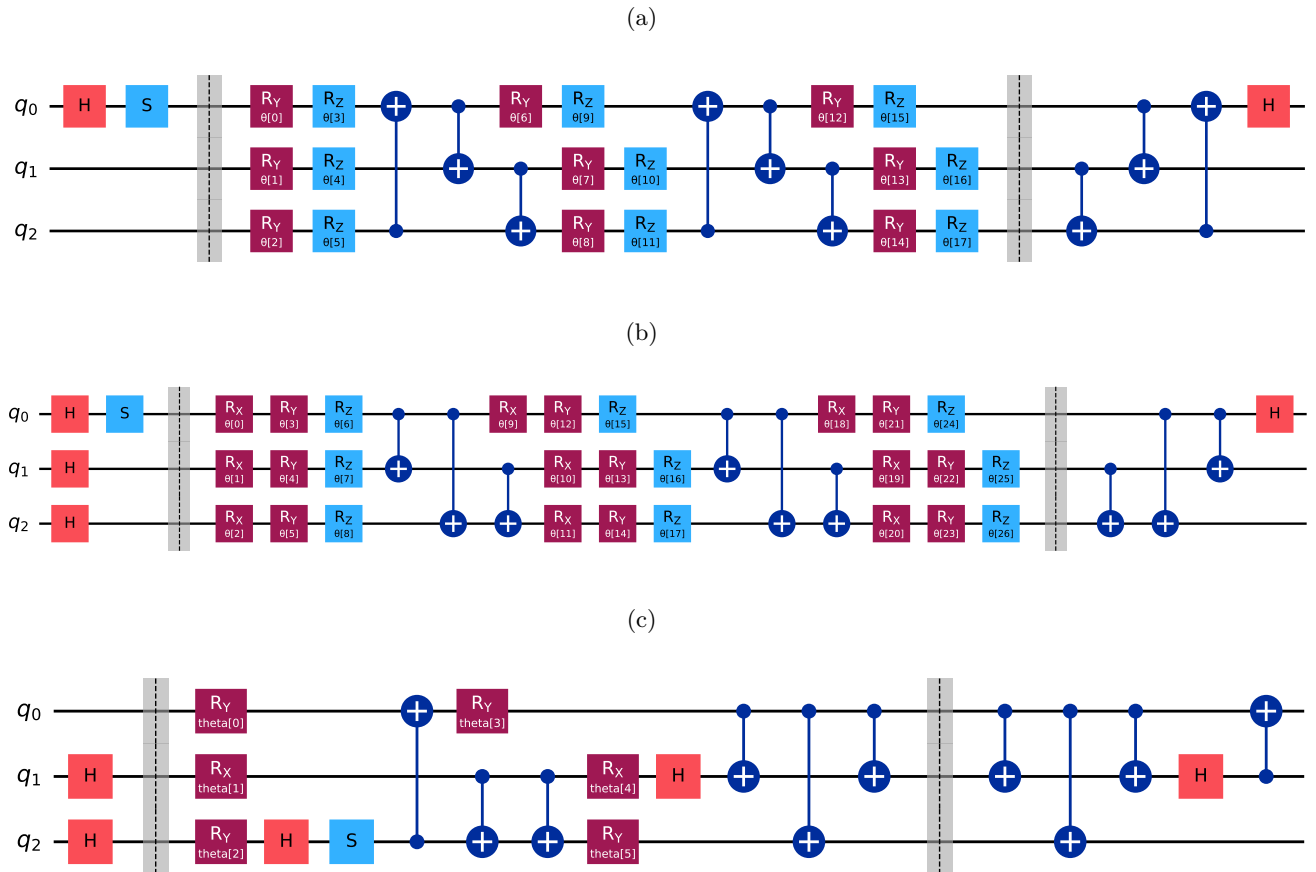


FIG. 8. Examples of two-layer PQCs after LCE transformation. (a) mHEA-circuit with  $N = 3$ ,  $D = 18$ ,  $k = 10$ ,  $P = XXZ$ . (b) fHEA-circuit with  $N = 3$ ,  $D = 27$ ,  $k = 16$ ,  $P = IIZ$ . (c) rPQC-circuit with  $N = 3$ ,  $D = 6$ ,  $k = 4$ ,  $P = IXI$ .

### Appendix C: PQC Ansatz Architectures

In this work, we consider three PQC model ansätze with  $L \geq 1$  layers:

1. **mHEA** [50]: minimalistic Hardware Efficient Ansatz based on Qiskit's `EfficientSU2` [51] with parameterized  $Y$ - and  $Z$ -single-qubit rotation layers, and circular entanglements. The number of parameters satisfies  $D = 2N(L + 1)$ .
2. **fHEA**: full Hardware Efficient Ansatz based on Qiskit's `EfficientSU2` [51] with parameterized  $X$ -,  $Y$ - and  $Z$ -single-qubit rotation layers, and full entanglements. The number of parameters satisfies  $D = 3N(L + 1)$ .
3. **rPQC**: We construct a layer-wise random PQC as follows: independently for each layer, we apply a layer of single-qubit  $H$ -gates followed by a layer of single-qubit  $S$ -gates. Each single-qubit gate appears with 0.5 probability. Then, we apply  $N$  uniformly random pairs of CX-gates. The number of parameters satisfies  $D = NL$ .

Fig. 8 illustrates representative examples of the PQC models used in our experiments after applying the LCE transformation ( $Q, \tilde{Q}$ ). The circuit starts with the Clifford  $Q$  to diagonalize the Pauli string, and ends with  $\tilde{Q}$ , used to induce a relative phase between two parameter-shifted terms  $C(\pm\pi/2 e_k)$ . Panel (a) shows mHEA with  $N = 3$  qubits and  $D = 18$  parameters, LCE transformed using  $k = 10$  and Pauli string  $P = XXZ$ . Panel (b) presents fHEA with  $N = 3$  qubits and  $D = 27$  parameters, LCE transformed using  $k = 16$  and  $P = IIZ$ . Panel (c) depicts rPQC with  $N = 3$  qubits,  $D = 6$  parameters, LCE transformed using  $k = 4$  and  $P = IXI$ .

## Appendix D: Comparing State-of-the-Art Simulation Techniques

In general, the computational resources needed to evaluate the cost  $C(\theta)$  in Eq. (6) is characterized by the number  $\mathcal{O}(|\mathcal{J}|)$  of operations in an estimator of the form

$$C(\theta) \approx \sum_{j \in \mathcal{J}} f_j(\theta), \quad (\text{D1})$$

where  $f_j : [-\pi, \pi]^D \rightarrow \mathbb{R}$  are certain parameter-dependent functions.

### 1. Naive Evaluation of the Exponential Quadratic Form

Recall that, if the  $n$ -qubit system is represented by a Hilbert space  $\mathcal{H}_N$  with state vectors of the general form

$$|\psi\rangle = \sum_{b \in \{0,1\}^N} a_b |b\rangle \quad \text{with amplitudes } a_b \in \mathbb{C} : \sum_{b \in \{0,1\}^N} |a_b|^2 = 1, \quad (\text{D2})$$

in the computational basis, then the cost is naively expressed as the exponential quadratic form (exponentially large matrix, and exponentially many terms depending on the state vector),

$$C(\theta) \stackrel{(6)}{=} \langle \psi(\theta) | H | \psi(\theta) \rangle = \sum_{b, b' \in \{0,1\}^N} a_b^* a_{b'} \langle b | H | b' \rangle = \sum_{b, b' \in \{0,1\}^N} \sum_{i \in \mathcal{I}} a_b^* a_{b'} \langle b | P_i | b' \rangle. \quad (\text{D3})$$

In that case, we find  $|\mathcal{J}| = |\mathcal{I}| \#\{0,1\}^{2N} = 2^{2N}$ , thus implying a worst-case runtime of  $\mathcal{O}(|\mathcal{I}| 2^{2N})$ .

The computational cost of evaluating the quadratic form (6) inherently depends on the specific parameter configuration  $\theta$ . In general, estimating quantum expectation values is exponentially hard [17, 23, 24], but depending on the values of the parameters we can classically approximate them more efficiently. For example, if  $\theta = 0$ , then we can simulate  $C(\theta = 0)$  in polynomial time due to the Gottesman-Knill theorem [20, 21].

In what follows, we provide a brief comparison of state-of-the-art simulation techniques for approximating the expectation value  $C(\theta)$  as a function of  $\theta$ . A short overview is found in Table III below.

	exact runtime	circuit restrictions	complexity in terms of $\theta$
Low-Rank Stabilizer Decomposition [17, 23]	$\mathcal{O}( \mathcal{I}  2^{0.48D})$	3-locality (cf. Eq. (D6))	bounding $m(\theta)$ (cf. Fig. 9)
Clifford Perturbation Theory [18, 24]	$\mathcal{O}( \mathcal{I}  2^D)$	none	none
Truncated Taylor series	$\mathcal{O}( \mathcal{I}  2^{2D})$	none	$m = \Theta(\ \theta\ _1)$ (cf. Lemma 9)

TABLE III. Comparing state-of-the-art simulation techniques with our classical Taylor surrogate method. These are applied to simulate near-Clifford circuits. The comparison is made in terms of the worst-case runtime required for exactly computing  $C(\theta)$ , assumptions on the quantum model ansatz, and the analysis performed of the computational complexity as a function of  $\theta$ .

### 2. Low-Rank Stabilizer Decomposition

Taking into consideration a parameterized state  $|\psi(\theta)\rangle = U(\theta)|0\rangle$ , setting the parameters to 0 results in a stabilizer state [20, 21],  $|\psi(0)\rangle \in \text{Stab}(N)$ . Such states can be efficiently represented and manipulated using Aaronson-Gottesman's check matrix algorithm [21] leveraging the Gottesman-Knill theorem [20] (cf. Theorem 6).

This observation led to the classical simulation technique of Bravyi et al. [17, 23] which is based on a *low-rank stabilizer decomposition* of  $|\psi(\theta)\rangle$ . Specifically,

$$|\psi(\theta)\rangle \approx \sum_{\ell=1}^m \gamma_{\ell}(\theta) |\phi_{\ell}\rangle, \quad (\text{D4})$$

where each  $|\phi_{\ell}\rangle$  defines a stabilizer state, efficiently described within the stabilizer formalism, and  $\gamma_{\ell}(\theta)$  are parameter-dependent complex coefficients.

The computational cost of calculating the expectation value in Eq. (D3) is directly characterized by the decomposition number  $m = \chi(\theta)$  (as a function of  $\theta$ ), also known as the *stabilizer rank*. Also, note that  $m = \sqrt{|\mathcal{I}|}$  in Eq. (D1) since taking the expectation value requires two copies of the low-rank stabilizer decomposition, hence an extra square root. In particular, starting from a Clifford configuration  $\theta = 0$ , as  $U(\theta)$  approaches a circuit containing an increasing number of non-Clifford gates, the number of terms in the decomposition (D4) grows, ultimately leading to an exponential scaling of the simulation cost (cf. Eq. (D3)).

Using the stabilizer decomposition, the expectation value can then be approximated as

$$C(\theta) \approx \sum_{\ell, \ell'=1}^m \gamma_{\ell}(\theta) \gamma_{\ell'}(\theta) \langle \phi_{\ell} | H | \phi_{\ell'} \rangle, \quad (\text{D5})$$

with the approximation error decreasing as  $m$  increases. As of this writing, the most efficient algorithm for implementing Eq. (D5) is reported by Bravyi et al. [17], achieving a worst-case computational complexity of  $\mathcal{O}(|\mathcal{I}| 2^{0.48D})$ .

Unfortunately, their analysis assumes a circuit architecture limited to 3-local qubit gates [17, Proposition 1], thereby imposing a lightcone constraint that reduces the computational complexity of their method. More precisely, they require that

$$|\psi(\theta)\rangle = |\psi_1\rangle \otimes \cdots \otimes |\psi_n\rangle \quad (\text{D6})$$

with each state  $|\psi_j\rangle$  describing a system of at most three qubits. Consequently, this strongly limits the expressive power of the ansatz model.

In Fig. 9, we analyze the stabilizer rank  $m = \chi(\theta)$  [17, Eq. (14)] as a function of the number of qubits  $N$ , under the same experimental setting as Fig. 3. In panel (a), where all parameters are deterministically initialized as  $\theta_1 = \cdots = \theta_D$ , we observe a clear phase transition in computational complexity, consistent with Fig. 3. The red-shaded region indicates the barren-plateau-free regime characterized in Theorem 2. In contrast, panel (b) shows that for randomly initialized parameters  $\theta \sim \mathcal{N}(0, \sigma^2 I_D)$ , the decomposition rank  $m = \chi(\theta)$  exhibits no meaningful dependence on  $N$ , since  $m \geq 1$  is always a positive integer. This demonstrates that the low-rank stabilizer decomposition technique fails to capture the statistical behavior of  $\chi(\theta)$  under random initialization  $\mathbb{P}_{\theta}$ . The key issue is that the formula used in [17] assumes parameter correlations not present under i.i.d. initializations, thereby violating the conditions required for the law of large numbers. In contrast, our formulation  $m = m(\|\theta\|_1)$  satisfies these assumptions asymptotically (cf. Lemma 9). As a result, the framework of Bravyi et al. is unsuitable for testing initialization strategies based on random sampling.

### 3. Pauli Path Formalism

Begušić et al. [24] take a fundamentally different approach to the problem. Instead of explicitly describing the quantum state  $|\psi(\theta)\rangle$  first, they directly expand the expectation value Eq. (D3) by iteratively applying commutator rules. Specifically, for each Pauli-rotation gate  $R_{V_k}$  with  $k \in [D]$  in the circuit ansatz, and each Pauli term  $P_i$  with  $i \in \mathcal{I}$  in the cost function, they use

$$R_{V_k}(\theta_k)^\dagger P_i R_{V_k}(\theta_k) = \begin{cases} P_i, & [P_i, V_k] = 0, \\ \cos \frac{\theta_k}{2} P_i + i \sin \frac{\theta_k}{2} V_k P_i, & \{P_i, V_k\} = 0, \end{cases} \quad (\text{D7})$$

to propagate each Pauli-rotation gate through the observable, where  $[\cdot, \cdot]$ , and  $\{\cdot, \cdot\}$  denote the commutator, and anti-commutator, respectively.

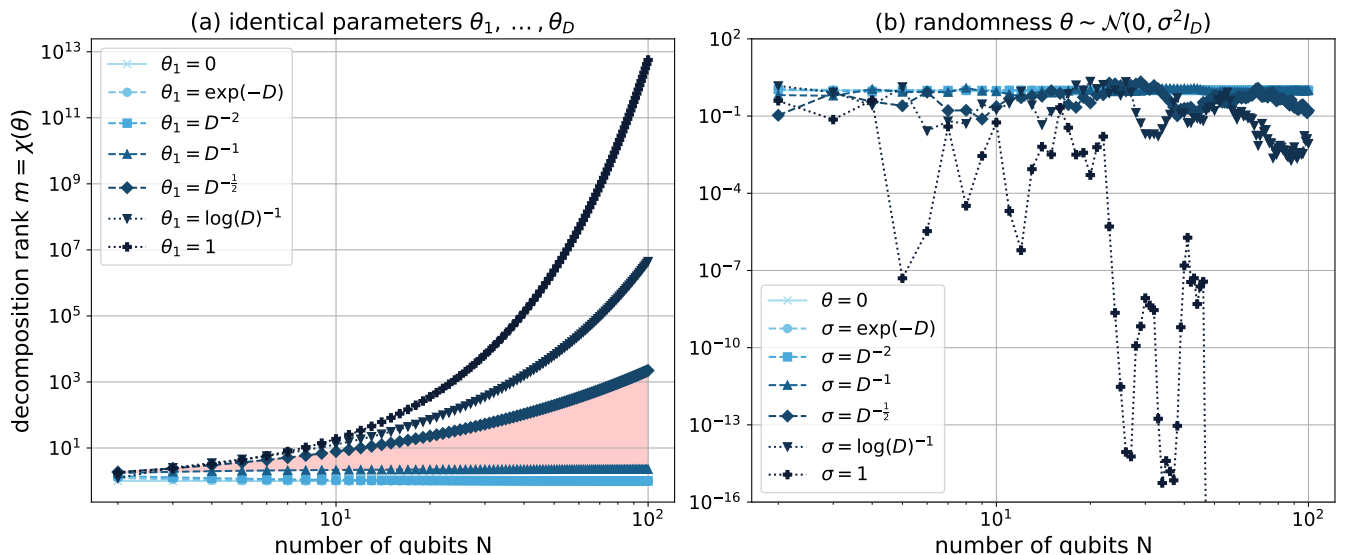


FIG. 9. Stabilizer rank  $m = \chi(\theta)$  as a function of qubit number  $N$  for a model with  $D = N$  parameters. (a) Deterministic parameters show a complexity phase transition and a barren-plateau-free region (red). (b) Randomly initialized parameters yield uninformative scaling of  $m$  with the number of qubits  $N$ .

This results in an alternative series expansion of the expectation value:

$$C(\theta) \approx \sum_{i \in \mathcal{I}} c_i \sum_{\ell=1}^m f_{\ell}(\theta) \langle 0 | \tilde{P}_{\ell} | 0 \rangle, \quad (\text{D8})$$

where  $f_{\ell}(\theta)$  are sinusoidal functions of  $\theta$ , and  $\tilde{P}_{\ell}$  are newly propagated Pauli strings. More concretely, the functions  $f_{\ell}(\theta)$  are products of sine and cosine functions so that if  $f_{\ell}(\theta)$  contains many sine factors, it will be negligibly small if  $\theta \approx 0$  due to  $\sin \theta \approx \theta$ . This motivates the idea behind the approximation in Eq. (D8), where one truncates the terms containing many sine factors which do not contribute much to the error. This simulation technique is used for surrogating near-Clifford patches in the works of Lerch et al. [18].

In this approach, the decomposition number  $m$  depends on how frequently the Pauli-rotation gates in the circuit ansatz fail to commute with the Pauli strings in the observable. Their simulation strategy has a worst-case complexity of  $\mathcal{O}(|\mathcal{I}| 2^D)$ , but if all involved Pauli matrices are uniformly random, the average-case scaling improves to  $\mathcal{O}(|\mathcal{I}| 2^{0.59D})$  [24].

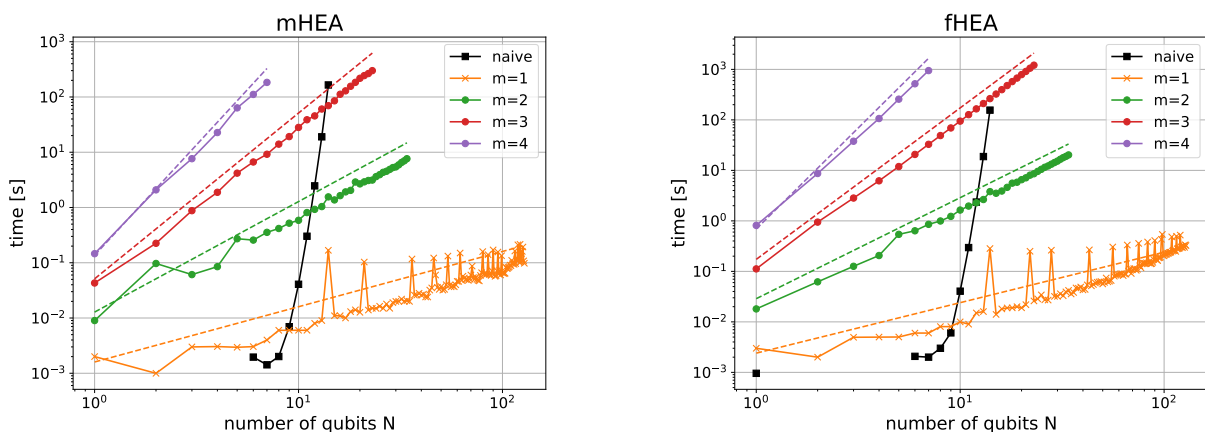


FIG. 10. Simulation time of  $C_m(\theta)$  using mHEA (left) and fHEA (right) for increasing qubit number  $N$  and Taylor orders  $m \leq 4$ . Due to the additional number of parameters, fHEA has a computational overhead of  $1.5^m$  compared to mHEA.

Although it exhibits worse scaling compared to Bravyi et al. [17, 23] this may be due to their analysis imposing no restrictions on the circuit model ansatz. However, their approach does not provide a closed-form expression for the truncation number  $m = K(\theta)$  as a function of  $\theta$ , making it less convenient for characterizing time complexity in terms of  $\theta$ . This may be due to the technical challenges of their perturbative expansion in the Heisenberg picture, which makes it difficult to analytically capture the dependency  $m = K(\theta)$ . In contrast, our approach offers a simple characterization of  $m = m(\theta)$  in Lemma 9, though at the expense of increased computational complexity when applied to simulating  $C(\theta)$ .

#### 4. Truncated Taylor series

Mitarai et al. [19] first introduced a Taylor approach for approximating the expectation value (D3) classically. Their method corresponds to the special case of a truncated Taylor expansion with  $m = 3$ :

$$C(\theta) \approx \sum_{\|\alpha\|_1 < m} (D_\theta^\alpha C)(0) \frac{\theta^\alpha}{\alpha!}, \quad (\text{D9})$$

where for each multi-index  $\alpha = (\alpha_1, \dots, \alpha_D)$  we use the notations  $D_\theta^\alpha := \partial_{\theta_1}^{\alpha_1} \dots \partial_{\theta_D}^{\alpha_D}$ ,  $\theta^\alpha := \theta_1^{\alpha_1} \dots \theta_D^{\alpha_D}$ ,  $\alpha! := \alpha_1! \dots \alpha_D!$ , and  $\|\alpha\|_1 := |\alpha_1| + \dots + |\alpha_D|$  denoting the  $\ell_1$ -norm of  $\alpha$ .

This expansion provides an explicit polynomial approximation of  $C(\theta)$ , enabling efficient classical evaluations for small values of  $\theta$ . Lerch et al. [18] also employed a truncated series of this form, not as a simulation method, but rather as part of their analysis in proving their results (cf. their Eq. (C6), and their Theorems 1 and 2).

One particularly interesting difference regarding the decomposition complexity  $|\mathcal{J}|$  is that the Taylor truncation threshold  $m$  is used to upper bound a set of multi-indices  $\{\alpha \in \mathbb{N}_0^D : \|\alpha\|_1 < m\}$ , while the other methods do not iterate over multi-indices. This distinction allows us to characterize complexity more easily as a function of  $\theta$  by focusing solely on the multi-index upper bound  $m = m(\theta)$  as evident from the proofs of Lemma 9 in Appendix I and Theorem 3 in the main text, respectively. Additionally, this explains why the scaling of our multi-index threshold  $m = m(\theta)$  in Fig. 3 is simpler compared to the full decomposition threshold used by Bravyi et al. [17] in Fig. 9, because an upper bound for multi-indices grows much smaller compared to the direct number of multi-indices. Furthermore, the simplicity of our formula ensures consistency with the law of large numbers, unlike the formula in [17, Eq. (14)] by Bravyi et al., which is not a sum of independent random variables.

Fig. 10 illustrates the cost of classically simulating  $C_m(\theta)$  under the two PQC models **mHEA** and **fHEA** (introduced in Appendix C), for various system sizes  $N$  and Taylor expansion orders  $m \leq 4$ . The simulations use uniformly random Pauli strings  $H = P_i$  (in particular  $|\mathcal{Z}| = 1$ ) and initialization  $\mathbb{P}_\theta \sim \mathcal{N}(0, \sigma^2 I_D)$  with  $\sigma = D^{-1}$ . Theorem 3 states that the time complexity of evaluating  $C_m(\theta)$  is a polynomial scaling as  $\mathcal{O}(D^m)$ . Using that **mHEA** and **fHEA** each satisfy  $D = 2N(L + 1)$  and  $D = 3N(L + 1)$ , respectively, we see that **fHEA** has a computational overhead of  $(3/2)^m = 1.5^m$ . For large  $m$ , computing  $3^m$  takes significantly more time and space resources than  $2^m$ . The special case  $m = 1$  corresponds to the Gottesman-Knill theorem [20, 21]. The dashed lines represent the theoretical prediction as per Theorem 3. As expected, higher-order approximations ( $m > 0$ ) lead to increased computational cost, especially as  $N$  grows.

The following sections present the proofs of our theoretical results, organized thematically for clarity. We begin by defining the PQC ansatz employed in our numerical experiments. This is followed by proofs of the high-order parameter-shift rules and cost function regularities. Subsequently, we introduce the Linear Clifford Encoder (LCE) and demonstrate how it can be leveraged to mitigate barren plateaus. We then establish that the LCE transformation preserves both the expressivity of the ansatz and the global structure of the optimization landscape. The subsequent sections address computational complexity. We first derive the minimal truncation threshold required for the Taylor surrogate and use this to characterize the associated computational cost. Finally, we provide additional numerical experiments to support our theoretical findings.

### Appendix E: High-Order Parameter-Shift Rules and Cost Regularity

In this section, we study the regularity properties of the cost function  $C(\cdot)$ . Recall from Eq. (6) that

$$C(\theta) := \langle \psi(\theta) | H | \psi(\theta) \rangle = \sum_{i \in \mathcal{I}} c_i \langle \psi(\theta) | P_i | \psi(\theta) \rangle. \quad (\text{E1})$$

We first establish smoothness and explicitly demonstrate differentiability using the standard parameter-shift rule [43, 44]. We then extend this to the higher-order parameter-shift rule [33] and leverage this structure to derive strong regularity bounds for the cost function.

For a fixed multi-index  $\alpha = (\alpha_1, \dots, \alpha_D) \in \mathbb{N}_0^D$ , we define the class  $\mathcal{C}^\alpha$  to be the space of functions  $f : [-\pi, \pi]^D \rightarrow \mathbb{R}$  for which the higher-order derivative  $D_\theta^\alpha f$  of  $f$  exists and is continuous. Note that the cost function  $C(\cdot)$  defines a smooth function, i.e.

$$C(\cdot) \in \bigcap_{\alpha \in \mathbb{N}_0^D} \mathcal{C}^\alpha =: \mathcal{C}^\infty. \quad (\text{E2})$$

Indeed, this immediately follows from the fact that the vector-valued mapping  $\theta \mapsto |\psi(\theta)\rangle = U(\theta)|0\rangle$  is smooth (since  $U(\theta)$  is a product involving smooth factors  $\exp(-i\theta_k/2 V_k)$  as per Eq. (4)), and that  $C(\theta) = \langle \psi(\theta) | H | \psi(\theta) \rangle$  is a quadratic form in the Hilbert space  $\mathcal{H}_N$  (that is, a multivariate polynomial).

The standard parameter-shift rule [43, 44] shows explicitly that  $C(\cdot)$  is differentiable:

**Lemma 2** (Vanilla Parameter-Shift Rule). *Consider an expectation of the form in Eq. (E1) with a variational ansatz  $U(\theta)$  involving  $D \geq 1$  parameters. Let  $\theta \in [-\pi, \pi]^D$  and  $k \in [D]$  be arbitrary. Then,  $C(\cdot)$  is continuous, and*

$$\partial_{\theta_k} C(\theta) = \frac{1}{2} \left\{ C\left(\theta + \frac{\pi}{2} e_k\right) - C\left(\theta - \frac{\pi}{2} e_k\right) \right\},$$

where  $e_k$  denotes the  $k$ -th unit vector.

*Proof.* Let  $\theta \in [-\pi, \pi]^D$  and  $k \in [D]$  be arbitrary. By definition of  $U(\cdot)$ , we may decompose

$$U(\theta) = \prod_{j=D}^1 U_j(\theta_j) W_j = \underbrace{\left( \prod_{j=D}^{k+1} U_j(\theta_j) W_j \right)}_{=: U_+} U_k(\theta_k) \underbrace{\left( W_k \prod_{j=k-1}^1 U_j(\theta_j) W_j \right)}_{=: U_-} = U_+ U_k(\theta_k) U_-, \quad (\text{E3})$$

where  $U_j(\theta_j) := \exp(-i\frac{\theta_j}{2} V_j)$  with each  $V_j \in \{X, Y, Z\}$  specifying the Pauli-rotation axis, and  $W_j \in \text{Clifford}(N)$ , respectively. Note that  $U_\pm$  are independent of  $\theta_k$ . In particular,

$$\partial_{\theta_k} C(\theta_k) = \partial_{\theta_k} \langle 0 | U(\theta)^\dagger H U(\theta) | 0 \rangle = \langle 0 | U_-^\dagger \partial_{\theta_k} \left\{ U_k(\theta_k)^\dagger U_+^\dagger H U_+ U_k(\theta_k) \right\} U_- | 0 \rangle. \quad (\text{E4})$$

Mitarai et al. [43] made the crucial observation that (redefining  $H_+ := U_+^\dagger H U_+$ )

$$[V_k, H_+] = i \left\{ U_k\left(\frac{\pi}{2}\right) H_+ U_k\left(-\frac{\pi}{2}\right) - U_k\left(-\frac{\pi}{2}\right) H_+ U_k\left(\frac{\pi}{2}\right) \right\}, \quad (\text{E5})$$

which directly follows from the fact that  $U_k(\pm\frac{\pi}{2}) = \frac{1}{\sqrt{2}}(I \mp iV_k)$ , obtained by applying Euler's identity  $U_k(\theta_k) = \exp(-i\frac{\theta_k}{2} V_k) = \cos\frac{\theta_k}{2} I - i \sin\frac{\theta_k}{2} V_k$ . Also, note that  $V_k = V_k^\dagger$  and  $V_k^2 = I$ . Indeed, Eq. (E5) allows us to compute the derivative

$$\begin{aligned} \partial_{\theta_k} \left\{ U_k(\theta_k)^\dagger U_+^\dagger H U_+ U_k(\theta_k) \right\} &= \left\{ \partial_{\theta_k} U_k(\theta_k) \right\}^\dagger H_+ U_k(\theta_k) + U_k(\theta_k)^\dagger H_+ \left\{ \partial_{\theta_k} U_k(\theta_k) \right\} \\ &= \frac{i}{2} U_k(\theta_k)^\dagger V_k H_+ U_k(\theta_k) - \frac{i}{2} U_k(\theta_k)^\dagger H_+ V_k U_k(\theta_k) \\ &= \frac{i}{2} U_k(\theta_k)^\dagger [V_k, H_+] U_k(\theta_k) \\ &\stackrel{(\text{E5})}{=} -\frac{1}{2} \left\{ U_k(\theta_k)^\dagger U_k\left(\frac{\pi}{2}\right) H_+ U_k\left(-\frac{\pi}{2}\right) U_k(\theta_k) - U_k(\theta_k)^\dagger U_k\left(-\frac{\pi}{2}\right) H_+ U_k\left(\frac{\pi}{2}\right) U_k(\theta_k) \right\} \\ &= \frac{1}{2} \left\{ U_k\left(\theta_k + \frac{\pi}{2}\right)^\dagger H_+ U_k\left(\theta_k + \frac{\pi}{2}\right) - U_k\left(\theta_k - \frac{\pi}{2}\right)^\dagger H_+ U_k\left(\theta_k - \frac{\pi}{2}\right) \right\}, \quad (\text{E6}) \end{aligned}$$

using  $\partial_{\theta_k} U_k(\theta_k) = -\frac{i}{2} V_k U_k(\theta_k)$ , and in the last equality,  $U_k(\pm\theta_k)^\dagger = U_k(\mp\theta_k)$  and  $U_k(\theta_k \pm \frac{\pi}{2}) = U_k(\theta_k) U_k(\pm\frac{\pi}{2})$ , respectively. Returning to Eq. (E4), it now easily follows that

$$\begin{aligned} \partial_{\theta_k} C(\theta_k) &= \langle 0 | U_-^\dagger \partial_{\theta_k} \{ U_k(\theta_k)^\dagger H_+ U_k(\theta_k) \} U_- | 0 \rangle \\ &= \frac{1}{2} \langle 0 | \left\{ U_-^\dagger U_k \left( \theta_k + \frac{\pi}{2} \right)^\dagger U_+^\dagger H U_+ U_k \left( \theta_k + \frac{\pi}{2} \right) U_- - U_-^\dagger U_k \left( \theta_k - \frac{\pi}{2} \right)^\dagger U_+^\dagger H U_+ U_k \left( \theta_k - \frac{\pi}{2} \right) U_- \right\} | 0 \rangle \\ &= \frac{1}{2} \left\{ \langle 0 | U \left( \theta + \frac{\pi}{2} e_k \right)^\dagger H U \left( \theta + \frac{\pi}{2} e_k \right) | 0 \rangle - \langle 0 | U \left( \theta - \frac{\pi}{2} e_k \right)^\dagger H U \left( \theta - \frac{\pi}{2} e_k \right) | 0 \rangle \right\} \\ &= \frac{1}{2} \left\{ C \left( \theta + \frac{\pi}{2} e_k \right) - C \left( \theta - \frac{\pi}{2} e_k \right) \right\}, \end{aligned} \quad (\text{E7})$$

as desired.  $\square$

The next lemma generalizes the previous result to arbitrary high-order derivatives  $D_\theta^\alpha C(\cdot)$ , and may be considered an explicit proof of the regularity property in Eq. (E2):

**Lemma 3.** *Consider an expectation of the form Eq. (E1) with a variational ansatz  $U(\theta)$  involving  $D \geq 1$  parameters. Let  $\theta \in [-\pi, \pi]^D$  and  $\alpha \in \mathbb{N}_0^D$  be arbitrary but fixed. Then, the higher-order derivative of  $C(\theta)$  satisfies*

$$D_\theta^\alpha C(\theta) = \frac{1}{2^{\|\alpha\|_1}} \sum_{j \leq \alpha} (-1)^{\|j\|_1} \binom{\alpha}{j} C \left( \theta + \frac{\pi}{2} (\alpha - 2j) \right), \quad (\text{E8})$$

where  $\binom{\alpha}{j} := \prod_{k=1}^D \binom{\alpha_k}{j_k}$ , and the indexing set  $\{j \leq \alpha\}$  defined as  $\{j \in \mathbb{N}_0^D : j_k \leq \alpha_k \forall k \in [D]\}$ . The multi-index expressions  $\alpha - 2j$  are to be understood point-wise. In particular,  $(D_\theta^\alpha C)(\cdot)$  is continuous. If  $\theta = 0$ , the computational cost of evaluating Eq. (E8) is of order  $\mathcal{O}(D |\mathcal{I}| 2^{\|\alpha\|_1})$ , which is polynomial if  $\|\alpha\|_1 = \mathcal{O}(\log D)$ . Furthermore,  $C(\cdot)$  satisfies the strong regularity property that for each  $\alpha \in \mathbb{N}_0^D$ ,

$$\sup_{\theta \in [-\pi, \pi]^D} |D_\theta^\alpha C(\theta)| \leq \|H\|,$$

where  $\|H\|$  denotes the operator norm of the observable in Eq. (5).

*Proof.* Let  $\theta \in [-\pi, \pi]^D$  and  $\alpha \in \mathbb{N}_0^D$  be arbitrary. By the vanilla parameter-shift rule, Lemma 2, we know that

$$\partial_{\theta_k} C(\theta) = \frac{1}{2} \left\{ C \left( \theta + \frac{\pi}{2} e_k \right) - C \left( \theta - \frac{\pi}{2} e_k \right) \right\} \quad (\text{E9})$$

for all  $k \in [D]$ , where  $e_k$  denotes the  $k$ -th unit vector. This is precisely the formula for the central finite difference of  $C(\cdot)$ . Inductively over  $\alpha_k \geq 1$ , one easily establishes the higher-order generalization of the central finite difference formula, i.e.

$$\partial_{\theta_k}^{\alpha_k} C(\theta) = \frac{1}{2^{\alpha_k}} \sum_{j_k=0}^{\alpha_k} (-1)^{j_k} \binom{\alpha_k}{j_k} C \left( \theta + \pi \left( \frac{\alpha_k}{2} - j_k \right) e_k \right) \quad (\text{E10})$$

for all  $k \in [D]$ . Indeed, the case  $\alpha_k = 1$  follows directly from Eq. (E9). Assume that Eq. (E10) is true for some fixed  $\alpha_k \geq 1$ . Then, by induction,

$$\begin{aligned} \partial_{\theta_k}^{\alpha_k+1} C(\theta) &= \partial_{\theta_k} \{ \partial_{\theta_k}^{\alpha_k} C(\theta) \} \\ &\stackrel{(\text{E10})}{=} \frac{1}{2^{\alpha_k}} \sum_{j_k=0}^{\alpha_k} (-1)^{j_k} \binom{\alpha_k}{j_k} \partial_{\theta_k} C \left( \theta + \pi \left( \frac{\alpha_k}{2} - j_k \right) e_k \right) \\ &= \frac{1}{2^{\alpha_k+1}} \sum_{j_k=0}^{\alpha_k} (-1)^{j_k} \binom{\alpha_k}{j_k} \left\{ C \left( \theta + \pi \left( \frac{\alpha_k+1}{2} - j_k \right) e_k \right) - C \left( \theta - \pi \left( \frac{\alpha_k+1}{2} - j_k \right) e_k \right) \right\} \\ &= \frac{1}{2^{\alpha_k+1}} \sum_{j_k=0}^{\alpha_k+1} (-1)^{j_k} \binom{\alpha_k+1}{j_k} C \left( \theta + \pi \left( \frac{\alpha_k+1}{2} - j_k \right) e_k \right), \end{aligned} \quad (\text{E11})$$

where the second equality makes use of Eq. (E9) as follows:

$$\begin{aligned} \partial_{\theta_k} C \left( \theta + \pi \left( \frac{\alpha_k}{2} - j_k \right) e_k \right) &\stackrel{(E9)}{=} \frac{1}{2} \left\{ C \left( \theta + \pi \left( \frac{\alpha_k}{2} - j_k \right) e_k + \frac{\pi}{2} e_k \right) - C \left( \theta - \pi \left( \frac{\alpha_k}{2} - j_k \right) e_k - \frac{\pi}{2} e_k \right) \right\} \\ &= \frac{1}{2} \left\{ C \left( \theta + \pi \left( \frac{\alpha_k + 1}{2} - j_k \right) e_k \right) - C \left( \theta - \pi \left( \frac{\alpha_k + 1}{2} - j_k \right) e_k \right) \right\}. \end{aligned} \quad (E12)$$

Next, note that for each pair  $k' \neq k$  in  $[D]$ ,

$$\begin{aligned} \partial_{\theta_{k'}}^{\alpha_{k'}} \partial_{\theta_k}^{\alpha_k} C(\theta) &= \frac{1}{2^{\alpha_k}} \sum_{j_k=0}^{\alpha_k} (-1)^{j_k} \binom{\alpha_k}{j_k} \cdot \partial_{\theta_{k'}}^{\alpha_{k'}} C \left( \theta + \pi \left( \frac{\alpha_k}{2} - j_k \right) e_k \right) \\ &= \frac{1}{2^{\alpha_k}} \sum_{j_k=0}^{\alpha_k} (-1)^{j_k} \binom{\alpha_k}{j_k} \cdot \frac{1}{2^{\alpha_{k'}}} \sum_{j_{k'}=0}^{\alpha_{k'}} (-1)^{j_{k'}} \binom{\alpha_{k'}}{j_{k'}} C \left( \theta + \pi \left( \frac{\alpha_k}{2} - j_k \right) e_k + \pi \left( \frac{\alpha_{k'}}{2} - j_{k'} \right) e_{k'} \right) \\ &= \frac{1}{2^{\alpha_k + \alpha_{k'}}} \sum_{j_k=0}^{\alpha_k} \sum_{j_{k'}=0}^{\alpha_{k'}} (-1)^{j_k + j_{k'}} \binom{\alpha_k}{j_k} \binom{\alpha_{k'}}{j_{k'}} C \left( \theta + \pi \left( \frac{\alpha_k}{2} - j_k \right) e_k + \pi \left( \frac{\alpha_{k'}}{2} - j_{k'} \right) e_{k'} \right). \end{aligned} \quad (E13)$$

Applying these calculations successively for each  $k \in [D]$ , one finally obtains the multi-variate higher-order formula

$$\begin{aligned} D_{\theta}^{\alpha} C(\theta) &= \partial_{\theta_1}^{\alpha_1} \dots \partial_{\theta_D}^{\alpha_D} C(\theta) = \frac{1}{2^{\alpha_1 + \dots + \alpha_D}} \sum_{j_1=0}^{\alpha_1} \dots \sum_{j_D=0}^{\alpha_D} (-1)^{j_1 + \dots + j_D} \binom{\alpha_1}{j_1} \dots \binom{\alpha_D}{j_D} C \left( \theta + \pi \sum_{k=1}^D \left( \frac{\alpha_k}{2} - j_k \right) e_k \right) \\ &= \frac{1}{2^{\|\alpha\|_1}} \sum_{\substack{j \in \mathbb{N}_0^D \\ j_k \leq \alpha_k \forall k}} (-1)^{|j|} \binom{\alpha}{j} C \left( \theta + \frac{\pi}{2} \sum_{k=1}^D (\alpha_k - 2j_k) e_k \right), \end{aligned} \quad (E14)$$

of the central finite difference, as desired.

In order to show the uniform bound, let  $j \in \mathbb{N}_0^D$  be arbitrary with  $j_k \leq \alpha_k$  for all  $k \in [D]$ . Let us define the shifted parameter  $\theta_{j,\alpha} := \theta + \frac{\pi}{2} \sum_{k=1}^D (\alpha_k - 2j_k) e_k$ . Then, we apply sub-multiplicativity of norms in order to establish the bound

$$|C(\theta_{j,\alpha})| = |\langle \psi_{\theta_{j,\alpha}} | H | \psi_{\theta_{j,\alpha}} \rangle| \leq \|H\| \cdot \underbrace{|\langle \psi_{\theta_{j,\alpha}} | \psi_{\theta_{j,\alpha}} \rangle|}_{=1} = \|H\|, \quad (E15)$$

using the notation  $|\psi_{\theta_{j,\alpha}}\rangle = U(\theta_{j,\alpha})|0\rangle$ . Since this holds for arbitrary  $j$  and  $\alpha$  as above, by the previous computations, we may conclude with the uniform bound

$$|D_{\theta}^{\alpha} C(\theta)| \leq \frac{1}{2^{|\alpha|}} \sum_{\substack{j \in \mathbb{N}_0^D \\ j_k \leq \alpha_k \forall k}} \binom{\alpha}{j} \underbrace{\left| C \left( \theta + \frac{\pi}{2} \sum_{k=1}^D (\alpha_k - 2j_k) e_k \right) \right|}_{=|C(\theta_{j,\alpha})| \leq \|H\|} \leq \|H\| \frac{1}{2^{|\alpha|}} \sum_{\substack{j \in \mathbb{N}_0^D \\ j_k \leq \alpha_k \forall k}} \binom{\alpha}{j} = \|H\|, \quad (E16)$$

where in the last step follows from the binomial theorem, i.e.

$$\sum_{\substack{j \in \mathbb{N}_0^D \\ j_k \leq \alpha_k \forall k}} \binom{\alpha}{j} = \sum_{j_1=0}^{\alpha_1} \dots \sum_{j_D=0}^{\alpha_D} \prod_{k=1}^D \binom{\alpha_k}{j_k} = \prod_{k=1}^D \left( \sum_{j_k=0}^{\alpha_k} \binom{\alpha_k}{j_k} \right) = \prod_{k=1}^D 2^{\alpha_k} = 2^{|\alpha|}. \quad (E17)$$

Since  $\theta \in \mathbb{R}^D$  and  $\alpha \in \mathbb{N}_0^D$  were arbitrary, this completes the first part of the lemma.

It remains to show that, if  $\theta = 0$ , then the computational cost of evaluating Eq. (E8) is of order  $\mathcal{O}(D |\mathcal{I}| 2^{\|\alpha\|_1})$ . Each evaluation of  $C(\xi_{j,\alpha})$  using Gottesman-Knill's theorem requires  $\mathcal{O}(D |\mathcal{I}|)$  operations since all unitaries  $U(\xi_{j,\alpha})$  involved are Clifford operators (cf. last part of the proof of Theorem 3 in Appendix J). The number of times we need to evaluate  $C(\xi_{j,\alpha})$  is given by the cardinality

$$\#\{j \leq \alpha\} = \#\{j \in \mathbb{N}_0^D : j_k \leq \alpha_k \forall k \in [D]\} = \prod_{k=1}^D \underbrace{(\alpha_k + 1)}_{\leq 2^{\alpha_k}} \leq 2^{\sum_{k=1}^D \alpha_k} = 2^{\|\alpha\|_1}. \quad (E18)$$

Therefore, the total cost of evaluating Eq. (E8) is indeed  $\mathcal{O}(D |\mathcal{I}| 2^{\|\alpha\|_1})$ .  $\square$

## Appendix F: Construction of the Linear Clifford Encoder (LCE)

We now construct the LCE transformation used to mitigate the barren plateau problem [12]. The approach involves modifying the PQC via a pair  $(Q, \tilde{Q})$  of Clifford operators such that the  $k$ -th gradient component satisfies  $(\partial_{\theta_k} C)(0) = \pm 1$ , ensuring it is non-zero at the origin. This is accomplished by propagating the shifted Clifford operators  $U(\xi_{j,\alpha})$  through the Pauli observable  $H = P$ , yielding diagonal Pauli strings  $\tilde{P}_j := U(\xi_{j,\alpha})^\dagger P U(\xi_{j,\alpha})$  with a relative phase. Afterwards, we generalize this result to arbitrary, non-identity observables of the general form

$$H = \sum_{i \in \mathcal{I}} c_i P_i, \quad (\text{F1})$$

with Pauli strings  $P_i \in \mathcal{P}_N \setminus \{I\}$  and real coefficients  $c_i \in \mathbb{R}$ .

In what follows, we use  $\langle A, B \rangle_N$  to denote the multiplicative subgroup of the unitary group  $U(2^N)$ , generated by the matrices  $A$  and  $B$ , modulo the global phase factors  $\pm, \pm i$ . For example, it is well-known [27] that the Clifford group is equal to  $\langle H, S, CX \rangle_N$ . In practice, this means that a Clifford circuit is constructed from elementary gates in the ensemble  $\{H, S, CX\}$ . As another example, recall that the  $N$ -qubit Pauli group is defined as

$$\mathcal{P}_N := \langle X, Y, Z \rangle_N = \{\pm P, \pm i P : P = P_1 \otimes \cdots \otimes P_N, \forall j \in [N] : P_j \in \{I, X, Y, Z\}\}. \quad (\text{F2})$$

We generally consider

$$U(\cdot) \in \langle R_X(\cdot), R_Y(\cdot), R_Z(\cdot), \text{Clifford}(N) \rangle_N \quad (\text{F3})$$

to be generated by single-qubit rotation gates and Clifford-operators,  $\text{Clifford}(N) = \langle H, S, CX \rangle_N$ , acting on a  $N$ -qubit system. It is well-known that this defines a universal gate set.

### 1. Explicit Construction of the Linear Clifford Encoder (LCE)

The following theorem shows how to explicitly construct the LCE pair  $(Q, \tilde{Q})$  which plays a central role in our barren plateau mitigation technique. We begin by handling the case where the observable  $H = P$  is a single Pauli string. Afterwards, we show that the same construction may be used for arbitrary observables.

**Theorem 7.** *Consider an expectation of the form Eq. (E1) with a variational ansatz  $U(\theta)$  consisting of Clifford-gates and single-qubit Pauli-rotation gates involving  $D \geq 1$  parameters. Assume that the observable  $H = P$  in Eq. (F1) is a single Pauli string. Then, for every  $k \in [D]$  there exist two explicitly determined Clifford operators  $Q \in \langle H, S, CX \rangle_N$  and  $\tilde{Q} \in \langle H, S \rangle_N$  such that*

$$(\partial_{\theta_k} C)(0) = \frac{1}{2} \left\{ \langle 0 | Q^\dagger \tilde{P}^{0, e_k} Q | 0 \rangle - \langle 0 | Q^\dagger \tilde{P}^{e_k, e_k} Q | 0 \rangle \right\} = \pm 1,$$

after replacing  $U(\theta)$  with  $\tilde{Q} U(\theta) Q$ , where  $\tilde{P}^{j, \alpha} := U(\xi_{j, \alpha})^\dagger \tilde{Q}^\dagger P \tilde{Q} U(\xi_{j, \alpha})$ , and  $\xi_{j, \alpha} := \frac{\pi}{2}(\alpha - 2j)$  for multi-indices  $\alpha \in \mathbb{N}_0^D$  and  $0 \leq j \leq \alpha$  (i.e.  $0 \leq j_k \leq \alpha_k$  for all  $k \in [D]$ ).

*Proof.* Let  $k \in [D]$  be arbitrary, and the Clifford pair  $(Q, \tilde{Q})$  to be determined.

**Step 1: Higher-Order Parameter-Shift Rule.** First, we apply the higher-order parameter-shift rule, Lemma 3, with  $\xi_{0, e_k} = \frac{\pi}{2} e_k$  and  $\xi_{e_k, e_k} = -\frac{\pi}{2} e_k$ , which results in

$$\begin{aligned} (\partial_{\theta_k} C)(0) &= \frac{1}{2} \{ C(\xi_{0, e_k}) - C(\xi_{e_k, e_k}) \} \\ &= \frac{1}{2} \left\{ \langle 0 | Q^\dagger U(\xi_{0, e_k})^\dagger \tilde{Q}^\dagger P \tilde{Q} U(\xi_{0, e_k}) Q | 0 \rangle - \langle 0 | Q^\dagger U(\xi_{e_k, e_k})^\dagger \tilde{Q}^\dagger P \tilde{Q} U(\xi_{e_k, e_k}) Q | 0 \rangle \right\} \\ &= \frac{1}{2} \left\{ \langle 0 | Q^\dagger \tilde{P}^{0, e_k} Q | 0 \rangle - \langle 0 | Q^\dagger \tilde{P}^{e_k, e_k} Q | 0 \rangle \right\}. \end{aligned} \quad (\text{F4})$$

The idea is to engineer the pair  $(Q, \tilde{Q})$  of Clifford operators as follows: First, we design  $\tilde{Q}$  explicitly for inducing a relative phase, i.e.

$$\text{sign } \tilde{P}^{0,e_k} \stackrel{!}{\neq} \text{sign } \tilde{P}^{e_k,e_k} \quad (\text{F5})$$

Here, the notation “!” means that we would like to achieve the desired relation by adjusting free parameters (in that case  $\tilde{Q}$ ). Next, after determining  $\tilde{Q}$ , we explicitly design  $Q$  such that it simultaneously diagonalizes  $\tilde{P}^{0,e_k}$  and  $\tilde{P}^{e_k,e_k}$ . That is,

$$Q^\dagger \tilde{P}^{0,e_k} Q, Q^\dagger \tilde{P}^{e_k,e_k} Q \in \langle Z \rangle_N. \quad (\text{F6})$$

Engineering the pair  $(Q, \tilde{Q})$  that way thus implies

$$\langle 0 | Q^\dagger \tilde{P}^{0,e_k} Q | 0 \rangle - \langle 0 | Q^\dagger \tilde{P}^{e_k,e_k} Q | 0 \rangle \stackrel{(\text{F6})}{=} \text{sign } \tilde{P}^{0,e_k} - \text{sign } \tilde{P}^{e_k,e_k} \stackrel{(\text{F5})}{=} \pm 2, \quad (\text{F7})$$

which, substituted into Eq. (F4), results in the desired equality.

**Step 2: Relative Phase via  $\tilde{Q}$ .** Let us begin by designing  $\tilde{Q} \in \langle H, S, CX \rangle_N$ . In general, since  $U(\cdot)$  is generated according to Eq. (F3), we may decompose

$$U(\xi_{j,e_k}) = W_a R_{V_k} \left( \pm \frac{\pi}{2} e_k \right) W_b \quad (\text{F8})$$

for some Clifford operators  $W_a, W_b \in \langle H, S, CX \rangle_N$ . Thus, evolving the input Pauli string  $P$  through the Clifford  $\tilde{Q} U(\xi_{j,e_k})$  in the Heisenberg picture yields the evolved Pauli string,

$$\tilde{P}^{j,e_k} = U(\xi_{j,\alpha})^\dagger \tilde{Q}^\dagger P \tilde{Q} U(\xi_{j,\alpha}) = W_b^\dagger R_{V_k} \left( \pm \frac{\pi}{2} e_k \right)^\dagger W_a^\dagger \tilde{Q}^\dagger P \tilde{Q} W_a R_{V_k} \left( \pm \frac{\pi}{2} e_k \right) W_b. \quad (\text{F9})$$

The only way to obtain a relative phase, specifically different signs as per Eq. (F5), is to design  $\tilde{Q}$  systematically such that

$$R_{V_k} \left( \pm \frac{\pi}{2} e_k \right)^\dagger W_a^\dagger \tilde{Q}^\dagger P \tilde{Q} W_a R_{V_k} \left( \pm \frac{\pi}{2} e_k \right) \in \{\pm \Pi, \mp \Pi\} \quad (\text{F10})$$

for some unsigned Pauli string  $\Pi \in \mathcal{P}_N$ .

TABLE IV. Update rules for conjugating Pauli strings  $\Pi$  with Clifford operators  $C$ .

Clifford $C$	Input Pauli $\Pi \rightarrow$ Output Pauli $C^\dagger \Pi C$		
$R_X(\pm \frac{\pi}{2})$	$X \rightarrow X$	$Y \rightarrow \mp Z$	$Z \rightarrow \pm Y$
$R_Y(\pm \frac{\pi}{2})$	$X \rightarrow \pm Z$	$Y \rightarrow Y$	$Z \rightarrow \mp X$
$R_Z(\pm \frac{\pi}{2})$	$X \rightarrow \mp Y$	$Y \rightarrow \pm X$	$Z \rightarrow Z$

With the help of Table IV one establishes that for every pair  $(V, \Pi_1)$  of unsigned, single-qubit Pauli-operators, there exists an unsigned Pauli-operator  $\Pi_2$  such that  $\Pi_1 \neq \Pi_2$  and

$$R_V \left( \pm \frac{\pi}{2} \right)^\dagger \Pi_1 R_V \left( \pm \frac{\pi}{2} \right) \in \{\pm \Pi_2, \mp \Pi_2\} \quad \text{if and only if} \quad \Pi_1 \notin \{I, V\}. \quad (\text{F11})$$

We make the ansatz  $\tilde{Q} := \tilde{W} W_a^\dagger$  for some Clifford  $\tilde{W}$  to be determined, and it will follow that Eq. (F10) holds true if and only if

$$(\tilde{W}^\dagger P \tilde{W})_k \notin \{I, V_k\}. \quad (\text{F12})$$

Indeed, the factor  $W_a^\dagger$  is used to cancel with  $W_a$ , and the Clifford operator  $\tilde{W}$  remains to be designed such that a relative phase is induced as per Eq. (F5).

We briefly recall the indexing convention for Pauli operators: For a Pauli string  $P \in \mathcal{P}_N$ , we use the notation  $P_k \in \{I, X, Y, Z\}$  to denote the  $k$ -th component of the tensor product  $P = P_1 \otimes \cdots \otimes P_N$ . Equivalently,  $P_k$  may be interpreted as the  $N$ -qubit operator  $I_{2^{k-1}} \otimes P_k \otimes I_{2^{N-k}}$ . For  $2 \times 2$  operators  $A$  (like  $H$  and  $S$ ), we analogously denote  $A_k := I_{2^{k-1}} \otimes A \otimes I_{2^{N-k}}$ . These conventions are used to simplify our construction. The goal is now to construct  $\tilde{W}$  such that Eq. (F12) is satisfied:

Recall that we have fixed  $k \in [D]$  for the LCE construction. First, consider the case where  $P_k \neq I$ . If  $V_k \neq P_k$ , then Eq. (F12) holds true with the identity  $\tilde{W} := I$ . If  $V_k = P_k$ , then define

$$\tilde{W} := \begin{cases} H_k, & V_k \in \{X, Z\}, \\ S_k, & V_k = Y, \end{cases} \quad (\text{F13})$$

and it follows from Table VI below that Eq. (F12) is satisfied.

For the case where  $P_k = I$ , we are going to decompose  $\tilde{W} := \tilde{W}_1 \tilde{W}_2$  into two Clifford operators  $\tilde{W}_1 \in \langle \text{CX} \rangle_N$ , and  $\tilde{W}_2 \in \langle H, S \rangle_N$ , respectively. Due to the fact that  $P \neq I$  is non-trivial, there exists  $i \in [N]$  such that  $P_i \neq I$ . Define

$$\tilde{W}_1 := \begin{cases} \text{CX}_{i,k}, & P_i \in \{X, Y\}, \\ \text{CX}_{k,i}, & P_i = Z, \end{cases} \quad (\text{F14})$$

where the entangling gate  $\text{CX}_{i,j}$  has control  $i$  and target  $j$ .

TABLE V. Update rules for conjugating Pauli strings  $R$  with Clifford operators  $C$ .

Clifford $C$	Input Pauli $R \rightarrow$ Output Pauli $C^\dagger R C$		
$\text{CX}_{i,j}$	$X_i \rightarrow X_i X_j$	$Y_i \rightarrow Y_i X_j$	$Z_i \rightarrow Z_i$
	$X_j \rightarrow X_j$	$Y_j \rightarrow Z_i Y_j$	$Z_j \rightarrow Z_i Z_j$

With the help of Table V we see that

$$(\tilde{W}_1^\dagger P \tilde{W}_1)_k = \begin{cases} X_k, & P_i \in \{X, Y\}, \\ Z_k, & P_i = Z, \end{cases} \neq I. \quad (\text{F15})$$

Hence, we may construct  $\tilde{W}_2$  analogous to the previous case,  $P_k \neq I$ . That is, if  $V_k \neq (\tilde{W}_1^\dagger P \tilde{W}_1)_k$ , then Eq. (F12) holds true with  $\tilde{W}_2 = I$ . Otherwise, if  $V_k = (\tilde{W}_1^\dagger P \tilde{W}_1)_k$ , we may define

$$\tilde{W}_2 := \begin{cases} H_k, & V_k \in \{X, Z\}, \\ S_k, & V_k = Y, \end{cases} \quad (\text{F16})$$

and it follows from Table VI below that Eq. (F12) is satisfied.

**Step 3: Simultaneous Diagonalization via  $Q$ .** It remains to design  $Q \in \langle H, S \rangle_N$ . We make the ansatz  $Q = Q_1 \otimes \cdots \otimes Q_N$  and define

$$Q_i := \begin{cases} H, & \tilde{P}_i^{0,e_k} = X, \\ SH, & \tilde{P}_i^{0,e_k} = Y, \\ I, & \text{else.} \end{cases} \quad (\text{F17})$$

With the help of Table VI, one obtains that

$$Q^\dagger \tilde{P}^{0,e_k} Q = \bigotimes_{i=1}^N \underbrace{Q_i^\dagger \tilde{P}_i^{0,e_k} Q_i}_{\in \{I, \pm Z\}} \in \langle Z \rangle_N \quad (\text{F18})$$

is diagonal. Since  $\tilde{P}^{0,e_k}$  and  $\tilde{P}^{e_k,e_k}$  only differ by the sign, we also have that  $Q^\dagger \tilde{P}^{e_k,e_k} Q \in \langle Z \rangle_N$  is diagonal.

TABLE VI. Update rules for conjugating Pauli strings  $R$  with Clifford operators  $C$ .

Clifford $C$	Input Pauli $R \rightarrow$ Output Pauli $C^\dagger R C$		
$H$	$X \rightarrow Z$	$Y \rightarrow -Y$	$Z \rightarrow X$
$S$	$X \rightarrow -Y$	$Y \rightarrow X$	$Z \rightarrow Z$
$SH$	$X \rightarrow Y$	$Y \rightarrow Z$	$Z \rightarrow X$

We have thus successfully constructed the pair  $(Q, \tilde{Q})$  of Clifford operators such that Eqs. (F5) and (F6) are simultaneously satisfied. Therefore, by Eq. (F4), we have established that

$$(\partial_{\theta_k} C)(0) = \frac{1}{2} \left\{ \langle 0 | Q^\dagger \tilde{P}^{0, e_k} Q | 0 \rangle - \langle 0 | Q^\dagger \tilde{P}^{e_k, e_k} Q | 0 \rangle \right\} \stackrel{\text{(F6)}}{=} \frac{1}{2} \left\{ \text{sign } \tilde{P}^{0, e_k} - \text{sign } \tilde{P}^{e_k, e_k} \right\} \stackrel{\text{(F5)}}{=} \pm 1, \quad (\text{F19})$$

which completes the proof of the theorem.  $\square$

We refer to the Clifford pair  $(Q, \tilde{Q})$  used to transform the circuit  $U(\cdot)$  into  $\tilde{Q}U(\cdot)Q$  as the *Linear Clifford Encoder (LCE)*, since it is constructed to render the  $k$ -th linear Taylor coefficient constant, i.e.  $(\partial_{\theta_k} C)(0) = \pm 1$ .

In Fig. 11 we use a numerical experiment to illustrate geometrically how LCE transforms the loss landscape  $C(\cdot)$ . We consider a  $N = 12$  qubit mHEA-model with  $L = 6$  layers, and focus on the global observable  $Z^{\otimes N}$ . For the LCE construction, we pick the direction  $k = 1$ , and evaluate the cost  $C(\theta_1 e_1 + \theta_k e_k)$  for all non-LCE directions  $k \neq 1$ , where  $e_k$  denotes the  $k$ -th unit vector. This results in an equidistant grid  $\{\theta_1 e_1 + \theta_k e_k\}$  (we use  $30 \times 30$  points) on which we evaluate the cost  $C(\cdot)$ . Then, we average over all non-LCE directions, i.e.  $\mathbb{E}_{k \in [D] \setminus 1} [C(\theta_1 e_1 + \theta_k e_k)]$ , which are always used as the vertical axis in the plot. We can see that LCE ensures a better gradient when initializing close to  $\theta = 0$ , as predicted by Theorem 2. This is due to initializing at the steepest slope of the landscape (green-blue area where  $C(\theta) \approx 0$ ), which ensures a gradient “boost” in the positive LCE-direction (which could be exploited for momentum). The landscape appears to be shifted to the left in the LCE direction by  $\pi/2$  (stemming from the operator  $Q$  causing a translation), and then slightly stretched in the non-LCE directions (stemming from the operator  $\tilde{Q}$  causing a change of basis). In the case of  $Z^{\otimes N}$ , this transformation guarantees faster convergence to the global minimum value  $-1$  when directly employing gradient descent with sufficiently small learning rates (cf. Fig. 7). On the other hand, the non-LCE loss landscape has a global maximum at  $\theta = 0$ , showing that using vanilla gradient descent requires more iterations compared to LCE. In fact, using LCE in this situation even results in closer parameter initialization to the solution.

We have explained how to make the gradient constant in one direction. This naturally raises the question of whether multiple gradient components can be controlled simultaneously. In principle, this is possible to some extent: one must

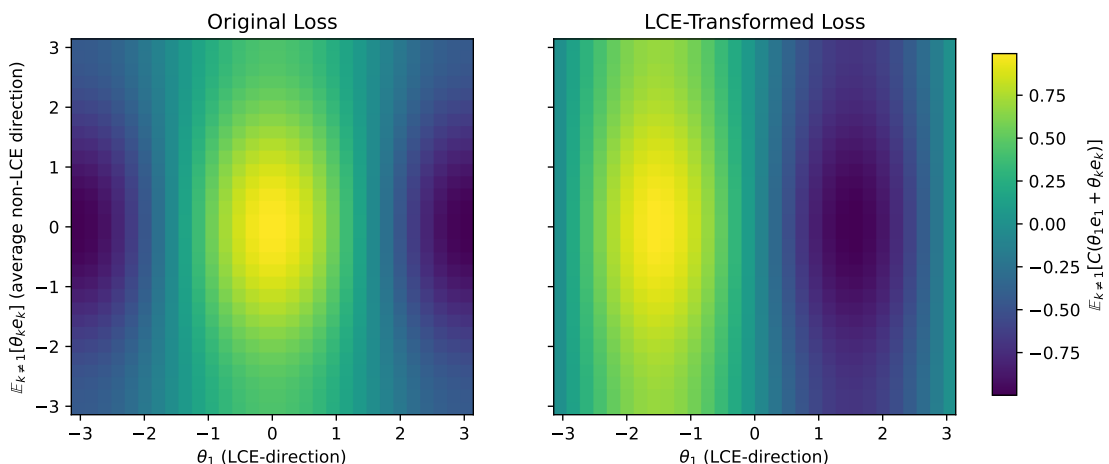


FIG. 11. Illustrating the landscape transformation effect of LCE for a mHEA-model with  $N = 12$  qubits,  $L = 6$  layers and  $H = Z^{\otimes N}$  as the observable. We fix  $k = 1$  as the LCE direction, and average the grids  $\{C(\theta_1 e_1 + \theta_k e_k) : \theta_1, \theta_k \in [-\pi, \pi]\}$  over non-LCE directions  $k \neq 1$  (always used as the vertical axis).

solve an over-determined system of operator equations. As the number of components increases, the likelihood of a solution decreases. The following elaborates the details:

Consider a collection  $\mathcal{K} \subseteq [D]$  of gradient elements we would like to control. We would like to construct a stronger LCE  $(Q, \tilde{Q})$  in the sense that

$$(\partial_{\theta_k} C)(0) = \pm 1 \quad \text{for all } k \in \mathcal{K} \quad (\text{F20})$$

after replacing  $U(\theta)$  with  $\tilde{Q} U(\theta) Q$ . To see how this works, for each  $k \in \mathcal{K}$  we decompose

$$U(\xi_{j,e_k}) = W_{a_k} R_{V_k} \left( \pm \frac{\pi}{2} e_k \right) W_{b_k} \quad (\text{F21})$$

for some Clifford operators  $W_{a_k}, W_{b_k} \in \langle H, S, CX \rangle_N$ . The solution (if it exists) is determined by the system of  $2\#\mathcal{K}$  operator equations:

$$\left\{ \begin{array}{l} (W_{a_k}^\dagger \tilde{Q}^\dagger P \tilde{Q} W_{a_k})_k \notin \{I, V_k\} \\ Q^\dagger W_{b_k}^\dagger R_{V_k} (\pm \frac{\pi}{2} e_k)^\dagger W_{a_k}^\dagger \tilde{Q}^\dagger P \tilde{Q} W_{a_k} R_{V_k} (\pm \frac{\pi}{2} e_k) W_{b_k} Q \in \langle Z \rangle_N \end{array} : k \in \mathcal{K} \right\}. \quad (\text{F22})$$

The difficulty of finding a solution  $(Q, \tilde{Q})$  in Eq. (F22) is influenced by the circuit ansatz first-order Clifford architecture  $\{(W_{a_k}, W_{b_k}) : k \in \mathcal{K}\}$ , which is obtained from the parameter shifts in Eq. (F21). If  $U(\cdot)$  exhibits additional structure, for example like a hardware-efficient, alternating ansatz (such as **EfficientSU2** [51]), and if  $\mathcal{K}$  chosen such that *all*  $V_k$  are identical and in the same layer, then Eq. (F22) reduces to a system of two equations (since  $W_{a_k} = W_a$  and  $W_{b_k} = W_b$  for all  $k \in \mathcal{K}$ ), and we may use the algorithm established in Theorem 1 to construct an explicit solution  $(Q, \tilde{Q})$ .

## 2. Generalization to Arbitrary Observables

We showed how to render the gradient constant along one direction for  $H = P$ . We now extend this result to an arbitrary linear combinations of Pauli strings. Consider a general observable of the form in Eq. (F1), i.e.

$$H = \sum_{i \in \mathcal{I}} c_i P_i. \quad (\text{F23})$$

The linear Clifford encoder constructed in Theorem 1 may still be used in that case:

**Theorem 1** Consider an expectation of the form Eq. (6) with a variational ansatz  $U(\theta)$  consisting of Clifford-gates and single-qubit Pauli-rotation gates involving  $D \geq 1$  parameters. Let  $H$  be an arbitrary observable as in Eq. (5). Then, for every  $k \in [D]$  and every  $j \in \mathcal{I}$  there exist two explicitly determined Clifford operators  $Q \in \langle H, S, CX \rangle_N$  and  $\tilde{Q} \in \langle H, S \rangle_N$  such that

$$(\partial_{\theta_k} C)(0) = \pm c_j + \frac{1}{2} \sum_{i \in \mathcal{I} \setminus \{j\}} c_i \left\{ \langle 0 | Q^\dagger \tilde{P}_i^{0,e_k} Q | 0 \rangle - \langle 0 | Q^\dagger \tilde{P}_i^{e_k,e_k} Q | 0 \rangle \right\}, \quad (\text{F24})$$

after replacing  $U(\theta)$  with  $\tilde{Q} U(\theta) Q$ , where, for each  $i \in \mathcal{I}$ ,  $\tilde{P}_i^{j,\alpha} := U(\xi_{j,\alpha})^\dagger \tilde{Q}^\dagger P_i \tilde{Q} U(\xi_{j,\alpha})$ , and  $\xi_{j,\alpha} := \frac{\pi}{2}(\alpha - 2j)$  for multi-indices  $\alpha \in \mathbb{N}_0^D$  and  $0 \leq j \leq \alpha$ .

*Proof.* Let  $j \in \mathcal{I}$  be arbitrary. By Theorem 7, there exists a pair  $(Q, \tilde{Q})$  of Clifford operators with the desired properties such that,

$$\frac{c_j}{2} \left\{ \langle 0 | Q^\dagger \tilde{P}_j^{0,e_k} Q | 0 \rangle - \langle 0 | Q^\dagger \tilde{P}_j^{e_k,e_k} Q | 0 \rangle \right\} = \pm c_j. \quad (\text{F25})$$

Hence, after replacing  $U(\theta)$  with  $\tilde{Q}U(\theta)Q$ , applying Lemma 3 with  $\xi_{0,e_k} = \frac{\pi}{2}e_k$  and  $\xi_{e_k,e_k} = -\frac{\pi}{2}e_k$ , yields

$$\begin{aligned}
(\partial_{\theta_k} C)(0) &= \frac{1}{2} \{C(\xi_{0,e_k}) - C(\xi_{e_k,e_k})\} \\
&= \frac{1}{2} \sum_{i \in \mathcal{I}} c_i \left\{ \langle 0|Q^\dagger U(\xi_{0,e_k})^\dagger \tilde{Q}^\dagger P_i \tilde{Q} U(\xi_{0,e_k}) Q|0\rangle - \langle 0|Q^\dagger U(\xi_{e_k,e_k})^\dagger \tilde{Q}^\dagger P_i \tilde{Q} U(\xi_{e_k,e_k}) Q|0\rangle \right\} \\
&= \frac{c_j}{2} \left\{ \langle 0|Q^\dagger \tilde{P}_j^{0,e_k} Q|0\rangle - \langle 0|Q^\dagger \tilde{P}_j^{e_k,e_k} Q|0\rangle \right\} + \frac{1}{2} \sum_{i \in \mathcal{I} \setminus \{j\}} c_i \left\{ \langle 0|Q^\dagger \tilde{P}_i^{0,e_k} Q|0\rangle - \langle 0|Q^\dagger \tilde{P}_i^{e_k,e_k} Q|0\rangle \right\} \\
&\stackrel{\text{(F25)}}{=} \pm c_j + \frac{1}{2} \sum_{i \in \mathcal{I} \setminus \{j\}} c_i \left\{ \langle 0|Q^\dagger \tilde{P}_i^{0,e_k} Q|0\rangle - \langle 0|Q^\dagger \tilde{P}_i^{e_k,e_k} Q|0\rangle \right\}, \tag{F26}
\end{aligned}$$

as claimed.  $\square$

## Appendix G: Escaping Barren Plateaus

In the previous section, we introduced the Linear Clifford Encoder (LCE) to ensure constant gradient directions at zero initialization. We employ this construction now to mitigate the barren plateau problem [12]. In what follows,  $\|H\|$  denotes the operator norm of the observable in Eq. (F1).

### 1. Taylor Perturbation around Clifford Points

The proposition below characterizes the perturbation of higher-order derivatives  $D_\theta^\alpha C(\theta)$  around their zero evaluation  $(D_\theta^\alpha C)(0)$ —interpreted here as Taylor coefficients—by an error term  $\mathcal{O}(\mathbb{P}_\theta)$  that depends on the initial distribution  $\mathbb{P}_\theta$ .

**Proposition 1.** *Consider an expectation of the form Eq. (E1) with a variational ansatz  $U(\theta)$  involving  $D \geq 1$  parameters. Then, for each multi-index  $\alpha \in \mathbb{N}_0^D$ , we have*

$$\mathbb{E}_\theta[D_\theta^\alpha C(\theta)] = (D_\theta^\alpha C)(0) + \|H\| \mathcal{O}(\mathbb{P}_\theta),$$

where the error term  $\mathcal{O}(\mathbb{P}_\theta)$  scaling depends on the probability distribution  $\mathbb{P}_\theta$ .

*Proof.* Let  $\alpha \in \mathbb{N}_0^D$  be an arbitrary multi-index. Since  $C(\cdot)$  is analytic, we may use a Taylor expansion, combined with the uniform bound in higher-order parameter-shift rule, Lemma 3, finding

$$\mathbb{E}_\theta[D_\theta^\alpha C(\theta)] = \sum_{\|\beta\|_1 \geq 0} \underbrace{(D_\theta^{\alpha+\beta} C)(0)}_{=\mathcal{O}(\|H\|)} \frac{\mathbb{E}_\theta[\theta^{\alpha+\beta}]}{\alpha! \beta!} = (D_\theta^\alpha C)(0) + \mathcal{O}(\|H\|) \sum_{\|\beta\|_1 > 0} \frac{\mathbb{E}_\theta[\theta^{\alpha+\beta}]}{\alpha! \beta!} = (D_\theta^\alpha C)(0) + \|H\| \mathcal{O}(\mathbb{P}_\theta), \tag{G1}$$

where we separated the zero term  $(D_\theta^\alpha C)(0)$  (i.e.  $\{\|\beta\|_1 = 0\}$ ) from the remaining terms in the summation over  $\{\|\beta\|_1 > 0\}$  for which we applied Lemma 3. Note that the bound  $(D_\theta^{\alpha+\beta} C)(0) = \mathcal{O}(\|H\|)$  also follows from Lemma 3. We defined the asymptotic error term

$$\mathcal{O}(\mathbb{P}_\theta) := \mathcal{O} \left( \sum_{\|\beta\|_1 > 0} \frac{\mathbb{E}_\theta[\theta^{\alpha+\beta}]}{\alpha! \beta!} \right), \tag{G2}$$

which has a scaling depending on the probability distribution  $\mathbb{P}_\theta$ .

Similar to Proposition 1, the following theorem lower bounds the scaling of the expected squared gradient norm  $\nabla_\theta C(\theta)$  under local Gaussian/uniform initialization  $\mathbb{P}_\theta$  of the parameters. We generally assume that  $\sigma < 1$ .

**Theorem 8.** Consider an expectation of the form Eq. (E1) with a variational ansatz  $U(\theta)$  involving  $D \geq 1$  parameters. Let  $\mathbb{P}_\theta \in \{\mathcal{N}(0, \sigma^2 I_D), \text{Unif}([- \sigma, \sigma]^D)\}$  be a probability distribution with i.i.d. components  $\theta_1, \dots, \theta_D$ . Then, for every  $k \in [D]$ ,

$$\mathbb{E}_\theta[\|\nabla_\theta C(\theta)\|^2] \geq \mathbb{E}_\theta[(\partial_{\theta_k} C(\theta))^2] = (\partial_{\theta_k} C)(0)^2 + \|H\|^2 \mathcal{O}(D\sigma^2).$$

*Proof.* Let  $k \in [D]$  be arbitrary. We may expand the gradient using the Taylor series, Eq. (10),

$$\partial_{\theta_k} C(\theta) = (\partial_{\theta_k} C)(0) + \sum_{\|\alpha\|_1 > 0} \underbrace{(D_\theta^{\alpha+e_k} C)(0)}_{=\mathcal{O}(\|H\|)} \frac{\theta^\alpha}{\alpha!} = (\partial_{\theta_k} C)(0) + \mathcal{O}(\|H\|) \sum_{\|\alpha\|_1 > 0} \frac{\theta^\alpha}{\alpha!}, \quad (\text{G3})$$

where we made use of the strong regularity property in Lemma 3, and using the observation that  $\partial_{\theta_k} D_\theta^\alpha = D_\theta^{\alpha+e_k}$  for all  $\alpha \in \mathbb{N}_0^D$ . Taking the expectation then involves the computation of the well-known moments ( $\delta$  denoting the Dirac delta function)

$$\mathbb{E}_\theta[\theta^\alpha] = \delta_{\{\alpha_k \in 2\mathbb{N} \forall k\}}(\alpha) \cdot \begin{cases} (\alpha-1)!! \sigma^\alpha, & \theta \sim \mathcal{N}(0, \sigma^2 I_D), \\ \sigma^\alpha \prod_{k=1}^D (\alpha_k + 1)^{-1}, & \theta \sim \text{Unif}([- \sigma, \sigma]^D), \end{cases} \quad (\text{G4})$$

which uses the assumption that  $\theta_1, \dots, \theta_D$  are independent. Again, we use the canonical notations for  $\sigma^\alpha := \sigma^{\alpha_1} \dots \sigma^{\alpha_D}$  and  $(\alpha-1)!! := \prod_{k \in [D]} (\alpha_k - 1)!!$ . This particularly implies that

$$\sum_{\|\alpha\|_1 > 0} \frac{1}{\alpha!} \mathbb{E}_\theta[\theta^\alpha] = \mathcal{O}(D\sigma^2) = \sum_{\|\alpha\|_1, \|\beta\|_1 > 0} \frac{1}{\alpha! \beta!} \mathbb{E}_\theta[\theta^{\alpha+\beta}], \quad (\text{G5})$$

noting that there are exactly  $D$  many multi-indices  $\alpha \in \mathbb{N}_0^D$  for which the error bound  $\mathbb{E}_\theta[\theta^\alpha] \stackrel{(\text{G4})}{=} \mathcal{O}(\sigma^2)$  holds true (namely  $\{\alpha = 2e_k : k \in [D]\}$ ). Note that the higher order terms  $\mathcal{O}(\sigma^r)$  with  $r > 2$  are dominated by  $\mathcal{O}(\sigma^2)$  since  $\sigma < 1$ . As a result, we find

$$\begin{aligned} \mathbb{E}_\theta[\|\nabla_\theta C(\theta)\|^2] &= \sum_{j=1}^D \mathbb{E}_\theta[(\partial_{\theta_j} C(\theta))^2] \\ &\geq \mathbb{E}_\theta[(\partial_{\theta_k} C(\theta))^2] \\ &\stackrel{(\text{G3})}{=} (\partial_{\theta_k} C)(0)^2 + 2 \underbrace{(\partial_{\theta_k} C)(0)}_{=\mathcal{O}(\|H\|)} \mathcal{O}(\|H\|) \sum_{\|\alpha\|_1 > 0} \frac{\mathbb{E}_\theta[\theta^\alpha]}{\alpha!} + \mathcal{O}(\|H\|^2) \sum_{\|\alpha\|_1, \|\beta\|_1 > 0} \frac{\mathbb{E}_\theta[\theta^{\alpha+\beta}]}{\alpha! \beta!} \\ &\stackrel{(\text{G5})}{=} (\partial_{\theta_k} C)(0)^2 + \|H\|^2 \mathcal{O}(D\sigma^2), \end{aligned} \quad (\text{G6})$$

as desired.  $\square$

## 2. Constant Gradient Lower Bound in Small Patches

Having derived a lower bound for the expected squared gradient norm with an error term perturbing a given component  $(\partial_{\theta_k} C)(0)$ , we combine this result with the LCE (cf. Theorem 1) to establish a constant lower bound. In particular, this guarantees a tight escape from barren-plateaus as per Eq. (9):

**Corollary 2.** Consider an expectation of the form Eq. (E1) with a variational ansatz  $U(\theta)$  consisting of Clifford-gates and single-qubit Pauli-rotation gates involving  $D \geq 1$  parameters. Assume that  $H = P_i$  is a single Pauli string. For any arbitrarily small  $\delta > 0$ , initialize  $\theta \sim \mathbb{P}_\theta \in \{\mathcal{N}(0, \sigma^2 I_D), \text{Unif}([- \sigma, \sigma]^D)\}$  with i.i.d. components  $\theta_1, \dots, \theta_D$ , where  $\sigma = \mathcal{O}(D^{-\frac{1+\delta}{2}})$ . Then, there exists a pair of Clifford operators  $(Q, \tilde{Q})$  (cf. Theorem 1) such that

$$\mathbb{E}_\theta[\|\nabla_\theta C(\theta)\|^2] \geq \mathbb{E}_\theta[(\partial_{\theta_k} C(\theta))^2] = 1 + \mathcal{O}(D^{-\delta}),$$

after replacing  $U(\theta)$  by  $\tilde{Q}U(\theta)Q$ .

*Proof.* Let  $k \in [D]$  be arbitrary. By Theorem 8 we know that

$$\mathbb{E}_\theta[\|\nabla_\theta C(\theta)\|^2] \geq \mathbb{E}_\theta[(\partial_{\theta_k} C(\theta))^2] = (\partial_{\theta_k} C)(0)^2 + \mathcal{O}(D\sigma^2), \quad (\text{G7})$$

noting that  $\|H\| = 1$  if  $H = P$ . On the other hand, Theorem 1 shows how to find the desired pair  $Q, \tilde{Q}$  of Clifford operators such that

$$(\partial_{\theta_k} C)(0) = \pm 1 \quad (\text{G8})$$

after replacing  $U(\theta)$  with  $\tilde{Q}U(\theta)Q$ . Therefore, observing that

$$\sigma = \mathcal{O}\left(D^{-\frac{1+\delta}{2}}\right) \implies \mathcal{O}(D\sigma^2) = \mathcal{O}(D^{-\delta}) \quad (\text{G9})$$

concludes the proof.  $\square$

As in Theorem 1, this result may be generalized to arbitrary observables  $H$  as defined in Eq. (F1) with a lower bound depending on the distribution of the Pauli coefficients  $\{c_i\}_{i \in \mathcal{I}}$ .

**Theorem 2.** *Let  $H$  be an arbitrary observable as in Eq. (5) with Pauli terms indexed by  $\mathcal{I}$ . Let  $\delta > 0$  and initialize  $\theta \sim \mathbb{P}_\theta \in \{\mathcal{N}(0, \sigma^2 I_D), \text{Unif}([- \sigma, \sigma]^D)\}$  with i.i.d. components and  $\sigma = \mathcal{O}(\|H\|^{-1} D^{-\frac{1+\delta}{2}})$ . Then, for each  $i_0 \in \mathcal{I}$ , there exists a pair of Clifford operators  $(Q, \tilde{Q})$  such that*

$$\mathbb{E}_\theta[\|\nabla_\theta \tilde{C}(\theta)\|^2] \geq \mathbb{E}_\theta[(\partial_{\theta_k} \tilde{C}(\theta))^2] = \beta_{i_0}(H)^2 + \mathcal{O}(D^{-\delta}),$$

where

$$\beta_{i_0}(H) := \pm c_{i_0} + \frac{1}{2} \sum_{i \in \mathcal{I} \setminus \{i_0\}} c_i \{ \langle 0 | \tilde{P}_i^{0, e_k} | 0 \rangle - \langle 0 | \tilde{P}_i^{e_k, e_k} | 0 \rangle \},$$

defining  $\tilde{P}_i^{j, \alpha} := Q^\dagger U(\xi_{j, \alpha})^\dagger \tilde{Q}^\dagger P_i \tilde{Q} U(\xi_{j, \alpha}) Q$  and  $\xi_{j, \alpha} := \frac{\pi}{2}(\alpha - 2j)$  for  $0 \leq j \leq \alpha$ , and  $\tilde{C}(\cdot)$  denoting the LCE transformed cost. In particular,  $\beta_{i_0}(H) = 1$  if  $H = P$  is a single Pauli string.

*Proof.* Let  $k \in [D]$  and  $i_0 \in \mathcal{I}$  be arbitrary. By Theorem 8 we know that

$$\mathbb{E}_\theta[\|\nabla_\theta C(\theta)\|^2] \geq \mathbb{E}_\theta[(\partial_{\theta_k} C(\theta))^2] = (\partial_{\theta_k} C)(0)^2 + \|H\|^2 \mathcal{O}(D\sigma^2), \quad (\text{G10})$$

On the other hand, Theorem 1 yields the desired pair  $(Q, \tilde{Q})$  of Clifford operators such that

$$(\partial_{\theta_k} \tilde{C})(0) = \pm c_{i_0} + \frac{1}{2} \sum_{i \in \mathcal{I} \setminus \{i_0\}} c_i \{ \langle 0 | \tilde{P}_i^{0, e_k} | 0 \rangle - \langle 0 | \tilde{P}_i^{e_k, e_k} | 0 \rangle \} = \beta_{i_0}(H), \quad (\text{G11})$$

after replacing  $U(\theta)$  with  $\tilde{Q}U(\theta)Q$  via the LCE transformation. Therefore, observing that

$$\sigma = \mathcal{O}\left(\|H\|^{-1} D^{-\frac{1+\delta}{2}}\right) \implies \|H\|^2 \mathcal{O}(D\sigma^2) = \mathcal{O}(D^{-\delta}) \quad (\text{G12})$$

concludes the proof.  $\square$

The observable-dependent lower bound  $\beta_{i_0}(H)^2$  in Theorem 2 is only meaningful if it behaves like  $\Omega(1)$ , i.e. when it dominates error term  $\mathcal{O}(D^{-\delta})$ . The scaling behavior of  $\beta_{i_0}(H)$  is less straightforward to analyze due to the cancellations between Pauli terms. The following lemma shows that the probability of total cancellation (i.e.  $\beta_{i_0}(H) = 0$ ), conditioned on  $P_{i_0}$  which is given for the LCE construction, is vanishing exponentially in the number of qubits  $N$ :

**Lemma 1.** *Let  $H = \sum_{i \in \mathcal{I}} c_i P_i$  be a random observable with  $P_i \stackrel{i.i.d.}{\sim} \text{Unif}(\mathcal{P}_N \setminus \{I\})$ . Then, for each  $i_0 \in \mathcal{I}$ , we have the conditional probability that*

$$\mathbb{P}(\beta_{i_0}(H)^2 = c_{i_0}^2 \mid P_{i_0}) \geq 1 - \mathcal{O}(|\mathcal{I}| 2^{-N}),$$

as  $N \rightarrow \infty$ .

*Proof.* Recall the definition of the  $N$ -qubit Pauli group,

$$\mathcal{P}_N := \{\pm P, \pm iP : P \in \{I, X, Y, Z\}^{\otimes N}\}, \quad (\text{G13})$$

which contains  $4 \cdot 4^N = 4^{N+1}$  elements. In the construction of LCE, we were particularly interested in the subgroup

$$\langle I, Z \rangle_N = \{\pm P, \pm iP : P \in \{I, Z\}^{\otimes N}\} \quad (\text{G14})$$

of diagonal Pauli strings, containing  $4 \cdot 2^N = 2^{N+2}$  elements.

First, we note that a uniformly random (non-identity) Pauli string  $P$  satisfies that

$$\mathbb{P}(\langle 0|P|0\rangle = 1) = \frac{\#\langle I, Z \rangle_N \setminus \{I\}}{\#\mathcal{P}_N \setminus \{I\}} = \frac{2^{N+2} - 1}{4^{N+1} - 1} = \mathcal{O}(2^{-N}), \quad (\text{G15})$$

since the only non-zero Pauli expectations are achieved by diagonal operators in  $\langle I, Z \rangle_N$ . In other words, the probability of having a non-zero expectation is determined by the total number of non-identity diagonal Pauli matrices divided by the total number of non-identity Pauli matrices. That is, for any uniformly random (non-identity) Pauli string  $P$  we have

$$\mathbb{P}(\langle 0|P|0\rangle = 0) = 1 - \mathcal{O}(2^{-N}), \quad (\text{G16})$$

which we will use to conclude with the lower bound.

Recall from the proof of Theorem 7 that for each  $(j, \alpha)$ , and  $i \in \mathcal{I}$ ,

$$\tilde{P}_i^{j, \alpha} := Q^\dagger U_{j, \alpha}^\dagger \tilde{Q}^\dagger P_i \tilde{Q} U_{j, \alpha} Q \quad (\text{G17})$$

for some deterministic  $U_{j, \alpha} \in \text{Clifford}(N)$  (i.e.  $U(\cdot)$  evaluated at certain grid points) depending on the LCE direction  $k \in [D]$  (since  $\alpha = e_k$  and  $j \in \{0, e_k\}$ ) which is deterministically fixed by assumption. On the other hand, the LCE pair  $(Q, \tilde{Q})$  depends on both the (deterministic) LCE direction  $k \in [D]$ , and Pauli term  $i_0 \in \mathcal{I}$ .

Crucially, the LCE pair  $(Q, \tilde{Q})$  is explicitly constructed from the random Pauli string  $P_{i_0}$  in order to isolate the Pauli coefficient  $c_{i_0}$ , thus causing  $(Q, \tilde{Q})$  to be random as well. Hence, given the choice of the Pauli string  $P_{i_0}$  for the LCE construction, the pair  $(Q, \tilde{Q})$  is also given, which in turn results in  $\tilde{P}_i^{j, \alpha}$  being pair-wise independent in  $i \in \mathcal{I}$  with respect to the conditional probability  $\mathbb{P}(\cdot | P_{i_0})$ .

Defining  $d_i := \langle 0|\tilde{P}_i^{0, e_k}|0\rangle - \langle 0|\tilde{P}_i^{e_k, e_k}|0\rangle$ , we thus obtain

$$\mathbb{P}(d_i = 0 \forall i \in \mathcal{I} \setminus \{i_0\} | P_{i_0}) \stackrel{i.i.d.}{=} \prod_{i \in \mathcal{I} \setminus \{i_0\}} \mathbb{P}(d_i = 0 | P_{i_0}) \stackrel{(\text{G16})}{\geq} (1 - \mathcal{O}(2^{-N}))^{|\mathcal{I}|} = 1 - \mathcal{O}(|\mathcal{I}| 2^{-N}). \quad (\text{G18})$$

Consequently, by the previous estimation,

$$\mathbb{P}\left(\sum_{i \in \mathcal{I} \setminus \{i_0\}} c_i d_i = 0 \mid P_{i_0}\right) \geq \mathbb{P}(d_i = 0 \forall i \in \mathcal{I} \setminus \{i_0\} | P_{i_0}) \geq 1 - \mathcal{O}(|\mathcal{I}| 2^{-N}), \quad (\text{G19})$$

which directly implies the desired claim since by definition,

$$\beta_{i_0}(H) = \pm c_{i_0} + \frac{1}{2} \sum_{i \in \mathcal{I} \setminus \{i_0\}} c_i d_i. \quad (\text{G20})$$

□

### 3. Polynomial Gradient Lower Bound beyond Small Patches

Utilizing the LCE method in conjunction with Lebesgue measure theory and previous results, we are ready to rigorously show that barren plateaus are mitigated beyond the threshold  $\sigma = \mathcal{O}(D^{-1/2})$ , a landscape patch lacking any known classical surrogate [18]. This outcome holds with probability one for all observables  $H$  as defined in Eq. (5), indexed by  $\mathcal{I}$ , provided that at least one Pauli term features a constant coefficient:

**Theorem 5.** *Let  $H$  be an arbitrary, uniformly randomly sampled observable as in Eq. (F1) with Pauli terms indexed by  $\mathcal{I}$ . Let  $r > 0$  be arbitrary, and initialize the parameters according to  $\mathbb{P}_{-\frac{r}{D}} := \text{Unif}([- \sigma, \sigma]^D)$  with  $\sigma = \|H\|^{-1} D^{-\frac{1-r/D}{2}}$ . Then, for each  $k \in [D]$  and  $i \in \mathcal{I}$  with  $c_i = \Omega(1)$ , there exists a pair of Clifford operators  $(Q, \tilde{Q})$  such that, with probability at least  $1 - \mathcal{O}(|\mathcal{I}| 2^{-N})$  (conditioned on  $P_i$ ), as  $D \rightarrow \infty$ ,*

$$\mathbb{E}_{\theta \sim \mathbb{P}_{-\frac{r}{D}}} [(\partial_{\theta_k} \tilde{C}(\theta))^2] \geq D^{-r} (\Omega(1) + \mathcal{O}(D^{-\frac{r}{D}})),$$

where  $\tilde{C}(\cdot)$  is the LCE transformed cost.

*Proof.* Let  $\delta > 0$  to be determined, and define  $\mathbb{P}_{\pm\delta} = \text{Unif}([- \sigma_{\pm\delta}, \sigma_{\pm\delta}]^D)$  where  $\sigma_{\pm\delta} := \|H\|^{-1} D^{-\frac{1\pm\delta}{2}}$ . Consider the two hypercubes  $Q_{\pm\delta} := [- \sigma_{\pm\delta}, \sigma_{\pm\delta}]^D$ . Their volumes in terms of the Lebesgue measure  $\lambda$  in  $\mathbb{R}^D$  are given by

$$\lambda(Q_{\pm\delta}) := \int_{Q_{\pm\delta}} d\lambda = \lambda([- \sigma_{\pm\delta}, \sigma_{\pm\delta}]^D) = (2\sigma_{\pm\delta})^D = 2^D \|H\|^{-D} D^{-\frac{1\pm\delta}{2}D}. \quad (\text{G21})$$

Note that  $Q_\delta \subseteq Q_{-\delta}$ . In particular  $\lambda(Q_\delta) \leq \lambda(Q_{-\delta})$  by monotonicity of the Lebesgue measure.

Furthermore, on the smaller patch  $Q_\delta$ , we know by Theorem 2 that (for all  $\delta > 0$ )

$$\mathbb{E}_{\theta \sim \mathbb{P}_\delta} [(\partial_{\theta_k} \tilde{C}(\theta))^2] = \frac{1}{\lambda(Q_\delta)} \int_{Q_\delta} ((\partial_{\theta_k} \tilde{C}(\theta))^2) d\theta = \Omega(\beta_i(H)) + \mathcal{O}(D^{-\delta}) \quad (\text{G22})$$

as  $D \rightarrow \infty$ .

As a result, we find

$$\begin{aligned} \mathbb{E}_{\theta \sim \mathbb{P}_{-\delta}} [(\partial_{\theta_k} \tilde{C}(\theta))^2] &= \frac{1}{\lambda(Q_{-\delta})} \int_{Q_{-\delta}} (\partial_{\theta_k} \tilde{C}(\theta))^2 d\theta \\ &= \frac{1}{\lambda(Q_{-\delta})} \int_{Q_\delta} ((\partial_{\theta_k} \tilde{C}(\theta))^2) d\theta + \frac{1}{\lambda(Q_{-\delta})} \int_{Q_{-\delta} \setminus Q_\delta} \underbrace{(\partial_{\theta_k} \tilde{C}(\theta))^2}_{\geq 0} d\theta \end{aligned} \quad (\text{G23})$$

$$\begin{aligned} &\geq \frac{\lambda(Q_\delta)}{\lambda(Q_{-\delta})} \underbrace{\frac{1}{\lambda(Q_\delta)} \int_{Q_\delta} (\partial_{\theta_k} \tilde{C}(\theta))^2 d\theta}_{\stackrel{(\text{G22})}{=} \Omega(\beta_i(H)) + \mathcal{O}(D^{-\delta})} = D^{-\delta D} (\Omega(\beta_i(H)) + \mathcal{O}(D^{-\delta})), \end{aligned} \quad (\text{G24})$$

where we computed

$$\frac{\lambda(Q_\delta)}{\lambda(Q_{-\delta})} \stackrel{(\text{G21})}{=} \left( \frac{D^{-\frac{1+\delta}{2}}}{D^{-\frac{1-\delta}{2}}} \right)^D = D^{\frac{D}{2}(-1-\delta+1-\delta)} = D^{-\delta D}. \quad (\text{G25})$$

Therefore, by choosing  $\delta = \frac{r}{D}$  in Eq. (G24), we obtain

$$\mathbb{E}_{\theta \sim \mathbb{P}_{-\frac{r}{D}}} [(\partial_{\theta_k} \tilde{C}(\theta))^2] \geq D^{-r} (\Omega(\beta_i(H)) + \mathcal{O}(D^{-\frac{r}{D}})). \quad (\text{G26})$$

We observe that the error term

$$D^{-\frac{r}{D}} = e^{-\frac{r \log D}{D}} = \sum_{s=1}^{\infty} \frac{(-1)^s}{s!} \left( \frac{r \log D}{D} \right)^s = 1 - \Theta\left(\frac{r \log D}{D}\right) \quad (\text{G27})$$

is dominated by the lower bound if  $\beta_i(H) = \Omega(1)$ . By Lemma 1 (and by assumption on  $c_i$ ) we know that  $\beta_i(H)^2 = c_i^2 = \Omega(1)$  with probability at least  $1 - \mathcal{O}(|\mathcal{I}| 2^{-N})$  (conditioned on  $P_i$  which is fixed for the LCE construction). This proves that the claimed polynomially decaying lower bound in Eq. (G26) is indeed satisfied.  $\square$

## Appendix H: State Expressivity of Parameterized Quantum Circuits

It is essential to verify that the LCE transformation  $C(\cdot) \mapsto \tilde{C}(\cdot)$  preserves desirable properties of the optimization landscape. Recall that  $\tilde{C}(\cdot)$  denotes the LCE transformed cost obtained by replacing  $U(\cdot)$  with  $\tilde{U}(\cdot) := \tilde{Q}U(\cdot)Q$  as in Theorem 1. We show that both expressivity and global optimality remain intact, using the following geometric notion of expressivity:

**Definition 2** ( $\varepsilon$ -State-Expressivity). *Let  $\varepsilon > 0$ . A PQC  $U(\cdot)$  is said to be  $\varepsilon$ -state-expressive if for every state  $|\psi\rangle \in \mathcal{H}_N$  and every stabilizer state  $|\psi_0\rangle \in \text{Stab}(N)$ , there exists a parameter configuration  $\theta \in [-\pi, \pi]^D$  such that*

$$\|U(\theta)|\psi_0\rangle - |\psi\rangle\|_2 < \varepsilon. \quad (\text{H1})$$

Here, it suffices to consider the metric

$$\| |\psi\rangle - |\phi\rangle \|_2 := \sqrt{2(1 - \text{Re}\langle\psi|\phi\rangle)}, \quad (\text{H2})$$

induced by the  $\ell_2$ -norm, to measure the distance between quantum states  $|\psi\rangle, |\phi\rangle \in \mathcal{H}_N$ . The reason for considering arbitrary stabilizer inputs  $|\psi_0\rangle \in \text{Stab}(N)$  is that the expressivity of the model  $U(\cdot)$  should not depend on a finite set of classically tractable input states.

This definition captures the geometric capacity of the ansatz  $U(\cdot)$  to explore the Hilbert space  $\mathcal{H}_N$ . Intuitively, if  $U(\cdot)$  explores  $\mathcal{H}_N$  in an unbiased fashion, then the KL-divergence  $D_{\text{KL}}(\hat{P}_{\text{PQC}}(F; \theta) \| P_{\text{Haar}}(F))$  in Ref. [15] is small if and only if  $U(\cdot)$  is  $\varepsilon$ -state-expressive for sufficiently small  $\varepsilon > 0$ .

Recall that we consider a Variational Quantum Eigensolver (VQE) [2] problem of the form

$$\theta_* = \arg \min_{\theta \in [-\pi, \pi]^D} C(\theta), \quad (\text{H3})$$

where  $C(\theta_*)$  approximates the ground state energy  $\lambda_{\min}(H)$  of the observable in Eq. (F1). We first show that sufficient  $\varepsilon$ -state-expressivity guarantees the existence of a good solution to Eq. (H3):

**Lemma 4.** *Assume that the quantum model  $U(\cdot)$  is  $\frac{\varepsilon}{2\|H\|}$ -state-expressive. Then, there exists a configuration  $\theta_* \in [-\pi, \pi]^D$  such that*

$$|C(\theta_*) - \lambda_{\min}(H)| < \varepsilon,$$

where  $\lambda_{\min}(H)$  denotes the smallest eigenvalue of the observable in Eq. (F1).

*Proof.* Let  $|\psi\rangle \in \mathcal{H}_N$  be the eigenstate corresponding to the smallest eigenvalue  $\lambda_{\min}(H)$  of  $H$ . That is,  $H|\psi\rangle = \lambda_{\min}(H)|\psi\rangle$ . Then, since  $U(\cdot)$  is  $\frac{\varepsilon}{2\|H\|}$ -state-expressive, there exists a configuration  $\theta_* \in [-\pi, \pi]^D$  such that

$$\|U(\theta_*)|0\rangle - |\psi\rangle\| < \frac{\varepsilon}{2\|H\|}. \quad (\text{H4})$$

As a consequence, defining  $|\phi\rangle := U(\theta_*)|0\rangle$ ,

$$\begin{aligned} |C(\theta_*) - \lambda_{\min}(H)| &= |\langle\phi|H|\phi\rangle - \langle\psi|H|\psi\rangle| \\ &= |(\langle\phi - \psi|H|\phi\rangle + \langle\psi|H(|\phi\rangle - |\psi\rangle))| \\ &\leq |(\langle\phi - \psi|H|\phi\rangle)| + |\langle\psi|H(|\phi\rangle - |\psi\rangle)| \\ &\leq \|H\| \underbrace{\| |\phi\rangle \|}_{=1} \| |\phi\rangle - |\psi\rangle \| + \|H\| \underbrace{\| |\psi\rangle \|}_{=1} \| |\phi\rangle - |\psi\rangle \| = 2\|H\| \| |\phi\rangle - |\psi\rangle \| \stackrel{(\text{H4})}{<} \varepsilon, \end{aligned} \quad (\text{H5})$$

where we employed the triangle inequality and Cauchy Schwarz, respectively.  $\square$

Lemma 4 proves that, under its assumptions,  $C(\theta_*)$  provides a good approximation of the ground energy of  $H$ , and thus solves the VQE problem in Eq. (H3). The next step is to establish that the LCE transformation  $C(\cdot) \mapsto \tilde{C}(\cdot)$  does not compromise  $\varepsilon$ -state-expressivity. That is, the quantum model is just as  $\varepsilon$ -state-expressive after replacing  $U(\cdot)$  with  $\tilde{Q}U(\cdot)Q$  as per Theorem 1:

**Lemma 5.** *If the quantum model  $U(\cdot)$  is  $\varepsilon$ -state-expressive, then so is  $\tilde{Q}U(\cdot)Q$  for each  $Q, \tilde{Q} \in \text{Clifford}(N)$ . In particular, the LCE transformation  $C(\cdot) \mapsto \tilde{C}(\cdot)$  leaves the  $\varepsilon$ -state-expressivity of the quantum model  $U(\cdot)$  invariant.*

*Proof.* Let  $|\psi_0\rangle \in \text{Stab}(N)$ , and  $|\psi\rangle \in \mathcal{H}_N$  be arbitrary. By assumption that  $U(\cdot)$  is  $\varepsilon$ -state-expressive, we find

$$\|\tilde{Q}U(\theta)Q|\psi_0\rangle - |\psi\rangle\| = \|\tilde{Q}U(\theta)|\tilde{\psi}_0\rangle - |\psi\rangle\| = \|U(\theta)|\tilde{\psi}_0\rangle - |\tilde{\psi}\rangle\| < \varepsilon, \quad (\text{H6})$$

using that  $|\tilde{\psi}_0\rangle := Q|\psi_0\rangle \in \text{Stab}(N)$  defines a stabilizer state, and that  $\tilde{Q}$  is unitary, leaving the norm invariant in the second equality with  $|\tilde{\psi}\rangle := \tilde{Q}^\dagger|\psi\rangle$ .  $\square$

It remains to show that the global quality of the optimization landscape is preserved under the LCE transformation  $C(\cdot) \mapsto \tilde{C}(\cdot)$ . Specifically, we prove that the global minimum value satisfies  $C(\theta_*) \approx \tilde{C}(\theta_*)$ , with an error controllable by assuming stronger  $\varepsilon$ -state-expressivity. The proof relies on ensuring that a change of basis leaves the eigenspectrum invariant:

**Lemma 6.** *Let  $\tilde{Q}$  be an arbitrary unitary operator, and define  $\tilde{H} := \tilde{Q}^\dagger H \tilde{Q}$ , where  $H$  denotes the observable in Eq. (5). Then,  $H$  and  $\tilde{H}$  share the same eigenspectrum.*

*Proof.* Let  $\lambda(H)$  be an arbitrary eigenvalue of  $H$ , and take the corresponding eigenstate  $|\psi\rangle \in \mathcal{H}_N$ . In other words,  $H|\psi\rangle = \lambda(H)|\psi\rangle$ . Define the state  $|\tilde{\psi}\rangle := \tilde{Q}^\dagger|\psi\rangle$ . Then,

$$\tilde{H}|\tilde{\psi}\rangle = \tilde{Q}^\dagger H \underbrace{\tilde{Q}\tilde{Q}^\dagger}_{=I}|\psi\rangle = \tilde{Q}^\dagger \underbrace{H|\psi\rangle}_{=\lambda(H)|\psi\rangle} = \lambda(H)\tilde{Q}^\dagger|\psi\rangle = \lambda(H)|\tilde{\psi}\rangle, \quad (\text{H7})$$

implying that  $\lambda(H) = \lambda(\tilde{H})$ . The claim follows since  $\lambda(H)$  was arbitrary.  $\square$

We are now ready to prove the remaining statement:

**Proposition 2.** *Assume that the quantum model  $U(\cdot)$  is  $\frac{\varepsilon}{4\|H\|}$ -state-expressive. Then, we have that*

$$\left| \min_{\theta \in [-\pi, \pi]^D} C(\theta) - \min_{\theta \in [-\pi, \pi]^D} \tilde{C}(\theta) \right| < \varepsilon,$$

where  $\tilde{C}(\cdot)$  denotes the cost after replacing  $U(\cdot)$  by  $\tilde{Q}U(\cdot)Q$ . This ensures that the LCE does not compromise the quality of the global minimum.

*Proof.* By definition, the LCE transformed cost equals

$$\tilde{C}(\theta) := \langle 0|Q^\dagger U(\theta)^\dagger \tilde{H} U(\theta) Q|0\rangle, \quad (\text{H8})$$

where we introduced the transformed observable  $\tilde{H} = \tilde{Q}^\dagger H \tilde{Q}$ . The goal is to prove that  $C(\cdot)$  and  $\tilde{C}(\cdot)$  have approximately the same global minimum. The idea is to first make use of state expressivity in order ensure that  $C(\cdot)$  is able to approximate the smallest eigenvalue  $\lambda_{\min}(H)$ . This step is achieved with the help of Lemma 4. Next, we use Lemma 5 to establish an identical bound for the LCE transformed cost  $\tilde{C}(\cdot)$  approximating  $\lambda_{\min}(\tilde{H})$ . To conclude with the proof, we employ Lemma 6 stating that the change of basis  $H \mapsto \tilde{Q}^\dagger H \tilde{Q} = \tilde{H}$  leaves the eigenspectrum invariant, i.e.  $\lambda_{\min}(H) = \lambda_{\min}(\tilde{H})$ , allowing us to combine both previous bounds for the desired result.

We now elaborate the above proof strategy more formally: Since  $U(\cdot)$  is  $\frac{\varepsilon}{4\|H\|}$ -state-expressive by assumption, it follows from Lemma 4 that we can approximate the lowest eigenvalue for the original cost:

$$\left| \min_{\theta \in [-\pi, \pi]^D} C(\theta) - \lambda_{\min}(H) \right| < \frac{\varepsilon}{2}. \quad (\text{H9})$$

By Lemma 5 we know that the LCE transformation leaves  $\varepsilon$ -expressivity invariant, thus establishing the exact same bound for the LCE transformed cost:

$$\left| \min_{\theta \in [-\pi, \pi]^D} \tilde{C}(\theta) - \lambda_{\min}(\tilde{H}) \right| < \frac{\varepsilon}{2}. \quad (\text{H10})$$

As a result, by the triangle inequality,

$$\begin{aligned} \left| \min_{\theta \in [-\pi, \pi]^D} C(\theta) - \min_{\theta \in [-\pi, \pi]^D} \tilde{C}(\theta) \right| &\leq \left| \min_{\theta \in [-\pi, \pi]^D} C(\theta) - \lambda_{\min}(H) \right| + \left| \min_{\theta \in [-\pi, \pi]^D} \tilde{C}(\theta) - \lambda_{\min}(H) \right| \\ &= \left| \min_{\theta \in [-\pi, \pi]^D} C(\theta) - \lambda_{\min}(H) \right| + \left| \min_{\theta \in [-\pi, \pi]^D} \tilde{C}(\theta) - \lambda_{\min}(\tilde{H}) \right| < \frac{\varepsilon}{2} + \frac{\varepsilon}{2} = \varepsilon, \end{aligned} \quad (\text{H11})$$

where we made use of Lemma 6, which states that  $\lambda_{\min}(H) = \lambda_{\min}(\tilde{H})$ .  $\square$

Proposition 2 confirms that the LCE transformation preserves the quality of the global minimum. Notably, we make no structural assumptions on the PQC ansatz  $U(\cdot)$  (e.g. no lightcone or locality constraints), allowing us to assume  $\varepsilon$ -state-expressivity for arbitrarily small  $\varepsilon > 0$ .

## Appendix I: Minimal Truncation Threshold of the Taylor Surrogate

We approximate the PQC using the Taylor surrogate  $C_m(\theta)$  from Eq. (10), where the truncation threshold  $m = m(\theta)$  determines computational complexity. To meet a prescribed surrogate error tolerance, we analyze the minimal necessary  $m$  via two approaches:

1. **Worst-Case Error:**  $m = m(\theta)$  is a deterministic function of a fixed configuration  $\theta \in [-\pi, \pi]^D$ ;
2. **Mean-Squared Error:**  $m = m(\mathbb{P}_\theta)$  is defined probabilistically based on an initialization distribution  $\mathbb{P}_\theta$ .

### 1. Worst-Case Error Analysis

The following lemma quantifies the (deterministic) worst-case error of the approximation  $C_m(\theta) \approx C(\theta)$  as a function of  $\theta$ .

**Lemma 7.** *Consider an expectation of the form Eq. (E1) with a variational ansatz  $U(\theta)$  involving  $D \geq 1$  parameters, and suppose we simulate it classically using the Taylor series  $C_m(\theta)$  defined in Eq. (D9). Let  $\theta \in [-\pi, \pi]^D$  and  $m \in \mathbb{N}$  be arbitrary. Then, for every  $\theta \in [-\pi, \pi]^D$  and  $m \in \mathbb{N}$ , we have*

$$|C(\theta) - C_m(\theta)| \leq \frac{\|H\|}{m!} \|\theta\|_1^m, \quad (\text{I1})$$

where  $\|H\|$  is the operator norm of the observable in Eq. (F1).

*Proof.* Let  $\theta \in [-\pi, \pi]^D$  and  $m \in \mathbb{N}$  be arbitrary. Using Lagrange's form of the remainder in the Taylor series, we find an element  $\xi \in [0, \theta]$  in the line segment from 0 to  $\theta$ , such that

$$\begin{aligned} C(\theta) - C_m(\theta) &= \sum_{\|\alpha\|_1 \geq m} (D_\theta^\alpha C)(0) \frac{\theta^\alpha}{\alpha!} = \sum_{\|\alpha\|_1 = m} \underbrace{(D_\theta^\alpha C)(\xi)}_{\leq \|H\|} \frac{\theta^\alpha}{\alpha!} \\ &\leq \|H\| \sum_{\|\alpha\|_1 = m} \left| \frac{\theta^\alpha}{\alpha!} \right| \leq \|H\| \frac{1}{m!} \left( \sum_{k=1}^D |\theta_k| \right)^m = \frac{\|H\|}{m!} \|\theta\|_1^m, \end{aligned} \quad (\text{I2})$$

where, in the first estimate we made use of the uniform bound in the higher-order parameter-shift rule, Lemma 3, and the multi-nomial theorem in the second, i.e.

$$\sum_{\|\alpha\|_1 = m} \binom{m}{\alpha} \theta^\alpha = \left( \sum_{k=1}^D \theta_k \right)^m, \quad \binom{m}{\alpha} := \frac{m!}{\alpha_1! \cdots \alpha_D!}. \quad (\text{I3})$$

$\square$

In order to solve for the truncation threshold  $m$ , we make use of asymptotic properties of the Lambert- $W$ -function [62]:

**Lemma 8.** Let  $W(\cdot)$  denote the main branch of the Lambert- $W$ -function [62]. Then,

$$W(x) = x + \mathcal{O}(x^2)$$

as  $x \rightarrow 0$ .

*Proof.* By definition,  $W(x)e^{W(x)} = x$ . In particular,  $W(0) = 0$ . We shall use the implicit function theorem to prove the lemma statement. For that purpose, let us define the analytic function  $F(w, x) := we^w - x$ . By the previous observation, we have  $F(0, 0) = 0$ . Next, we note that  $\partial_w F(w, x) = (w+1)e^w$  which implies  $(\partial_w F)(0, 0) = 1 \neq 0$ . By the implicit function theorem, there exists a unique analytic function  $W(\cdot)$  satisfying  $W(0) = 0$  and  $F(W(x), x) = 0$  in a neighborhood of  $x = 0$ . By uniqueness,  $W(\cdot)$  has to coincide with the principal branch of the Lambert- $W$ -function [62]. Since  $W(\cdot)$  is analytic (in a neighborhood of  $x = 0$ ), we may consider the Taylor expansion,

$$W(x) = W(0) + W'(0)x + \mathcal{O}(x^2). \quad (\text{I4})$$

Taking the derivative on both sides of  $W(x)e^{W(x)} = x$  yields

$$W'(x)e^{W(x)}(1 + W(x)) = 1 \implies W'(x) = \frac{e^{-W(x)}}{1 + W(x)} \implies W'(0) = 1 \quad (\text{I5})$$

making use of  $W(0) = 0$ . Thus, Eq. (I4) reduces to the desired asymptotics  $W(x) = x + \mathcal{O}(x^2)$  as  $x \rightarrow 0$ .  $\square$

We are now ready to deterministically lower bound the truncation threshold  $m(\theta)$ :

**Lemma 9.** Consider an expectation in Eq. (E1) with a variational ansatz  $U(\theta)$  involving  $D \geq 1$  parameters, simulated classically via the Taylor series  $C_m(\theta)$  from Eq. (D9). Assume the Taylor remainder in Eq. (I1) is bounded by a tolerance  $\varepsilon > 0$ , and let  $m = m(\theta)$  be the truncation order in Eq. (D9). Then, the truncation threshold  $m = m(\theta)$  satisfies the lower bound

$$m(\theta) \geq e\|\theta\|_1 \exp\left(W\left(\frac{1}{e\|\theta\|_1} \log\left(\frac{\|H\|}{\varepsilon\sqrt{e^3\|\theta\|_1}}\right)\right)\right) - \frac{1}{2},$$

where  $e \approx 2.71828$  is the natural constant,  $W(\cdot)$  denotes the main branch of the Lambert- $W$  function [62], and  $\|H\|$  is the operator norm of the observable in Eq. (F1). In particular, if  $\|\theta\|_1 \rightarrow \infty$  increases as  $D \rightarrow \infty$ , then the asymptotic equivalence  $m(\theta) \sim e\|\theta\|_1$  is sufficient for the truncation threshold to ensure the error tolerance  $\varepsilon$  (where the contributions of  $\|H\|$  and  $\varepsilon$  become negligible).

*Proof.* Let  $\varepsilon > 0$  be a given error tolerance. Without loss of generality  $\theta \neq 0$ , so that  $m(\theta) \geq 2$ . Otherwise if  $\theta = 0$ , the Taylor approximation is exact with  $m(0) = 1$ . Utilizing a Stirling approximation yields the lower bound

$$m! \leq e\sqrt{m} \left(\frac{m}{e}\right)^m \quad (\text{I6})$$

for all  $m \geq 2$ . This bound is derived from the remark of Robbins [63] that for all  $m \geq 1$ ,

$$m! \leq \sqrt{2\pi m} \left(\frac{m}{e}\right)^m e^{\frac{1}{12m}}, \quad (\text{I7})$$

and verifying that for all  $m \geq 2$ ,

$$\sqrt{2\pi}e^{\frac{1}{12m}} \leq e. \quad (\text{I8})$$

As a result, we require by Lemma 7 that, that the Taylor approximation error is bounded by

$$\log \varepsilon \stackrel{!}{\geq} \log\left(\frac{\|H\|}{m!} \|\theta\|_1^m\right) \stackrel{(\text{I6})}{\geq} \log\left(\frac{\|H\|}{e\sqrt{m}} \frac{(e\|\theta\|_1)^m}{m^m}\right) = \log\|H\| - \frac{1}{2}\log(e^2m) - m \log\left(\frac{m}{e\|\theta\|_1}\right). \quad (\text{I9})$$

Noting that  $\log \varepsilon = -\log(1/\varepsilon)$ , we may manipulate the following expression:

$$\begin{aligned} \gamma &:= \frac{1}{e\|\theta\|_1} \log \left( \frac{\|H\|}{\varepsilon\sqrt{e^3\|\theta\|_1}} \right) = -\frac{1}{e\|\theta\|_1} \log \varepsilon + \frac{1}{e\|\theta\|_1} \log \|H\| - \frac{1}{2e\|\theta\|_1} \log(e^3\|\theta\|_1) \\ &\stackrel{(19)}{\leq} \frac{1}{2e\|\theta\|_1} \log(e^2m) + \frac{m}{e\|\theta\|_1} \log \left( \frac{m}{e\|\theta\|_1} \right) - \frac{1}{2e\|\theta\|_1} \log(e^3\|\theta\|_1) \\ &= \frac{1}{2e\|\theta\|_1} \underbrace{\{\log(e^2m) - \log(e^3\|\theta\|_1)\}}_{=\log\left(\frac{m}{e\|\theta\|_1}\right)} + \frac{m}{e\|\theta\|_1} \log \left( \frac{m}{e\|\theta\|_1} \right) \end{aligned} \quad (I10)$$

$$= \frac{2m+1}{2e\|\theta\|_1} \log \left( \frac{m}{e\|\theta\|_1} \right) \leq \frac{2m+1}{2e\|\theta\|_1} \log \left( \frac{2m+1}{2e\|\theta\|_1} \right). \quad (I11)$$

We have therefore established the bound

$$\gamma \stackrel{(I11)}{\leq} y \log y =: f(y), \quad \text{substituting } y := \frac{2m+1}{2e\|\theta\|_1}. \quad (I12)$$

The equation  $f(y) = \gamma$  is known to be solved by the main branch of the Lambert- $W$ -function [62] with solution  $y = e^{W(\gamma)}$ . Moreover, the function  $f$  is invertible on  $y > 1$ . In that case,

$$\frac{2m+1}{2e\|\theta\|_1} = y \stackrel{(I12)}{\geq} f^{-1}(\gamma) = e^{W(\gamma)} = \frac{1}{e\|\theta\|_1} \log \left( \frac{\|H\|}{\varepsilon\sqrt{e^3\|\theta\|_1}} \right), \quad (I13)$$

or equivalently,

$$m \geq e\|\theta\|_1 \exp \left( W \left( \frac{1}{e\|\theta\|_1} \log \left( \frac{\|H\|}{\varepsilon\sqrt{e^3\|\theta\|_1}} \right) \right) \right) - \frac{1}{2} =: b(\theta). \quad (I14)$$

In order to prove that  $y > 1$  always holds true in our case, we prove the following: If  $\|\theta\|_1 \rightarrow \infty$  as  $D \rightarrow \infty$ , then there exists a lower bound  $b(\theta) \sim e\|\theta\|_1$  as  $D \rightarrow \infty$ , where  $b(\theta)$  is the lower bound defined in Eq. (I14). Let us substitute

$$x := \frac{1}{e\|\theta\|_1} \log \left( \frac{\|H\|}{\varepsilon\sqrt{e^3\|\theta\|_1}} \right). \quad (I15)$$

Observe that  $x \rightarrow 0$  as  $D \rightarrow \infty$  by assumption on the asymptotics of  $\|\theta\|_1$  (even if  $\|H\|$  and/or  $\varepsilon > 0$  depend on  $D$ , provided that their ratio is not exponential in  $D$  which is insured by  $|\mathcal{I}| = \mathcal{O}(\text{Poly}(D))$ ). Moreover, by definition of the Lambert- $W$ -function [62], we have  $W(x)e^{W(x)} = x$ . Therefore, applying Lemma 8 (which tells us that  $x/W(x) \sim 1$  as  $x \rightarrow 0$ ),

$$m(x) \stackrel{(I14)}{\geq} b(\theta) = e\|\theta\|_1 \exp(W(x)) - \frac{1}{2} = e\|\theta\|_1 \frac{x}{W(x)} - \frac{1}{2} \sim e\|\theta\|_1 \quad (I16)$$

as  $D \rightarrow \infty$  (since  $x \rightarrow 0$ ). In particular, recalling Eq. (I12),  $y > 1$  equivalently means that

$$m > e\|\theta\|_1 - 1, \quad (I17)$$

which always holds true by Eq. (I16). Moreover, Eq. (I16) also shows that  $m(\theta) \sim e\|\theta\|_1$  as  $D \rightarrow \infty$  is sufficient for the truncation threshold to ensure the error tolerance  $\varepsilon > 0$ .  $\square$

The asymptotics of the lower bound in Lemma 9 may be used to establish useful statistical insights about the expected truncation threshold, given a certain initial distribution  $\mathbb{P}_\theta$ :

**Proposition 3.** Consider an expectation of the form in Eq. (E1) with a variational ansatz  $U(\theta)$  involving  $D \geq 1$  parameters, and suppose we simulate it classically using the Taylor series  $C_m(\theta)$  defined in Eq. (D9) within some error tolerance  $\varepsilon$ . Let  $m = m(\theta)$  be the truncation threshold in the Taylor-approximation in Eq. (D9). Initialize  $\theta \sim \mathbb{P}_\theta \in \{\mathcal{N}(0, \sigma^2 I_D), \text{Unif}([- \sigma, \sigma]^D)\}$  with i.i.d. components  $\theta_1, \dots, \theta_D$ , where  $\sigma = D^{-r}$  for some  $r \in [0, 1)$ . Then, as  $D \rightarrow \infty$ , the expected truncation threshold behaves according to

$$\mathbb{E}_\theta[m(\theta)] = \Theta(D^{1-r}).$$

*Proof.* Let  $r \in [0, 1)$  be arbitrary. By Lemma 9 we know that  $m(\theta) \sim e\|\theta\|_1$  as  $D \rightarrow \infty$  is sufficient to simulate  $C_m(\theta)$  within some error tolerance  $\varepsilon > 0$ . By the law of large numbers we may simply take the expectation value of the  $\ell_1$ -norm which gives

$$\mathbb{E}_\theta[\|\theta\|_1] = \sum_{k=1}^D \mathbb{E}_\theta[|\theta_k|] = D \underbrace{\mathbb{E}_\theta[|\theta_1|]}_{=\Theta(\sigma)} = D \Theta(D^{-r}) = \Theta(D^{1-r}), \quad (\text{I18})$$

where the second equality uses that the components of  $\theta$  are i.i.d.  $\square$

## 2. Mean-Squared Error Analysis

Next, we quantify the mean squared error of the approximation  $C_m(\theta) \approx C(\theta)$  with respect to the local distribution  $\mathbb{P}_\theta \in \{\mathcal{N}(0, \sigma^2 I_D), \text{Unif}([- \sigma, \sigma]^D)\}$  for some  $\sigma > 0$ . However, we first require the following counting argument to conclude with the result:

**Lemma 10.** Let  $m = \mathcal{O}(1)$  be of constant order, i.e. independent of  $D$ . Then,

$$\sum_{\|\alpha\|_1 < m} 1 = \mathcal{O}(D^{m-1}), \quad (\text{I19})$$

where  $\{\|\alpha\|_1 < m\} := \{\alpha \in \mathbb{N}_0^D : |\alpha_1| + \dots + |\alpha_D| < m\}$ . Moreover,

$$\sum_{\substack{\|\alpha\|_1, \|\beta\|_1 = m \\ \alpha_k + \beta_k \text{ even } \forall k}} 1 = \mathcal{O}(D^m), \quad (\text{I20})$$

where  $\{\|\alpha\|_1, \|\beta\|_1 < m : \alpha_k + \beta_k \text{ even } \forall k\} := \{(\alpha, \beta) \in \mathbb{N}_0^D \times \mathbb{N}_0^D : \|\alpha\|_1 = \|\beta\|_1 = m, \forall k \in [D] : \alpha_k + \beta_k \in 2\mathbb{N}\}$ .

*Proof.* We begin by proving Eq. (I19). By the ‘‘balls and cells’’ formula [64, Eq. (5.2)], we count

$$\sum_{\|\alpha\|_1 < m} 1 = \sum_{i=0}^{m-1} \left( \sum_{\|\alpha\|_1 = i} 1 \right) = \sum_{i=0}^{m-1} \binom{D+i-1}{i} = \mathcal{O} \left( \binom{D+m-2}{m-1} \right) = \mathcal{O}(D^{m-1}), \quad (\text{I21})$$

due of the assumption that  $m = \mathcal{O}(1)$ , leading to

$$\begin{aligned} \binom{D+m-2}{m-1} &= \frac{(D+m-2)!}{(m-1)!(D+m-2-(m-1))!} = \frac{(D-1+(m-1))!}{(m-1)!(D-1)!} \\ &= \frac{1}{(m-1)!} \prod_{i=1}^{m-1} (D-1+i) = \mathcal{O}(D^{m-1}). \end{aligned} \quad (\text{I22})$$

Next, let us show Eq. (I20). First, note that  $\alpha_k + \beta_k$  are even if and only if for each  $k \in [D]$  there exists  $\gamma_k \in \mathbb{N}_0$  such that  $\alpha_k + \beta_k = 2\gamma_k$ . Therefore, combined with  $\|\alpha\|_1 = \|\beta\|_1 = m$ , we find

$$2m = \|\alpha\|_1 + \|\beta\|_1 = \sum_{k=1}^D \{\alpha_k + \beta_k\} = 2 \sum_{k=1}^D \gamma_k = 2\|\gamma\|_1 \iff \|\gamma\|_1 = m. \quad (\text{I23})$$

Furthermore, once again utilizing the ‘‘balls and cells’’ formula [64, Eq. (5.2)], we find

$$\#\{\gamma \in \mathbb{N}_0^D : \|\gamma\|_1 = m\} = \sum_{\|\gamma\|_1=m} 1 = \binom{D+m-1}{m} = \mathcal{O}(D^m), \quad (\text{I24})$$

where the last equality follows from Eq. (I22). As a result,

$$\sum_{\substack{\|\alpha\|_1, \|\beta\|_1=m \\ \alpha_k + \beta_k \text{ even } \forall k}} 1 \stackrel{(\text{I23})}{=} \#\{\gamma \in \mathbb{N}_0^D : \|\gamma\|_1 = m\} = \mathcal{O}(D^m). \quad (\text{I25})$$

□

We are now equipped with all necessary tools to bound the mean-squared error:

**Lemma 11.** *Consider an expectation of the form in Eq. (E1) with a variational ansatz  $U(\theta)$  involving  $D \geq 1$  parameters, and suppose we simulate it classically using the Taylor series  $C_m(\theta)$  defined in Eq. (D9). Initialize  $\theta \sim \mathbb{P}_\theta \in \{\mathcal{N}(0, \sigma^2 I_D), \text{Unif}([- \sigma, \sigma]^D)\}$  with i.i.d. components  $\theta_1, \dots, \theta_D$ . Then, the mean squared error satisfies the bound*

$$\mathbb{E}_\theta[(C(\theta) - C_m(\theta))^2] = \mathcal{O}(\|H\|^2 D^m \sigma^{2m}), \quad (\text{I26})$$

where  $\|H\|$  is the operator norm of the observable in Eq. (F1). In particular, if  $\sigma = \mathcal{O}(\|H\|^{-\frac{1}{m}} D^{-\frac{1+\delta}{2}})$  for some arbitrarily small  $\delta > 0$ , then the mean squared error decays like  $\mathcal{O}(D^{-\delta m})$ . Alternatively, if  $\sigma = q \|H\|^{-\frac{1}{m}} D^{-\frac{1}{2}}$  for some  $0 < q < 1$ , then the mean squared error decays like  $\mathcal{O}(q^{2m})$ .

*Proof.* We use the Lagrange-remainder to quantify the error,

$$C(\theta) - C_m(\theta) = \sum_{\|\alpha\|_1 \geq m} (D_\theta^\alpha C)(0) \frac{\theta^\alpha}{\alpha!} = \sum_{\|\alpha\|_1=m} \underbrace{(D_\theta^\alpha C)(\xi)}_{\leq \mathcal{O}(\|H\|)} \frac{\theta^\alpha}{\alpha!} = \mathcal{O}(\|H\|) \sum_{\|\alpha\|_1=m} \frac{\theta^\alpha}{\alpha!}, \quad (\text{I27})$$

employing the uniform bound  $(D_\theta^\alpha C)(\xi) \leq \mathcal{O}(\|H\|)$  in the higher-order parameter-shift rule, Lemma 3, in the last estimation.

Moreover, we shall employ the well-known moments formula,

$$\mathbb{E}_\theta[\theta^\alpha] = \delta_{\{\alpha_k \in 2\mathbb{N} \forall k\}}(\alpha) \cdot \begin{cases} (\alpha - 1)!! \sigma^\alpha, & \theta \sim \mathcal{N}(0, \sigma^2 I_D), \\ \sigma^\alpha \prod_{k=1}^D (\alpha_k + 1)^{-1}, & \theta \sim \text{Unif}([- \sigma, \sigma]^D), \end{cases} \quad (\text{I28})$$

in order to evaluate the mean squared error. Here, we use the assumption that  $\theta_1, \dots, \theta_D$  are independent. We employ the canonical notations  $\sigma^\alpha := \sigma^{\alpha_1} \dots \sigma^{\alpha_D}$  and  $(\alpha - 1)!! := \prod_{k \in [D]} (\alpha_k - 1)!!$ . Consequently,

$$\begin{aligned} \mathbb{E}_\theta[(C(\theta) - C_m(\theta))^2] &\stackrel{(\text{I27})}{=} \mathcal{O}(\|H\|^2) \mathbb{E}_\theta \left[ \left( \sum_{\|\alpha\|_1=m} \frac{\theta^\alpha}{\alpha!} \right)^2 \right] = \mathcal{O}(\|H\|^2) \sum_{\|\alpha\|_1, \|\beta\|_1=m} \frac{\mathbb{E}_\theta[\theta^{\alpha+\beta}]}{\alpha! \beta!} \\ &\stackrel{(\text{I28})}{=} \mathcal{O}(\|H\|^2 \sigma^{2m}) \sum_{\substack{\|\alpha\|_1, \|\beta\|_1=m \\ \alpha_k + \beta_k \text{ even } \forall k}} 1 = \mathcal{O}(\|H\|^2 D^m \sigma^{2m}), \end{aligned} \quad (\text{I29})$$

where the last bound follows from Eq. (I20) in Lemma 10.

The second statement is immediately obtained by solving for  $\sigma$  in  $\|H\|^2 D^m \sigma^{2m} \stackrel{!}{=} D^{-\delta m}$ , and  $\|H\|^2 D^m \sigma^{2m} \stackrel{!}{=} q^{2m}$ , respectively. □

The next step is to establish a lower bound for the necessary truncation threshold  $m = m(\mathbb{P}_\theta)$  in order to Taylor surrogate the cost in Eq. (E1), i.e. evaluate  $C_m(\theta)$  with high probability and error of at most  $\varepsilon > 0$ :

**Lemma 12.** Consider an expectation of the form in Eq. (E1) with a variational ansatz  $U(\theta)$  involving  $D \geq 1$  parameters, and suppose we simulate it classically using the Taylor series  $C_m(\theta)$  defined in Eq. (D9). Assume that the mean squared error in Eq. (I26) is bounded by a given tolerance  $\varepsilon > 0$ . Initialize  $\theta \sim \mathbb{P}_\theta \in \{\mathcal{N}(0, \sigma^2 I_D), \text{Unif}([- \sigma, \sigma]^D)\}$  with i.i.d. components  $\theta_1, \dots, \theta_D$ , where  $\sigma = \mathcal{O}(\|H\|^{-\frac{1}{m}} D^{-\frac{1+\delta}{2}})$  for some arbitrarily small  $\delta > 0$ . Then, there exists a constant  $c > 0$  such that, with probability at least  $1 - \rho$ , a constant truncation threshold  $m = m(\mathbb{P}_\theta)$  satisfying

$$m(\mathbb{P}_\theta) \geq \frac{1}{\delta} \frac{\log\left(\frac{c}{\rho \varepsilon^2}\right)}{\log D}$$

is sufficient to simulate  $C_m(\theta)$  with error at most  $\varepsilon > 0$ . Alternatively, if  $\sigma = q \|H\|^{-\frac{1}{m}} D^{-\frac{1}{2}}$  for some  $0 < q < 1$ , then we have the analogous result with

$$m(\mathbb{P}_\theta) \geq \frac{1}{2} \frac{\log\left(\frac{c}{\rho \varepsilon^2}\right)}{\log\left(\frac{1}{q}\right)}.$$

*Proof.* Let  $\delta, \varepsilon, \rho > 0$  be arbitrary. By Lemma 11, since  $\sigma = \mathcal{O}(\|H\|^{-\frac{1}{m}} D^{-\frac{1+\delta}{2}})$ , we know that the mean squared error satisfies

$$\mathbb{E}_\theta[(C(\theta) - C_m(\theta))^2] \leq c D^{-\delta m} \quad (\text{I30})$$

for some constant  $c > 0$ . Therefore, by Markov's inequality, we may bound the probability of failure,

$$\mathbb{P}_\theta(|C(\theta) - C_m(\theta)| \geq \varepsilon) = \mathbb{P}_\theta((C(\theta) - C_m(\theta))^2 \geq \varepsilon^2) \leq \frac{\mathbb{E}_\theta[(C(\theta) - C_m(\theta))^2]}{\varepsilon^2} \stackrel{(\text{I30})}{\leq} \frac{c D^{-\delta m}}{\varepsilon^2} \stackrel{!}{\leq} \rho. \quad (\text{I31})$$

Hence, it remains to solve for the truncation threshold  $m$  in  $\varepsilon^{-2} c D^{-\delta m} \leq \rho$ . Taking the logarithm on both sides,

$$-\delta m \log D \leq \log\left(\frac{\rho \varepsilon^2}{c}\right), \quad (\text{I32})$$

or equivalently,

$$\delta m \log D \geq \log\left(\frac{c}{\rho \varepsilon^2}\right), \quad (\text{I33})$$

which yields the desired constant lower bound for  $m$ .

Analogously, if  $\sigma = q \|H\|^{-\frac{1}{m}} D^{-\frac{1}{2}}$ , Lemma 11 yields

$$\mathbb{E}_\theta[(C(\theta) - C_m(\theta))^2] \leq c q^{2m} \quad (\text{I34})$$

for some constant  $c > 0$ . In that case, the probability of failure satisfies

$$\mathbb{P}_\theta(|C(\theta) - C_m(\theta)| \geq \varepsilon) \leq \frac{\mathbb{E}_\theta[(C(\theta) - C_m(\theta))^2]}{\varepsilon^2} \stackrel{(\text{I34})}{\leq} \frac{c q^{2m}}{\varepsilon^2} \stackrel{!}{\leq} \rho. \quad (\text{I35})$$

Solving for the truncation threshold  $m$  in  $\varepsilon^{-2} c q^{2m} \leq \rho$  implies

$$2m \log q \leq \log\left(\frac{\rho \varepsilon^2}{c}\right), \quad (\text{I36})$$

or equivalently, since  $\log q = -\log\left(\frac{1}{q}\right)$  because of  $0 < q < 1$ ,

$$m \geq \frac{1}{2} \frac{\log\left(\frac{c}{\rho \varepsilon^2}\right)}{\log\left(\frac{1}{q}\right)}. \quad (\text{I37})$$

□

## Appendix J: Computational Complexity

This part leverages the results of the previous section, and focuses on the computational complexity of simulating the cost function  $C(\theta)$  in Eq. (E1) with the help of the Taylor surrogate  $C_m(\theta)$  in Eq. (D9). We shall use  $\text{Time } C_m(\theta)$  to denote the time complexity of evaluating  $C_m(\theta)$ , which is, by definition, the number of operations required for evaluating the expression for  $C_m(\theta)$ . Furthermore, we use the following Landau notations to characterize asymptotic behavior of a function  $f : \mathbb{R}_{\geq 1} \rightarrow \mathbb{R}$  in terms of some  $g : \mathbb{R}_{\geq 1} \rightarrow \mathbb{R}$ , as  $x \rightarrow \infty$ :

$$\begin{aligned} f(x) = \mathcal{O}(g(x)) & : \iff \lim_{x \rightarrow \infty} \left| \frac{f(x)}{g(x)} \right| \in [0, \infty) \\ f(x) = \Omega(g(x)) & : \iff \lim_{x \rightarrow \infty} \left| \frac{f(x)}{g(x)} \right| \in (0, \infty] \\ f(x) = \Theta(g(x)) & : \iff \lim_{x \rightarrow \infty} \left| \frac{f(x)}{g(x)} \right| \in (0, \infty), \end{aligned} \quad (\text{J1})$$

assuming that there exists  $x_0 \geq 1$  such that  $g(x) \neq 0$  for all  $x \geq x_0$ . Furthermore, we say that  $f(x)$  and  $g(x)$  are *asymptotically equivalent* if the much stronger condition,

$$\lim_{x \rightarrow \infty} \frac{f(x)}{g(x)} = 1, \quad (\text{J2})$$

holds true. In that case, we write  $f(x) \sim g(x)$  as  $x \rightarrow \infty$ .

### 1. Deterministic Worst-Case Simulation Complexity

We begin with the deterministic error analysis, where we are able to highlight a computational phase transition from polynomial to super-polynomial complexity, which is characterized by the  $\ell_1$ -norm  $\|\theta\|_1$  of the parameter configuration:

**Theorem 3.** (Deterministic Complexity) *Consider an expectation of the form Eq. (E1) with a variational ansatz  $U(\theta)$  involving  $D \geq 1$  parameters, and suppose we simulate it classically using the Taylor series  $C_m(\theta)$  defined in Eq. (D9) with truncation threshold  $m = m(\theta)$  given by Lemma 9. Assume that almost every component  $\theta_k$  contributes comparably to  $\|\theta\|_1$ . Then, if  $\|\theta\|_1 = \mathcal{O}(1)$ , the runtime of computing  $C_m(\theta)$  is polynomial, namely  $\mathcal{O}(|\mathcal{I}|D^m)$ . On the other hand, if  $\|\theta\|_1 \rightarrow \infty$  as  $D \rightarrow \infty$ , the runtime becomes super-polynomial,*

$$\text{Time } C_m(\theta) = \mathcal{O} \left( |\mathcal{I}| \sqrt{\frac{D(D + e\|\theta\|_1)}{2\pi e\|\theta\|_1}} \exp \left[ e\|\theta\|_1 \left( 1 + \log \left( 2 + \frac{2D}{e\|\theta\|_1} \right) \right) \right] \right), \quad (\text{J3})$$

which saturates to exponential scaling (at most  $\mathcal{O}(|\mathcal{I}|D^{2^D})$ ) if and only if  $\|\theta\|_1 = \Theta(D)$ .

*Proof.* By the higher-order parameter-shift rule, Lemma 3, we may write

$$C_m(\theta) = \sum_{|\alpha| < m} (D_\theta^\alpha C)(0) \frac{\theta^\alpha}{\alpha!} = \sum_{|\alpha| < m} \frac{\theta^\alpha}{\alpha!} \sum_{\substack{j \in \mathbb{N}_0^D \\ j_k \leq \alpha_k \forall k}} (-1)^{|j|} \binom{\alpha}{j} C(\xi_{j,\alpha}) = \sum_{(j,\alpha) \in \Lambda_m} \frac{\theta^\alpha}{\alpha!} (-1)^{|j|} \binom{\alpha}{j} C(\xi_{j,\alpha}), \quad (\text{J4})$$

where  $\xi_{j,\alpha} := \frac{\pi}{2} \sum_{k=1}^D (\alpha_k - 2j_k) e_k$ , with  $e_k$  denoting the  $k$ -th unit vector, and indexing set

$$\Lambda_m := \{(j, \alpha) \in \mathbb{N}_0^D \times \mathbb{N}_0^D : |\alpha| < m, \forall k \in [D] : 0 \leq j_k \leq \alpha_k\}. \quad (\text{J5})$$

The computational complexity for each of the evaluation of  $C(\xi_{j,\alpha})$  using Gottesman-Knill is of order  $\mathcal{O}(D|\mathcal{I}|)$  [20, 21], which is the most expensive computation in our simulation strategy. At the end of the proof, we will justify why Gottesman-Knill may be applied for each  $\xi_{j,\alpha}$ . As a result, the time resources required to compute  $C_m(\theta)$  scales like

$$\begin{aligned} \text{Time } C_m(\theta) &= \mathcal{O}(D|\mathcal{I}|) \cdot \#\{C(\xi_{j,\alpha}) : (j, \alpha) \in \Lambda_m\} \\ &\leq \mathcal{O}(D|\mathcal{I}|) \#\Lambda_m = \mathcal{O}(D|\mathcal{I}|) \sum_{|\alpha| < m} \underbrace{\prod_{k=1}^D (\alpha_k + 1)}_{\leq 2^{\|\alpha\|_1} \leq 2^{m-1}} \leq \mathcal{O} \left( D|\mathcal{I}| 2^m \sum_{\|\alpha\|_1 < m} 1 \right). \end{aligned} \quad (\text{J6})$$

If  $\|\theta\|_1 = \mathcal{O}(1)$ , then we know that  $m = m(\theta) = \mathcal{O}(1)$  by Lemma 9. Therefore, we may employ Eq. (I19) in Lemma 10 to establish the polynomial complexity,

$$\text{Time } C_m(\theta) = \mathcal{O} \left( D |\mathcal{I}| \sum_{\|\alpha\|_1 < m} 1 \right) = \mathcal{O}(|\mathcal{I}| D^m), \quad (\text{J7})$$

as claimed.

Next, we will prove the super-polynomial case where  $\|\theta\|_1 \rightarrow \infty$  as  $D \rightarrow \infty$ . By Lemma 9 we know that  $m = m(\theta) = \Omega(\|\theta\|_1)$  as  $D \rightarrow \infty$ . By the ‘‘balls and cells’’ formula [64, Eq. (5.2)], we count

$$\sum_{\|\alpha\|_1 < m} 1 = \sum_{i=0}^{m-1} \left( \sum_{\|\alpha\|_1=i} 1 \right) = \sum_{i=0}^{m-1} \binom{D+i-1}{i} = \mathcal{O} \left( \binom{D+m-2}{m-1} \right). \quad (\text{J8})$$

Thus, the time complexity in Eq. (J6) is bounded by

$$\text{Time } C_m(\theta) = \mathcal{O} \left( D |\mathcal{I}| 2^m \binom{D+m-2}{m-1} \right). \quad (\text{J9})$$

We shall utilize Stirling’s formula

$$n! \sim \sqrt{2\pi n} \left( \frac{n}{e} \right)^n, \quad (\text{J10})$$

to approximate the binomial coefficient. Note asymptotic equivalence ‘‘ $\sim$ ’’ is sufficient for the tight asymptotics ‘‘ $\Theta$ ’’, allowing us to use it without problems for deriving an asymptotic upper bound ‘‘ $\mathcal{O}$ ’’ for the time complexity  $\text{Time } C_m(\theta)$ . Indeed, this is due to Eq. (J2) always implying Eqs. (J1). We also approximate  $D+m-2 \sim D+m$ , and  $m-1 \sim m$  (recall from above the  $m \sim e\|\theta\|_1 \rightarrow \infty$  as  $D \rightarrow \infty$ ). That is,

$$\begin{aligned} 2^m \binom{D+m-2}{m-1} &\sim 2^m \binom{D+m}{m} \sim 2^m \sqrt{\frac{D+m}{2\pi m D}} \frac{(D+m)^{D+m}}{D^D m^m} \\ &= 2^m \sqrt{\frac{D+m}{2\pi m D}} \left( \frac{D+m}{D} \right)^D \left( \frac{D+m}{m} \right)^m \\ &= \sqrt{\frac{D+m}{2\pi m D}} \exp \left\{ D \log \left( 1 + \frac{m}{D} \right) + m \log \left( 2 + \frac{2D}{m} \right) \right\}, \end{aligned} \quad (\text{J11})$$

using  $2^m = e^{m \log 2}$ . Assuming  $m < \Theta(D)$ , i.e.  $\frac{m}{D} \rightarrow 0$  as  $D \rightarrow \infty$ , we may use the elementary approximation

$$\log \left( 1 + \frac{m}{D} \right) \sim \frac{m}{D}, \quad (\text{J12})$$

and find, as  $D \rightarrow \infty$ ,

$$\begin{aligned} \exp \left\{ D \log \left( 1 + \frac{m}{D} \right) + m \log \left( 2 + \frac{2D}{m} \right) \right\} &= \exp \left[ m \left( 1 + \log \left( 2 + \frac{2D}{m} \right) \right) \right] \\ &\sim \exp \left[ e\|\theta\|_1 \left( 1 + \log \left( 2 + \frac{2D}{e\|\theta\|_1} \right) \right) \right], \end{aligned} \quad (\text{J13})$$

once again employing Lemma 9 which states that  $m(\theta) \sim e\|\theta\|_1$  as  $D \rightarrow \infty$  is sufficient for simulating  $C_m(\theta)$  within some error tolerance  $\varepsilon$ . Therefore, combining Eq. (J6) with the approximations in Eq. (J11) and Eq. (J13) yields

$$\text{Time } C_m(\theta) = \mathcal{O} \left( |\mathcal{I}| \sqrt{\frac{D(D+e\|\theta\|_1)}{2\pi e\|\theta\|_1}} \exp \left[ e\|\theta\|_1 \left( 1 + \log \left( 2 + \frac{2D}{e\|\theta\|_1} \right) \right) \right] \right), \quad (\text{J14})$$

as  $D \rightarrow \infty$ , as claimed.

Finally, let us consider the worst-case scenario where  $\|\theta\|_1 = \Theta(D)$  grows linearly in  $D$ . As discussed in Eq. (J6), we have

$$\text{Time } C_m(\theta) = \mathcal{O}(D|\mathcal{I}|) \cdot \#\{C(\xi_{j,\alpha}) : (j,\alpha) \in \Lambda_m\}. \quad (\text{J15})$$

What one could think about is whether it is possible to significantly reduce the cardinality of  $\Lambda_m$  by using the fact that  $C(\cdot)$  is  $2\pi$ -periodic in each direction in parameter space.

Indeed, note that  $(\xi_{j,\alpha})_k$  corresponds to a shift of  $2\pi$  in the  $k$ -th coordinate if and only if  $\alpha_k - 2j_k = 4$ . Therefore,  $C(\xi_{j,\alpha})$  depends only on  $\alpha_k - 2j_k \bmod 4$  for all  $k \in [D]$ . In other words:

$$\text{for each } (j,\alpha) \in \Lambda_m \text{ there exists } \beta_{j,\alpha} \in \{0, 1, 2, 3\}^D \text{ such that } C(\xi_{j,\alpha}) = C\left(\frac{\pi}{2}\beta_{j,\alpha}\right). \quad (\text{J16})$$

This particularly means that in the worst case scenario, we require at most  $4^D = 2^{2D}$  different evaluations of  $C(\xi_{j,\alpha})$ . As a result, it is possible to optimize the worst-case runtime to achieve

$$\text{Time } C_m(\theta) = \mathcal{O}(|\mathcal{I}| D 2^{2D}), \quad (\text{J17})$$

as claimed. Note that this scales worse compared to the computational complexity  $\mathcal{O}(|\mathcal{I}| 2^{2N})$  of naively evaluating the exponential quadratic form in Eq. (6), since high expressivity requires that  $N \ll D$ .

It remains to justify the application of Gottesman-Knill's theorem for each  $\xi_{j,\alpha}$ . It suffices to show that  $U(\xi_{j,\alpha}) \in \text{Clifford}(N)$  because of  $C(\xi_{j,\alpha}) = \langle 0|U(\xi_{j,\alpha})^\dagger \hat{O}U(\xi_{j,\alpha})|0\rangle$ . Indeed, note that  $e^{-i\frac{\pi}{4}}R_X\left(\frac{\pi}{2}\right) = HSH \in \text{Clifford}(N)$ ,  $R_Y\left(\frac{\pi}{2}\right) = XH \in \text{Clifford}(N)$ , and  $e^{-i\frac{\pi}{4}}R_Z\left(\frac{\pi}{2}\right) = S \in \text{Clifford}(N)$  (global phases are irrelevant). This particularly means for multiples of  $\frac{\pi}{2}$  that  $R_X\left(\frac{\pi}{2}\mathbb{Z}\right), R_Y\left(\frac{\pi}{2}\mathbb{Z}\right), R_Z\left(\frac{\pi}{2}\mathbb{Z}\right) \subset \text{Clifford}(N)$ , respectively. This follows from the fact that  $\text{Clifford}(N)$  defines a group. As a result, since  $\frac{\pi}{2}(\alpha_k - 2j_k) \in \frac{\pi}{2}\mathbb{Z}$  is also multiple of  $\frac{\pi}{2}$ , we find

$$U(\xi_{j,\alpha}) \in \left\langle R_X\left(\frac{\pi}{2}\mathbb{Z}\right), R_Y\left(\frac{\pi}{2}\mathbb{Z}\right), R_Z\left(\frac{\pi}{2}\mathbb{Z}\right), \text{Clifford}(N) \right\rangle_N \subset \text{Clifford}(N). \quad (\text{J18})$$

By the Gottesman-Knill theorem, we thus know that the cost evaluation  $C(\xi_{j,\alpha})$  is easy to simulate classically, i.e. it can be computed in polynomial time  $\mathcal{O}(D|\mathcal{I}|)$  on a conventional computer [20, 21].  $\square$

## 2. Probabilistic Mean-Squared Simulation Complexity

Next, we use the mean-squared error analysis in order to determine the Gaussian/uniform initialization strategy  $\mathbb{P}_\theta$  that covers the largest landscape patch where Taylor surrogating the cost  $C(\cdot)$  remains polynomially efficient.

**Theorem 4.** *Consider an expectation of the form in Eq. (E1) with a variational ansatz  $U(\theta)$  involving  $D \geq 1$  parameters, and suppose we simulate it classically using the Taylor series  $C_m(\theta)$  defined in Eq. (D9). Initialize the parameters  $\theta \sim \mathbb{P}_\theta \in \{\mathcal{N}(0, \sigma^2 I_D), \text{Unif}([- \sigma, \sigma]^D)\}$  with i.i.d. components  $\theta_1, \dots, \theta_D$  according to Eq. (20) with constant  $c > 0$ . Then, with probability at least  $1 - \rho$ , the computational cost  $\text{Time } C_m(\theta \sim \mathbb{P}_\theta)$  of simulating  $C(\theta)$  up to an error  $\varepsilon > 0$ , is of polynomial order,*

$$\mathcal{O}\left(|\mathcal{I}| D^{\frac{1}{\delta \log D} \log\left(\frac{c}{\rho \varepsilon^2}\right)}\right)$$

for asymptotic local initialization, i.e.  $\sigma = \mathcal{O}(\|H\|^{-\frac{1}{m}} D^{-\frac{1+\delta}{2}})$  for some  $\delta > 0$  and

$$\mathcal{O}\left(|\mathcal{I}| D^{\frac{1}{2 \log\left(\frac{1}{q}\right)} \log\left(\frac{c}{\rho \varepsilon^2}\right)}\right)$$

for non-asymptotic local initialization, i.e.  $\sigma = q \|H\|^{-\frac{1}{m}} D^{-\frac{1}{2}}$  for some  $0 < q < 1$ , respectively.

*Proof.* By the higher-order parameter-shift rule, Lemma 3, we may write

$$C_m(\theta) = \sum_{|\alpha| < m} (D_\theta^\alpha C)(0) \frac{\theta^\alpha}{\alpha!} = \sum_{|\alpha| < m} \frac{\theta^\alpha}{\alpha!} \sum_{\substack{j \in \mathbb{N}_0^D \\ j_k \leq \alpha_k \forall k}} (-1)^{|j|} \binom{\alpha}{j} C(\xi_{j,\alpha}) = \sum_{(j,\alpha) \in \Lambda_m} \frac{\theta^\alpha}{\alpha!} (-1)^{|j|} \binom{\alpha}{j} C(\xi_{j,\alpha}), \quad (\text{J19})$$

where  $\xi_{j,\alpha} := \frac{\pi}{2} \sum_{k=1}^D (\alpha_k - 2j_k) e_k$ , with  $e_k$  denoting the  $k$ -th unit vector, and indexing set

$$\Lambda_m := \{(j, \alpha) \in \mathbb{N}_0^D \times \mathbb{N}_0^D : |\alpha| < m, \forall k \in [D] : 0 \leq j_k \leq \alpha_k\}. \quad (\text{J20})$$

The computational complexity for each of the evaluation of  $C(\xi_{j,\alpha})$  using Gottesman-Knill is of order  $\mathcal{O}(D |\mathcal{I}|)$ , which is the most expensive computation in our simulation strategy. We have already justified in the proof of Theorem 3 why Gottesman-Knill may be applied for each  $\xi_{j,\alpha}$ . As a result, the time resources requires to compute  $C_m(\theta)$  scales like

$$\begin{aligned} \text{Time } C_m(\theta) &= \mathcal{O}(D |\mathcal{I}|) \cdot \#\{C(\xi_{j,\alpha}) : (j, \alpha) \in \Lambda_m\} \\ &\leq \mathcal{O}(D |\mathcal{I}|) \#\Lambda_m = \mathcal{O}(D |\mathcal{I}|) \sum_{|\alpha| < m} \underbrace{\prod_{k=1}^D (\alpha_k + 1)}_{\leq 2^{\|\alpha\|_1} \leq 2^{m-1}} \leq \mathcal{O} \left( D |\mathcal{I}| 2^m \sum_{\|\alpha\|_1 < m} 1 \right). \end{aligned} \quad (\text{J21})$$

For  $\|\theta\|_1 = \mathcal{O}(1)$ , we have already establish polynomial complexity in Eq. (J7), i.e.

$$\text{Time } C_m(\theta) = \mathcal{O} \left( D |\mathcal{I}| \sum_{\|\alpha\|_1 < m} 1 \right) = \mathcal{O}(|\mathcal{I}| D^m), \quad (\text{J22})$$

By Lemma 12 we know that, with probability at least  $1 - \rho$ , a constant truncation threshold satisfying

$$m \geq \frac{1}{\delta} \frac{\log \left( \frac{c}{\rho \varepsilon^2} \right)}{\log D}, \quad \text{and} \quad m \geq \frac{1}{2} \frac{\log \left( \frac{c}{\rho \varepsilon^2} \right)}{\log \left( \frac{1}{q} \right)} \quad (\text{J23})$$

for the other initialization strategy, respectively, is sufficient to simulate  $C_m(\theta)$  with error at most  $\varepsilon > 0$ .  $\square$

### 3. Complexity Comparison with the Pauli Path Surrogate

We conclude our complexity analysis by showing that our Taylor surrogate outperforms the Pauli path surrogate employed by Lerch et al. [18], as long as the patch is sufficiently small:

**Corollary 3.** *Consider an expectation of the form in Eq. (E1) with a variational ansatz  $U(\theta)$  involving  $D \geq 1$  parameters, and suppose we simulate it classically using the Taylor series  $C_m(\theta)$  defined in Eq. (D9). Initialize  $\theta \sim \mathbb{P}_\theta \in \{\mathcal{N}(0, \sigma^2 I_D), \text{Unif}([- \sigma, \sigma]^D)\}$  with i.i.d. components  $\theta_1, \dots, \theta_D$ , where  $\sigma = q \|H\|^{-\frac{1}{m}} D^{-\frac{1}{2}}$  for some  $0 < q < 1$ , so that*

$$\mathbb{E}_\theta [(C(\theta) - C_m(\theta))^2] \leq c q^{2m}$$

for some constant  $c > 0$  as per Lemma 11.

As shown by Lerch et al. in Ref. [18, Theorem 2, Eq. (13)], with probability at least  $1 - \rho$ , the Pauli-propagation algorithm  $\hat{C}(\theta)$  can simulate the cost  $C(\theta)$  up to error  $\varepsilon > 0$  using

$$\text{Time } \hat{C}(\theta \sim \mathbb{P}_\theta) = \gamma_1 |\mathcal{I}| D^{\log \left( \frac{1}{\rho \varepsilon^2} \right)}$$

many operations for some constant  $\gamma_1 > 0$ . On the other hand, by Theorem 4, we know that, with probability at least  $1 - \rho$ , the Taylor-simulation algorithm  $C_m(\theta)$  can simulate the cost  $C(\theta)$  up to error  $\varepsilon > 0$  using

$$\text{Time } C_m(\theta \sim \mathbb{P}_\theta) = \gamma_2 |\mathcal{I}| D^{\frac{1}{2 \log \left( \frac{1}{4} \right)} \log \left( \frac{c}{\rho \varepsilon^2} \right)}$$

many operations for some constant  $\gamma_2 > 0$ .

Then, setting  $\gamma := \frac{\gamma_1}{\gamma_2} > 0$ , our algorithm outperforms the Pauli-propagation technique, i.e.  $\text{Time } C_m(\theta) < \text{Time } \hat{C}(\theta)$ , if and only if

$$q < \exp\left(-\frac{\log\left(\frac{c}{\rho\varepsilon^2}\right)}{2\log\left(\frac{1}{\rho\varepsilon^2}\right) + \frac{2\log\gamma}{\log D}}\right), \quad (\text{J24})$$

provided that

$$D > \exp\left(\frac{\log\gamma}{\log\rho + 2\log\varepsilon}\right) \quad (\text{J25})$$

in the case where  $\gamma < 1$ .

*Proof.* As shown by Lerch et al. in Ref. [18, Theorem 2, Eq. (13)], with probability at least  $1 - \rho$ , the Pauli-propagation algorithm  $\hat{C}(\theta)$  can simulate the cost  $C(\theta)$  up to error  $\varepsilon > 0$  using

$$\text{Time } \hat{C}(\theta) = \gamma_1 |\mathcal{I}| D^{\log\left(\frac{1}{\rho\varepsilon^2}\right)} \quad (\text{J26})$$

many operations for some constant  $\gamma_1$ . On the other hand, by Theorem 4, we know that, with probability at least  $1 - \rho$ , the Taylor surrogate  $C_m(\theta)$  can simulate the cost  $C(\theta)$  up to error  $\varepsilon > 0$  using

$$\text{Time } C_m(\theta) = \gamma_2 |\mathcal{I}| D^{\frac{1}{2\log\left(\frac{1}{q}\right)} \log\left(\frac{c}{\rho\varepsilon^2}\right)} \quad (\text{J27})$$

many operations for some constant  $\gamma_2 > 0$ . Setting  $\gamma := \frac{\gamma_1}{\gamma_2} > 0$ , we see that  $\text{Time } C_m(\theta) < \text{Time } \hat{C}(\theta)$  if and only if

$$\gamma D^{\log\left(\frac{1}{\rho\varepsilon^2}\right)} = D^{\log\left(\frac{1}{\rho\varepsilon^2}\right) + \frac{\log\gamma}{\log D}} > D^{\frac{1}{2\log\left(\frac{1}{q}\right)} \log\left(\frac{c}{\rho\varepsilon^2}\right)}. \quad (\text{J28})$$

Taking the logarithm on both sides yields

$$\log\left(\frac{1}{\rho\varepsilon^2}\right) + \frac{\log\gamma}{\log D} > \frac{1}{2\log\left(\frac{1}{q}\right)} \log\left(\frac{c}{\rho\varepsilon^2}\right), \quad (\text{J29})$$

which may equivalently be rewritten as

$$\log\left(\frac{1}{q}\right) > \frac{\log\left(\frac{c}{\rho\varepsilon^2}\right)}{2\log\left(\frac{1}{\rho\varepsilon^2}\right) + \frac{2\log\gamma}{\log D}}, \quad (\text{J30})$$

if and only if the inequality

$$\log\left(\frac{1}{\rho\varepsilon^2}\right) + \frac{\log\gamma}{\log D} > 0 \quad (\text{J31})$$

holds true. Eq. (J31) holds true trivially if  $\gamma > 1$  because of  $\rho, \varepsilon < 1$ . On the other hand, if  $\gamma < 1$ , then Eq. (J31) is equivalent to

$$\log\left(\frac{1}{\rho\varepsilon^2}\right) > \frac{\log\left(\frac{1}{\gamma}\right)}{\log D} \iff D > \exp\left(\frac{\log\left(\frac{1}{\gamma}\right)}{\log\left(\frac{1}{\rho\varepsilon^2}\right)}\right) = \exp\left(\frac{\log\gamma}{\log\rho + 2\log\varepsilon}\right), \quad (\text{J32})$$

as assumed by the statement of the corollary.

Returning to Eq. (J30), we find that it equivalently reads

$$q < \exp\left(-\frac{\log\left(\frac{c}{\rho\varepsilon^2}\right)}{2\log\left(\frac{1}{\rho\varepsilon^2}\right) + \frac{2\log\gamma}{\log D}}\right), \quad (\text{J33})$$

which concludes the proof.  $\square$

To better understand the practical implications of Corollary 3, we numerically evaluate the bound on the surrogate patch size parameter  $q$  and, if  $\gamma < 1$ , the number of parameters  $D$  required for outperforming the Pauli-propagation technique. Fig. 12 panels (a) to (c) shows the upper bounds on  $q$  (cf. Eq. (J24)) across various values of the constants  $c, \gamma$  and parameter dimensions  $D$ . Panel (d) separately shows the behavior of the lower bound for  $D$  (cf. Eq. (J25)) when  $\gamma < 1$ . The plots clarify that our Taylor-based surrogate becomes advantageous in practically relevant scenarios, especially for large-scale models with high precision and low probability of failure (i.e. small  $\varepsilon, \rho > 0$ ). For constants  $c, \gamma \in [10^{-6}, 10^6]$  and arbitrary model sizes  $D \geq 1$ , the worst case scenario requires  $q \geq 0.35$ , which does not limit practicality.

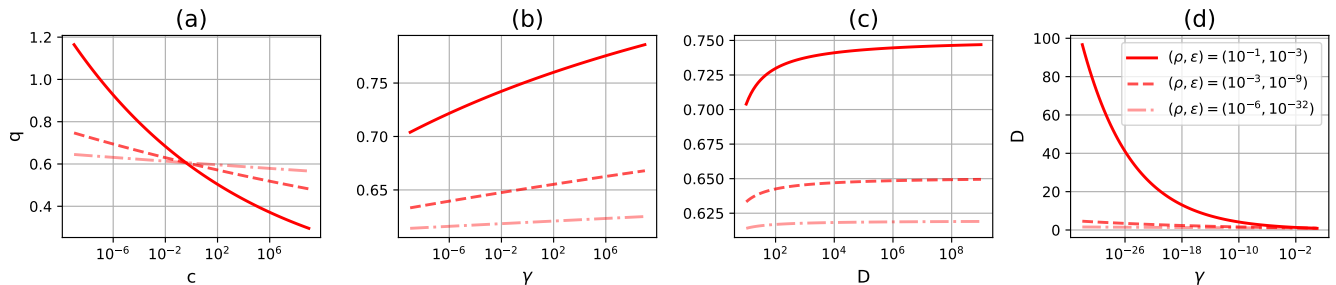


FIG. 12. Behavior of the required quantities  $q$  and  $D$ , for a polynomial speedup compared to the Pauli path simulation technique [18], as established by Corollary 3. (a) - (b): Upper bound of  $q$ . (d): Lower bound of  $D$ .

#### 4. Efficient Recursive Classical Implementation

In a practical implementation of our simulation strategy, one has to iterate over the summation  $\{\|\alpha\|_1 < m\}$  in Eq. (D9). Concretely, we are interested in finding all multi-index combinations in the set:

$$\mathcal{A}_{m,D} := \{\alpha = (\alpha_1, \dots, \alpha_D) \in \mathbb{N}_D : \|\alpha\|_1 < m\}. \quad (\text{J34})$$

When using a `for`-loop naively, one will be confronted with unnecessary computational overheads. Alternatively, we propose a recursive method that generates all combinations in the set  $\mathcal{A}_{m,D}$ , which indeed turns out to avoid the aforementioned overheads (cf. Fig. 10).

For that purpose, let us define  $\mathbb{N}_0^0 := \{\emptyset\}$ ,  $\|\emptyset\|_1 := 0$  and  $\dim(\emptyset) := -\infty$ . Consider the recursion

$$G_{m,D}(\alpha, \sigma) := \begin{cases} \bigcup_{s=0}^{m-\sigma-1} \{G_{m,D}(\alpha \cup (s), s)\}, & \dim(\alpha) < D, \\ (\alpha), & \dim(\alpha) = D, \end{cases} \quad (\text{J35})$$

where for tuples we use  $\alpha \cup (s) := (\alpha, s)$  to denote the operation of appending elements to the tuple. Also,  $\dim(\alpha) \geq 0$  denotes the number of components of non-empty tuples  $\alpha$ .

**Lemma 13.** *We have that*

$$G_{m,D}(\emptyset, 0) = \mathcal{A}_{m,D}$$

for all  $m, D \in \mathbb{N}$ .

*Proof.* Let  $m \in \mathbb{N}$  be arbitrary. First, we are going to establish for all  $D \geq 1$  that

$$G_{m,D}(\emptyset, 0) = \bigcup_{(s_1, \dots, s_{D-1}) \in \mathcal{A}_{m,D-1}} \bigcup_{s_D=0}^{m - (\sum_{j=1}^{D-1} s_j) - 1} \{(s_1, \dots, s_{D-1}, s_D)\}. \quad (\text{J36})$$

We do this by showing  $G_{m,D-1}(\emptyset, 0) = \mathcal{A}_{m,D-1}$  by induction. Indeed, if  $D = 1$ , we find

$$G_{m,1}(\emptyset, 0) = \bigcup_{s_1=0}^{m-1} \{G_{m,1}(\underbrace{(s_1)}_{\dim(\cdot)=1=D}, s_1)\} = \bigcup_{s_1=0}^{m-1} \{(s_1)\} = \{(0), (1), \dots, (m-1)\} = \mathcal{A}_{m,1}. \quad (\text{J37})$$

Assume by induction that  $G_{m,D-1}(\emptyset, 0) = \mathcal{A}_{m,D-1}$  holds true for some fixed  $D$ . In that case,

$$\begin{aligned} G_{m,D}(\emptyset, 0) &= \bigcup_{s_1=0}^{m-1} \{G_{m,D}((s_1), s_1)\} = \bigcup_{s_1=0}^{m-1} \bigcup_{s_2=0}^{m-s_1-1} \{G_{m,D}((s_1, s_2), s_1 + s_2)\} \\ &= \dots = \bigcup_{s_1=0}^{m-1} \bigcup_{s_2=0}^{m-s_1-1} \dots \bigcup_{s_{D-1}=0}^{m-(\sum_{j=1}^{D-2} s_j)-1} \bigcup_{s_D=0}^{m-(\sum_{j=1}^{D-1} s_j)-1} \{G_{m,D}(\underbrace{(s_1, \dots, s_{D-1}, s_D)}_{\dim(\cdot)=D}, \sum_{j=1}^D s_j)\} \\ &= \bigcup_{s_1=0}^{m-1} \bigcup_{s_2=0}^{m-s_1-1} \dots \bigcup_{s_{D-1}=0}^{m-(\sum_{j=1}^{D-2} s_j)-1} \left( \bigcup_{s_D=0}^{m-(\sum_{j=1}^{D-1} s_j)-1} \{(s_1, \dots, s_{D-1}, s_D)\} \right) \\ &= \bigcup_{(s_1, \dots, s_{D-1}) \in \underbrace{G_{m,D-1}(\emptyset, 0)}_{=\mathcal{A}_{m,D-1}}} \left( \bigcup_{s_D=0}^{m-(\sum_{j=1}^{D-1} s_j)-1} \{(s_1, \dots, s_{D-1}, s_D)\} \right), \end{aligned} \quad (\text{J38})$$

where in the last equality we simply used that, by definition,

$$\bigcup_{(s_1, \dots, s_{D-1}) \in G_{m,D-1}(\emptyset, 0)} \{(s_1, \dots, s_{D-1})\} = \underbrace{G_{m,D-1}(\emptyset, 0)}_{\mathcal{A}_{m,D-1}} = \bigcup_{s_1=0}^{m-1} \bigcup_{s_2=0}^{m-s_1-1} \dots \bigcup_{s_{D-1}=0}^{m-(\sum_{j=1}^{D-2} s_j)-1} \{(s_1, \dots, s_{D-1})\}, \quad (\text{J39})$$

Therefore, by induction, we know that (J36) holds true. Let us now use this identity to conclude with the claim  $G_{m,D}(\emptyset, 0) = \mathcal{A}_{m,D}$ .

“ $\subseteq$ ”: If  $\alpha = (\alpha_1, \dots, \alpha_D) \in G_{m,D}(\emptyset, 0)$ , then (J36) implies  $\alpha_D \leq m - (\sum_{j=1}^{D-1} s_j) - 1$ . This immediately results in the bound

$$\|\alpha\|_1 = \alpha_D + \sum_{j=1}^{D-1} \alpha_j \leq m - 1. \quad (\text{J40})$$

In particular,  $\alpha \in \mathcal{A}_{m,D}$ .

“ $\supseteq$ ”: On the other hand, if  $\alpha = (\alpha_1, \dots, \alpha_D) \in \mathcal{A}_{m,D}$ , then  $\|\alpha\|_1 = \alpha_D + \sum_{j=1}^{D-1} \alpha_j < m$  yields

$$\alpha_D \leq m - \left( \sum_{j=1}^{D-1} \alpha_j \right) - 1. \quad (\text{J41})$$

In particular

$$\alpha = (\alpha_1, \dots, \alpha_{D-1}, \alpha_D) \in \bigcup_{s_D=0}^{m-(\sum_{j=1}^{D-1} \alpha_j)-1} \{(\alpha_1, \dots, \alpha_{D-1}, s_D)\}. \quad (\text{J42})$$

Additionally,  $\|\alpha\|_1 < m$  means that one necessarily must have  $(\alpha_1, \dots, \alpha_{D-1}) \in \mathcal{A}_{m,D-1}$ . Indeed, otherwise we have the contradiction

$$m \leq \sum_{j=1}^{D-1} \alpha_j \leq \sum_{j=1}^D \alpha_j = \|\alpha\|_1 < m. \quad (\text{J43})$$

Therefore,

$$\alpha \in \bigcup_{(s_1, \dots, s_{D-1}) \in \mathcal{A}_{m, D-1}} \bigcup_{s_D=0}^{m - (\sum_{j=1}^{D-1} \alpha_j) - 1} \{(s_1, \dots, s_{D-1}, s_D)\} = G_{m, D}(\emptyset, 0), \quad (\text{J44})$$

where in the last equality we made use of our previous claim (J36).  $\square$

## Appendix K: Additional Numerical Experiments

This section expands upon the numerical experiments in Sec. V. In particular, we show the scaling of initial gradients for all circuit designs considered in this work, VQE experiments with finite sampling and different learning rates, and ultimately VQE experiments for the Heisenberg model.

### 1. Gradient Scaling Experiments

We repeat the initial gradient scaling experiments (cf. Figs. 5 and 6) comparing all models considered in this work: mHEA, fHEA, and rPQC (defined in Appendix C).

Fig. 13 illustrates the expected behavior of the initial gradient norm at  $\theta = 0$  employing various PQC models with  $L = 1$  layer. Gradients are computed analytically via Eq. (15). Results are averaged over 10 independent runs, each involving a randomly selected single Pauli string  $H = P$  and a random direction  $k \in [D]$  used in constructing the LCE transformation. As shown, the initial gradient norm for the non-LCE model decays exponentially and becomes indistinguishable from zero beyond  $N = 10$  qubits. In contrast, the LCE model consistently maintains an initial gradient norm of at least 1, in agreement with the theoretical prediction of Theorem 1.

Fig. 14 compares initial gradient norms at  $\theta = 0$  with and without LCE, employing mHEA with  $L = 1$  layer. Gradients are computed analytically via Eq. (15). Each run uses a randomly sampled observable  $H$ , and a random LCE construction. Panel (a) of Fig. 5 focus on uniformly random single Pauli strings  $H = P$ . Without LCE, constructive contributions in Eq. (15) vanish with increasing  $N$ , leading to zero expected gradient for sufficiently large  $N$ . With LCE, gradient norms remain constant in  $N$ . Panels (b) and (c) of Fig. 5 extend results to random observables with  $|\mathcal{I}| = \lfloor \sqrt{N} \rfloor$  Pauli terms. For observables with uniformly sampled Pauli strings  $P_i$  and  $c_i = 1$  for all  $i \in \mathcal{I}$  (called random unweighted  $H$ ), the scaling compares to the single-Pauli case. For observables with uniformly sampled Pauli strings  $P_i$  and i.i.d.  $c_i \sim \text{Unif}([-1, 1])$  for all  $i \in \mathcal{I}$  (called random weighted  $H$ ), gradient norms tend to behave more randomly due to random Pauli coefficients. This is evidence that the LCE transformation remains effective for arbitrary observables.

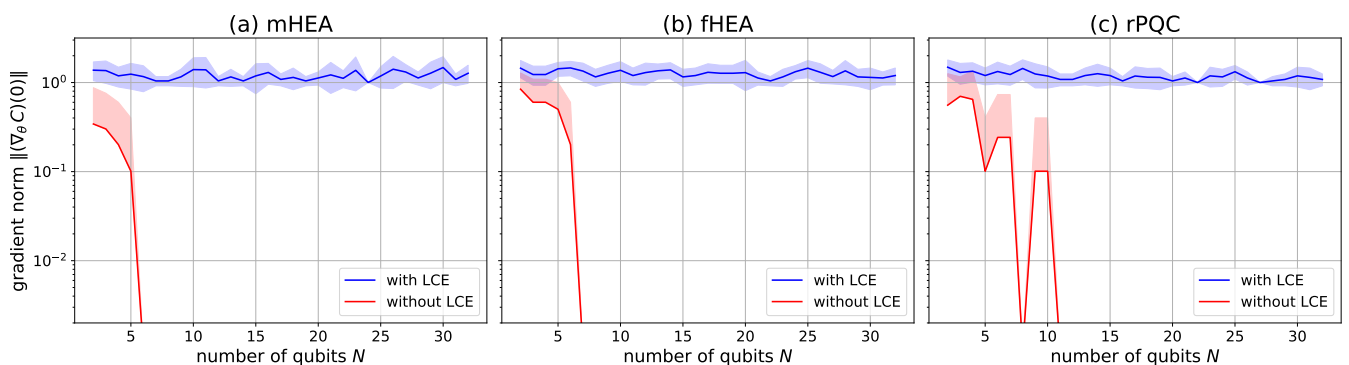


FIG. 13. Scaling behavior of the initial gradient norm at  $\theta = 0$  for across various PQCs with  $L = 1$  layer. We average over 10 samples of random single Pauli strings  $H = P$ , and random directions  $k \in [D]$  for the LCE transformation.

Fig. 15 repeats the experiment of Fig. 13 on near-Clifford patches, comparing various linear-depth PQC models, and varying patch sizes via Gaussian initialization  $\sigma = D^{-\tau}$ . Each run uses a randomly sampled parameter, a

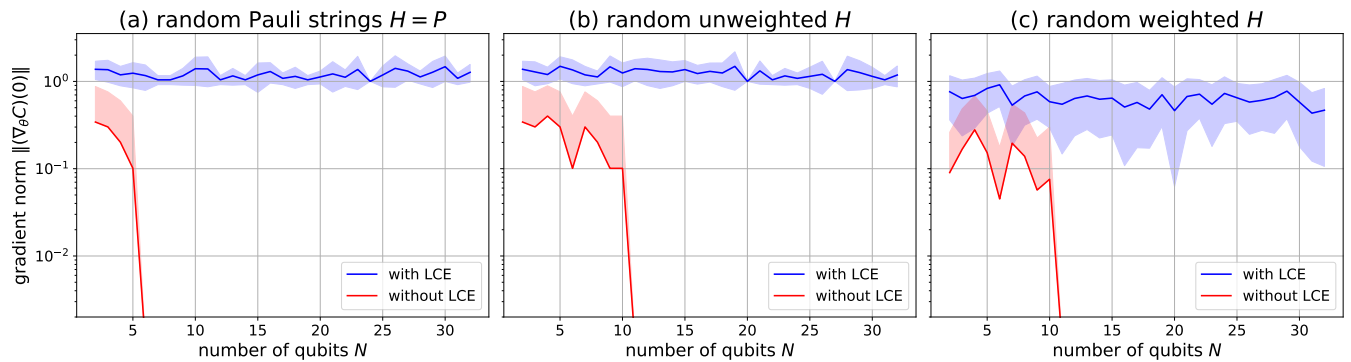


FIG. 14. Scaling behavior of the initial gradient norm at  $\theta = 0$  for the mHEA-model with  $L = 1$  layer. The panels vary across types of random observables. The experiment highlights the effect of the LCE transformation. We average over 10 independent runs.

random single-Pauli string observable  $H = P$ , and a random LCE construction. The red-shaded region corresponds to classically efficient regimes (cf. Fig. 3); blue-shaded to super-polynomial regimes, where gradients still decay only polynomially. Interestingly, the LCE construction not only preserves trainability but also regularizes gradient scaling in  $N$ . LCE transformed norms scale predictably, while non-LCE trends are erratic. Within the constant-scaling regime (red-shaded), LCE ensures trainability. For large  $\sigma$ , gradients decay exponentially. This confirms the existence of a larger patch size where gradient transition from constant decay to polynomial decay (cf. Eq. (9)) as established by Theorem 5.

The same experiment is performed using shallow PQC's with a single layer ( $L = 1$ ) as shown in Fig. 16. Comparing the results of linear-depth and single-layer setups reveals the impact on gradient scalability: as the number of parameters increases (i.e. in deeper circuits), the gradient norm tends to diminish more rapidly, especially for larger patch sizes.

## 2. VQE Optimization with different Learning Rates and Finite Sampling Noise

Here, we demonstrate that LCE is effective for smaller learning rates in vanilla gradient descent. Furthermore, we address the issue of finite sampling noise [53]. We use a small number of finite shots to evaluate the gradients in order to emphasize that LCE remains relevant for near-term practical applications.

Fig. 17 shows VQE optimization of the global observable  $Z^{\otimes N}$ , employing the mHEA ansatz ( $L = 5$ ,  $N = 15$ ), averaging over 5 runs with Gaussian initializations  $\theta \sim \mathcal{N}(0, \sigma^2 I_D)$  across varying patch sizes. Optimization is performed with vanilla gradient descent, where we compare various constant learning rates. The gradients are evaluated exactly as per Eq. (15). LCE consistently yields faster convergence, independent of the learning rate. Fastest convergence is achieved with a learning rate of 0.1, and continuously slows down as the learning rate increases. While our theory guarantees trainability up to  $\sigma = D^{-1/2}$ , numerical results continue to demonstrate successful convergence slightly beyond, even in classically intractable regimes (cf. Theorem 3). LCE advantage is less pronounced as  $\sigma$  increases (cf. Fig. 6).

Fig. 18 repeats the same VQE experiment, but this time using finite shots sampling, and a learning rate of 0.01. The improved gradient due to LCE allows fewer sampling shots. In this case, 8 shots are already sufficient for fast convergence up to the patch size  $\sigma = D^{-1/3}$ . Finite shots sampling explaining the increase of noise in the first three rows. Interestingly, using finite shots sampling appears to converge slightly faster compared to the exact dynamics in the last row. Hence, it may be possible that finite sampling noise may be exploited to improve the dynamics of LCE transformed VQEs. Inspecting the column containing  $\sigma = D^{-1/5}$ , one notices that a 15-qubit model suffering from barren plateaus generally requires  $2^{15}$  shots to accurately estimate the gradient in order to eventually achieve convergence, whereas employing exact gradients (cf. Eq. (15)) barely enables slow convergence. These findings can be seen as evidence that LCE has the potential to enhance finite sampling efficiency in VQEs.

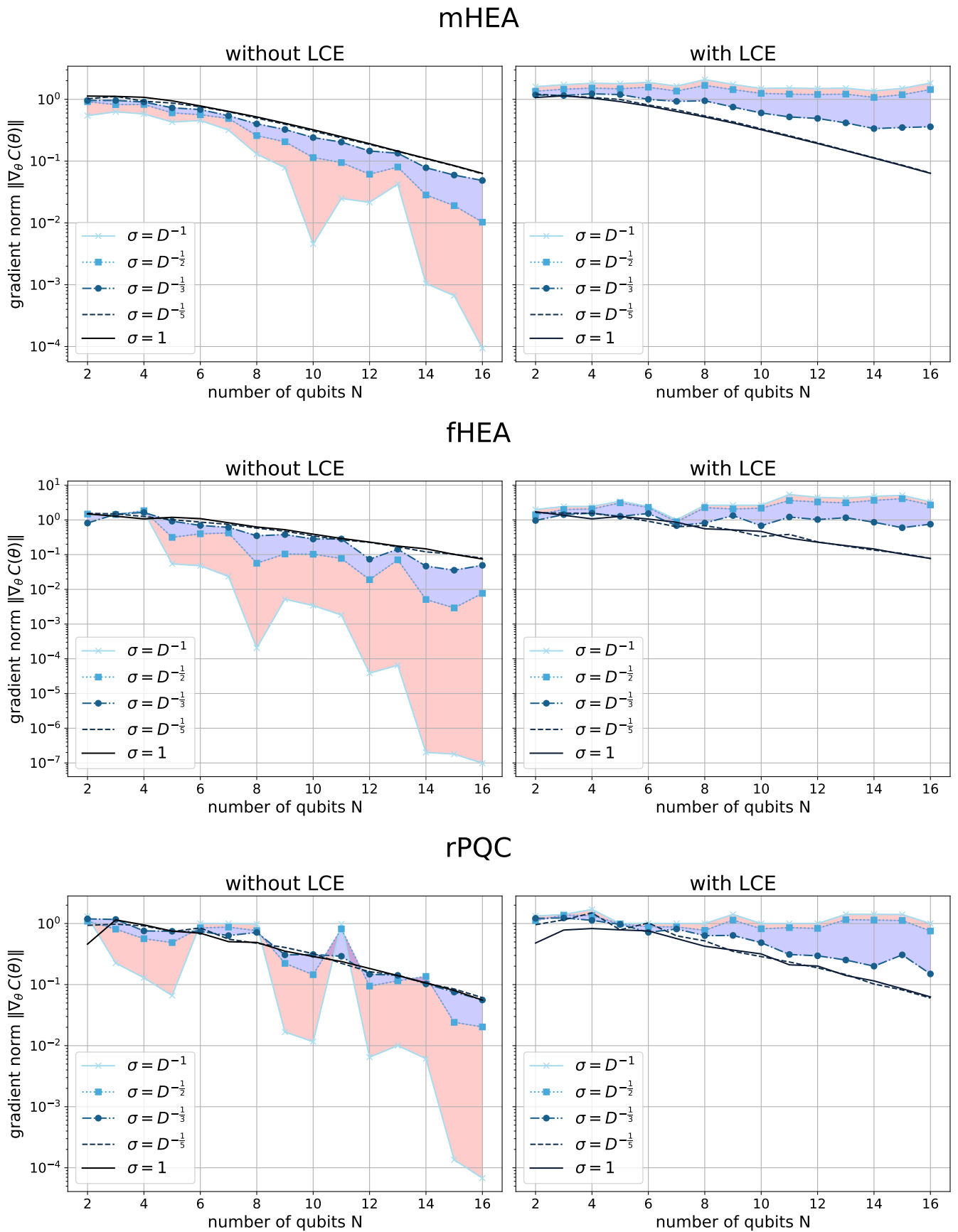


FIG. 15. Scaling behavior of the gradient norm on various surrogate patches for PQC models with  $L = N$  layers. We average over 50 independent runs.

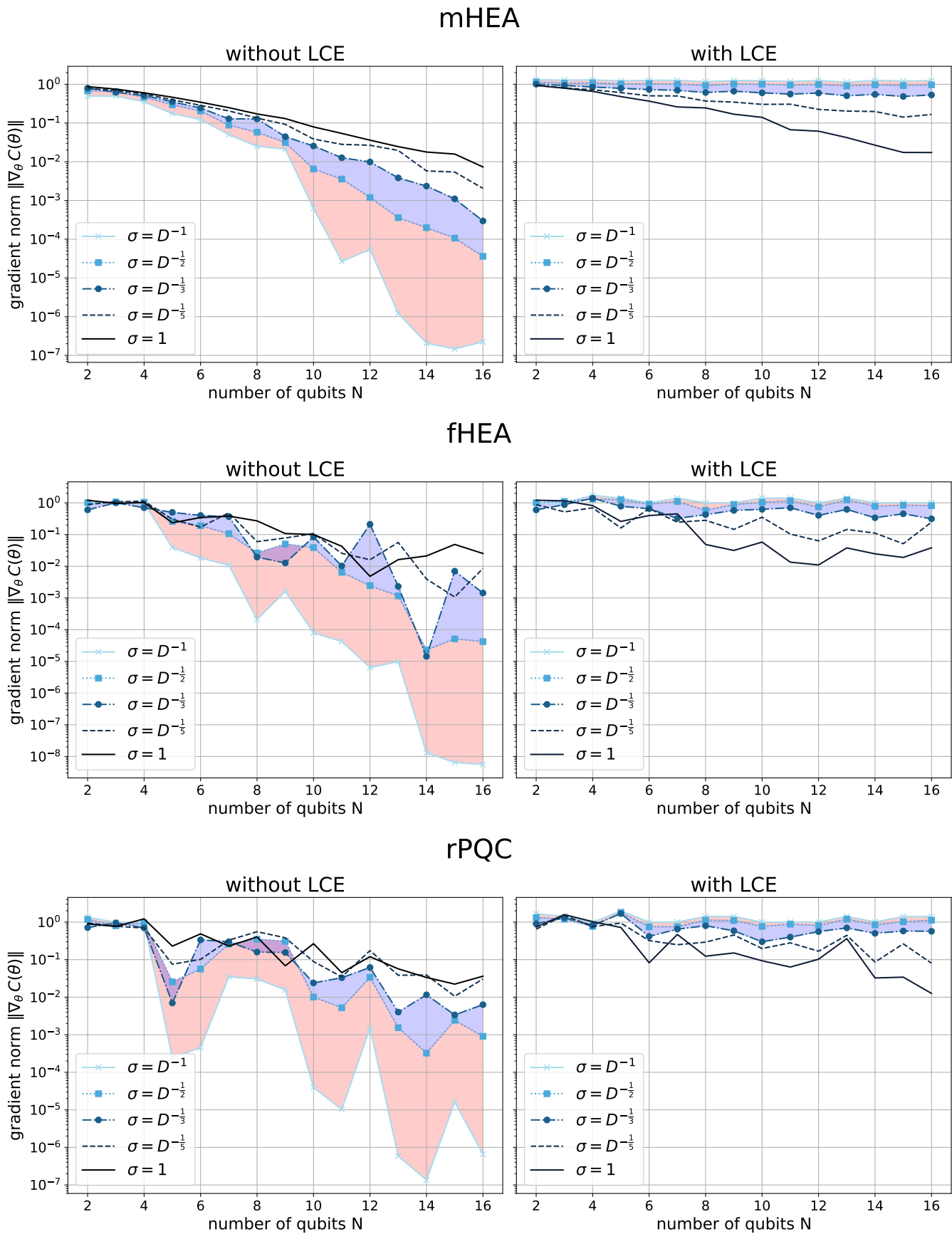


FIG. 16. Scaling behavior of the gradient norm on various surrogate patches for PQC models with  $L = 1$  layer. We average over 50 independent runs.

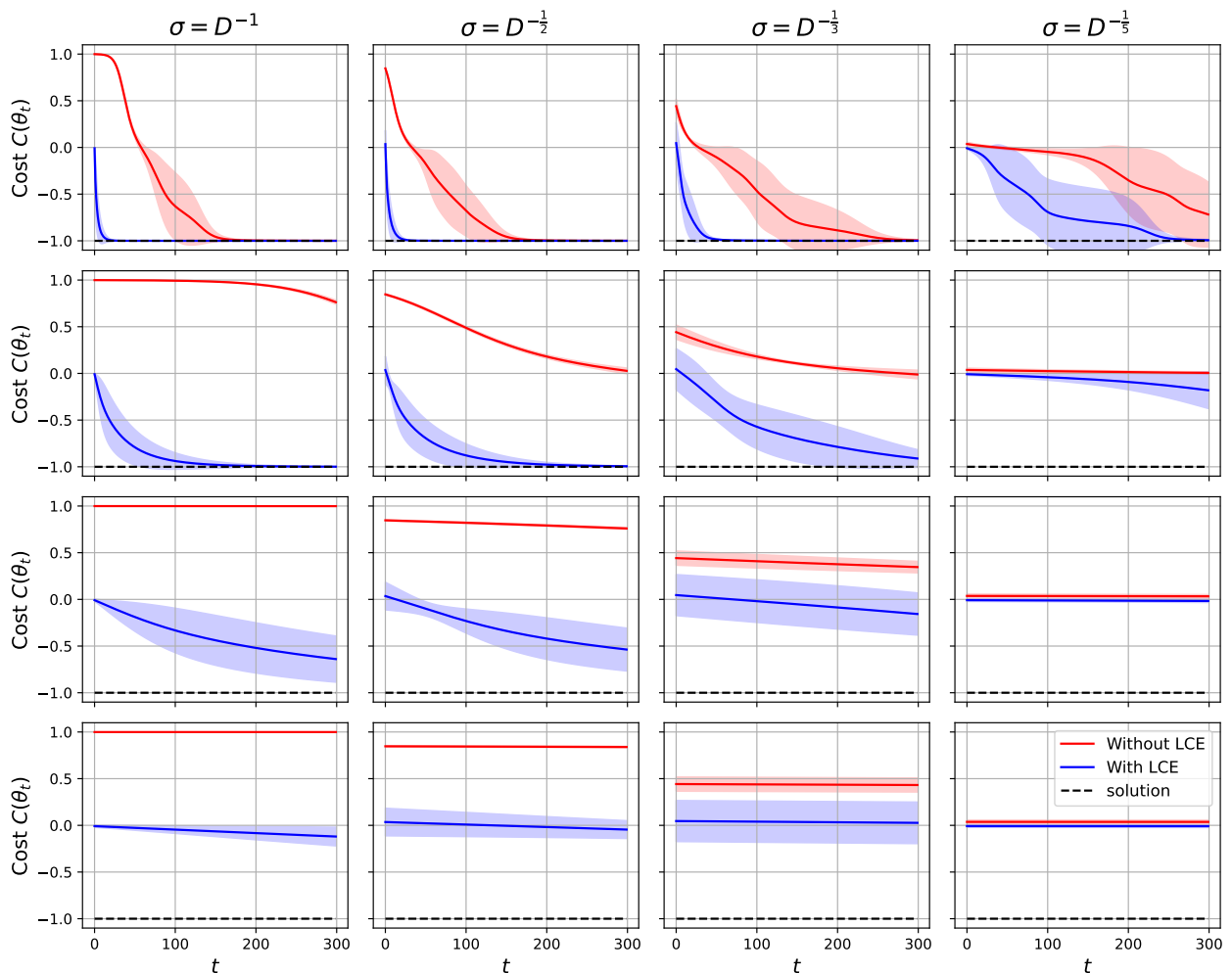


FIG. 17. VQE Optimization using vanilla gradient descent with various learning rates of 0.1 (top row), 0.01 (second row), 0.001 (third row), and 0.0001 (bottom row). We evaluate exact gradients, and average over 5 runs of random Gaussian initialization across varying patch sizes. We find the ground energy of the global observable  $Z^{\otimes N}$  with  $N = 15$ , employing the mHEA ansatz with  $L = 5$  layers.

### 3. VQE Optimization of the Heisenberg Model

In this experiment, we leverage the benchmarked initial gradient scaling statistics to optimize the VQE of the  $N = 12$  qubit Heisenberg model [54],

$$H_{\text{Heisenberg}} := \sum_{j=1}^{N-1} \{X_j X_{j+1} + Y_j Y_{j+1} + Z_j Z_{j+1}\}. \quad (\text{K1})$$

Eq. (K1) defines a local observable and thus is less prone to the barren plateau problem [52]. In order to increase the chance of inducing barren plateaus, one may consider deep circuit ansätze which result in expressivity-induced barren plateaus [16]. Therefore, when employing shallow circuits to find the ground state of a local observable, the effectiveness of LCE is expected to disappear.

We compare the optimization dynamics of the Heisenberg model in Eq. (K1) with and without the LCE transformation. We employ mHEA with  $L = 32$  layers, and average over 5 independent runs of random Gaussian initialization of parameters across varying patch sizes. The results are presented in Fig. 19. We can see the advantage of LCE on sufficiently large patch sizes stemming from the improved initial gradient as per Fig. 6, while the non-LCE model

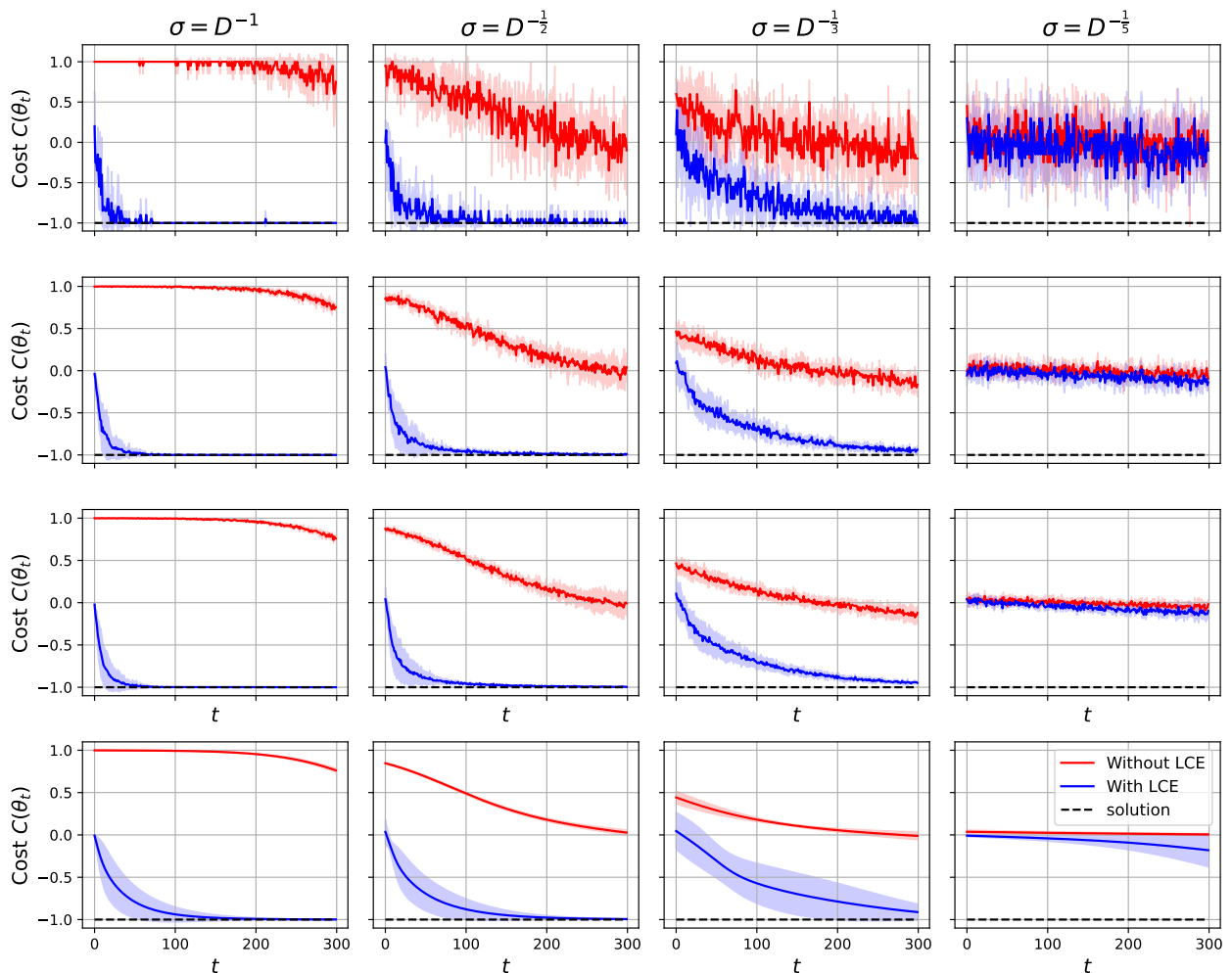


FIG. 18. VQE Optimization using vanilla gradient descent with a learning rate of 0.01, estimating gradients with 8 shots (top row), 64 shots (second row), 512 shots (third row), and exact gradients (bottom row). We average over 5 runs of random Gaussian initialization across varying patch sizes. We find the ground energy of the global observable  $Z^{\otimes N}$  with  $N = 15$ , employing the mHEA ansatz with  $L = 5$  layers.

remains stuck on a local minimum. If the patch size is too large (e.g.  $\sigma = D^{-1/5}$ ), then the advantage of LCE is less pronounced.

Recalling the VQE experiment with  $H_{\text{global}} = Z^{\otimes N}$  (cf. Fig. 7 in Sec. V), we note that the converge rates when using LCE are far slower compared to the Heisenberg model. This could be due to the assumption that  $|\mathcal{I}| = \mathcal{O}(1)$  (see the discussion following Theorem 2) which may explain why LCE yields significantly improved VQE dynamics for  $Z^{\otimes N}$  compared to the dynamics of the Heisenberg model for which  $|\mathcal{I}| = 3N$ .

As a further point of comparison, we conduct the same experiment using a shallower mHEA model with  $L = 6$  layers, as shown in Fig. 20. This model, having fewer trainable parameters, is expected to be less susceptible to the barren plateau problem. The results indicate that the beneficial impact of LCE (being particularly effective for mitigating barren plateaus) is less pronounced compared to the deeper mHEA model with  $L = 36$  layers. This means that LCE should only be applied for VQEs with observables giving rise to barren plateaus. Interestingly, this experiment also suggests that the non-LCE initialization might, in some cases, begin closer to a global minimum, whereas the LCE transformation could potentially lead to entrapment in a local minimum (particularly in under-parameterized models). We hypothesize that such behavior is less prevalent in larger-scale models, and that alternative optimization strategies, such as the ADAM optimizer [29], may offer a way to escape local minima.

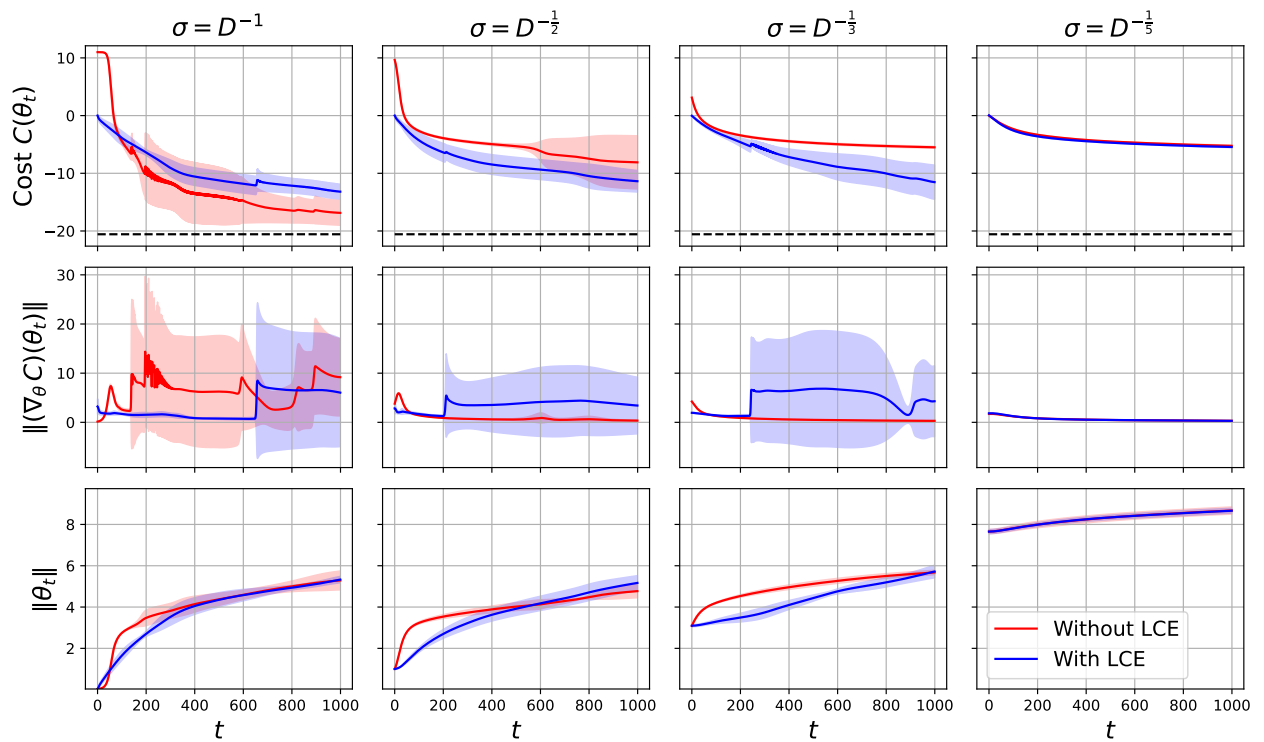


FIG. 19. VQE Optimization using vanilla gradient descent with a learning rate of 0.01, averaging over 5 runs of random Gaussian initialization across varying patch sizes. We employ the mHEA ansatz with  $L = 36$  layers to find the ground energy of 12-qubit Heisenberg model.

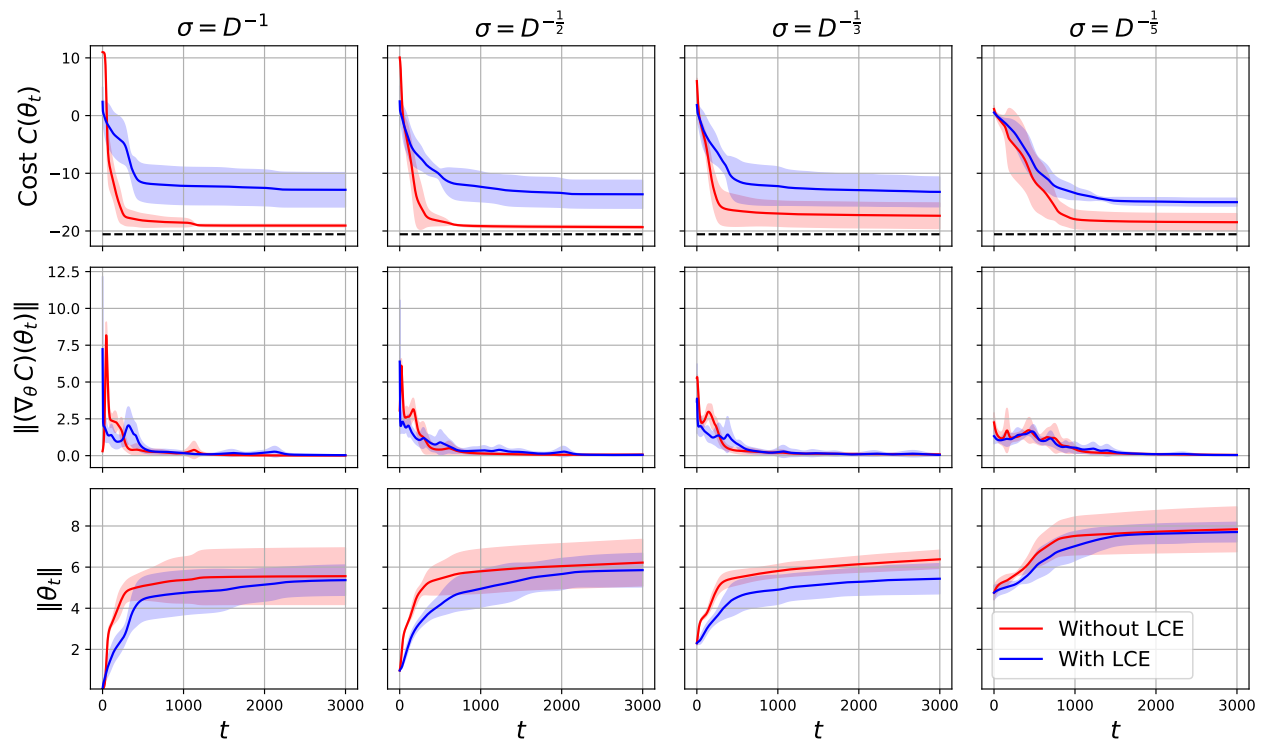


FIG. 20. VQE Optimization using vanilla gradient descent with a learning rate of 0.01, averaging over 5 runs of random Gaussian initialization across varying patch sizes. We employ the mHEA ansatz with  $L = 6$  layers to find the ground energy of 12-qubit Heisenberg model.